**Nonlinear Processes
in Geophysics**

Finite-time Lagrangian transport analysis: stable and unstable manifolds of hyperbolic trajectories and finite-time Lyapunov exponents

M. Branicki[1,2] **and S. Wiggins**[1]

[1]School of Mathematics, University of Bristol, University Walk, Bristol BS8 1TW, UK
[2]College of Earth, Ocean, and Environment, University of Delaware, Robinson Hall, Newark, USA

Abstract. We consider issues associated with the Lagrangian characterisation of flow structures arising in aperiodically time-dependent vector fields that are only known on a finite time interval. A major motivation for the consideration of this problem arises from the desire to study transport and mixing problems in geophysical flows where the flow is obtained from a numerical solution, on a finite space-time grid, of an appropriate partial differential equation model for the velocity field. Of particular interest is the characterisation, location, and evolution of transport barriers in the flow, i.e. material curves and surfaces. We argue that a general theory of Lagrangian transport has to account for the effects of transient flow phenomena which are not captured by the infinite-time notions of hyperbolicity even for flows defined for all time. Notions of finite-time hyperbolic trajectories, their finite time stable and unstable manifolds, as well as finite-time Lyapunov exponent (FTLE) fields and associated Lagrangian coherent structures have been the main tools for characterising transport barriers in the time-aperiodic situation. In this paper we consider a variety of examples, some with explicit solutions, that illustrate in a concrete manner the issues and phenomena that arise in the setting of finite-time dynamical systems. Of particular significance for geophysical applications is the notion of flow transition which occurs when finite-time hyperbolicity is lost or gained. The phenomena discovered and analysed in our examples point the way to a variety of directions for rigorous mathematical research in this rapidly developing and important area of dynamical systems theory.

Correspondence to: M. Branicki
(m.branicki@bristol.ac.uk)

1 Introduction

Organised or "coherent" structures in fluid flows have been a subject of intense study for some time, especially since the seminal paper of Brown and Roshko (1974). The dynamical systems approach to the Lagrangian aspects of fluid transport, which became widespread in the 1980's and 90's, has provided a variety of techniques for determining the existence and quantifying "organised structures" in fluid flows. Hyperbolic trajectories and their associated stable and unstable manifolds have provided one approach to this problem, in both the periodic and aperiodic time-dependent settings, that dates back to the beginning of studies of "chaotic advection" in fluid flows (Ottino, 1989; Aref and El Naschie, 1994; Acrivos et al., 1991; Babiano et al., 1994; Wiggins, 2005; Jones and Winkler, 2002; Samelson and Wiggins, 2006). More recently, the notion of "Lagrangian coherent structure" (henceforth LCS) derived from finite-time Lyapunov exponent (FTLE) fields has provided another means of identifying coherent flow structures in fluid flows which can be used in Lagrangian transport analysis (Haller and Yuan, 2000; Haller, 2001a,b; Shadden et al., 2005; Lekien et al., 2007). The purpose of this paper is to compare the methods based on determination of stable and unstable manifolds of hyperbolic trajectories with LCS's derived from FTLE's as techniques for uncovering organised structures in fluid flows and quantifying their influence on transport.

We begin in Sect. 2 by reviewing some theoretical issues associated with Lagrangian transport analysis in time-dependent vector fields defined over a finite time interval. We also take the opportunity to clarify a number of misconceptions that have arisen in the literature concerning the applicability of hyperbolic trajectories and their stable and unstable

manifolds in analysing Lagrangian transport in fluid flows, especially with respect to their comparison with LCS's. This will naturally lead to the issue of a relationship between the stable and unstable manifolds of hyperbolic trajectories and LCS's. We will particularly focus on the performance and applicability of these techniques in flows undergoing transitions associated with a loss or gain of *finite-time* hyperbolicity by some trajectories. An understanding of this relationship is essential for understanding the role that each of these structures plays in Lagrangian transport. Both methods can have drawbacks as tools for diagnosing the finite-time Lagrangian flow structure. In Sect. 3 we consider a series of examples which aim at providing a guide for choosing the most suitable technique for a particular application. We begin the discussion by studying a 1-D non-autonomous system which can be solved analytically and which provides a good illustration of issues concerning the finite-time hyperbolic trajectories and FTLE fields in higher dimensions. The subsequent examples of 2-D non-autonomous systems are chosen to highlight various properties and problems arising in the invariant manifolds and FTLE analysis.

We summarise our findings in Sect. 4 where we also discuss a number of outstanding problems. The Appendices contain a number of technical details and definitions, as well as a discussion of some important facts necessary for computation of finite-time stable and unstable manifolds.

2   Some theoretical background and questions

In this section we describe some of the relevant theoretical issues related to hyperbolic trajectories and their stable and unstable manifolds, and LCS's. This will serve to highlight some practical issues arising from applications, as well as the need for further theoretical and computational developments. We will not go into great detail in describing the theoretical results and computational methods since they are already covered in numerous papers in the literature; relevant references will be provided wherever appropriate in the discussion. Rather, we will discuss ideas and concepts and provide a guide to the existing literature. In order to achieve a relative self-containment of the following discussion, we also provide a number of important definitions in the Appendix A in order to make this discussion easier to follow.

The notion of *hyperbolicity of a trajectory* has been around for some time. It is particularly worth remembering in the context of the present discussion that hyperbolicity is not dependent on the nature of the considered time dependence (although continuity in time, which is also our operating assumption here, eliminates many technical issues). In particular, if hyperbolicity is determined by Lyapunov exponents (Katok and Hasselblatt, 1995) or exponential dichotomies (Coppel, 1978), then the nature of the time dependence, e.g. periodicity, quasiperiodicity, or aperiodicity plays no role in any of these definitions (equivalence between these

definitions is considered in Dieci and Vleck, 2002). Once a hyperbolic trajectory is located, the stable and unstable manifold theorem for hyperbolic trajectories immediately applies. It can be verified that the statement of this theorem is also independent of the nature of the time dependence by examining, for example, its proof in the classic ordinary differential equations textbook of Coddington and Levinson (1955). Additional resources on the stable and unstable manifold theorem for arbitrary time dependence can be found in de Blasi and Schinas (1973); Irwin (1973); Katok and Hasselblatt (1995).

Of course, a central issue in practical applications is the location of relevant hyperbolic trajectories in aperiodically time-dependent velocity fields. Historically, there have been many algorithms for finding equilibrium points (stagnation points) of steady velocity fields and periodic orbits of time-periodic velocity fields. However, relatively little work had been done on algorithms for finding hyperbolic trajectories of aperiodically time-dependent velocity fields (and quite a few new issues arise, in comparison to the issues associated with steady and time periodic velocity fields, which we will mention below). An algorithm for determining hyperbolic trajectories in arbitrary unsteady flows was given in Ide et al. (2002) and further refined in Ju et al. (2003); Mancho et al. (2004). This technique is based on an iterative method defined on a space of "paths" and, provided it converges, is guaranteed to yield a *hyperbolic trajectory* on a specified time interval which is bounded in most practical applications. (The "finiteness" of the considered time interval brings up yet another technical issue that we will shortly address.) The iterative algorithm requires an initial 'guess' in the form of a C^1 hyperbolic path (see Definition A.4) defined on the appropriate time interval. It is important to stress here that such a path need not be a trajectory of the velocity field. Nevertheless, the construction of the initial guess is often nontrivial and problem dependent. We provide a few more details regarding some necessary properties of the initial guess in the Appendix A (see remarks after Definition A.5). The initial guess is often chosen to be a path of hyperbolic instantaneous stagnation points, ISPs (cf. A18, Appendix A). This particular choice of the initial path has lead to numerous misleading and incorrect statements in the LCS literature related to the notion of "Galilean invariance" and the nature of this algorithm (Lekien and Coulliette, 2007; Lekien et al., 2007; Shadden et al., 2005). Galilean transformations consist of spatial translations, time translations, shear transformations, reflections, and rotations. Paths of ISPs are *not*, in general, particle trajectories and they are not invariant under Galilean transformations. This has been a known fact in the fluid dynamics community for some time and a simple proof can be found, for example, in an appendix in Ide et al. (2002). However, it is well-known in the dynamical systems community that trajectories are invariant under Galilean transformations (i.e. a trajectory maps to a trajectory under a Galilean transformation) and *hyperbolic* trajectories to which

the iterative algorithm converges are likewise invariant under Galilean transformations[1]. Consequently, the fact that a non-Galilean invariant path is used as an initial guess for the iterative algorithm is irrelevant since if the algorithm converges, it yields a hyperbolic trajectory which is manifestly Galilean invariant. Likewise, since the stable and unstable manifolds of a hyperbolic trajectory are, by definition, composed of trajectories, they are also Galilean invariant. The importance of Galilean invariance to specific oceanographic investigations is another matter entirely. Oceanographers require a fixed reference frame to describe the ocean through measurements and grid based computations. In the chosen frame, the behavior and stability of ISPs have historically played an important role in describing observed Eulerian flow structures. While ISPs *may* bear little relation to particle trajectories, we believe that dismissal of their utility on the grounds of not being Galilean-invariant is unjustified.

A more serious issue worth mentioning here is that hyperbolicity, and therefore hyperbolic trajectories and their stable and unstable manifolds, are "infinite-time objects". More precisely, hyperbolicity of a trajectory is determined on the basis of the asymptotic behaviour of neighbouring trajectories in the infinite time limit. The stable and unstable manifolds associated with a hyperbolic trajectory are proven to exist via a fixed point, or iterative, argument where the limit as time goes to either positive or negative infinity is taken. If the velocity field is aperiodic in time, and it is obtained from the output of a numerical computation, then we have knowledge of the velocity field only on a *finite time interval*. This fact creates a host of new problems in applying the "traditional" dynamical systems approach to fluid transport. The main difficulty in the "finite-time" description of Lagrangian transport stems from the fact that the dynamical systems theory is generally concerned with the "long time behavior" of systems of ODE's (many of these problems are discussed in Wiggins, 2005; Mancho et al., 2006). In particular, the standard definitions of hyperbolicity of trajectories do not apply to velocity fields that are only known on a finite time interval (henceforth *finite-time velocity fields*).

The subject of "finite-time dynamical systems theory" gives rise to many new issues that require new theoretical and computational results. These are discussed in Wiggins (2005); Mancho et al. (2006). There have also been a number of mathematical papers developing various aspects of this subject in recent years (Duc and Siegmund, 2008; Berger et al., 2008). The "finite-time" framework is intrinsically dependent on the time interval one considers in the analysis and the implications of non-uniqueness associated with this setting have been discussed in numerous papers, see, e.g., Miller et al. (1997); Haller and Poje (1998); Haller (2000); Ide et al. (2002); Mancho et al. (2006). In particu-

lar, in the context of finite-time dynamical systems, hyperbolicity of a trajectory is defined over a finite time interval (cf. Definitions A.4 and A.11 in the Appendix A) and the stable and unstable manifolds associated with the trajectory no longer have a lower dimension than the underlying phase space (cf. Appendix B and Duc and Siegmund, 2008). Consequently, a trajectory which is hyperbolic over some time interval (in the finite-time sense) may not be hyperbolic over a longer time interval. In other words, given $a, b, c, d \in \mathbb{R}$ such that $a < b < c < d$, it is possible for a trajectory to possess finite-time hyperbolic characteristics on all intervals contained in $I_{ab} = [a, b]$, and then lose such characteristics on some intervals contained in I_{bc}, possibly regaining the finite-time hyperbolic properties for all intervals contained in I_{cd}. We refer to such a scenario as a "loss" and a subsequent "gain" of finite-time hyperbolicity and point out that one cannot pin these transitions to a particular time instant. Purists in dynamical systems theory may immediately object by saying that hyperbolicity is a notion that only has meaning for trajectories defined for all time. According to the traditional definition, this is certainly correct. However, applications to transport in velocity fields defined for finite time have motivated this new definition of hyperbolic-like properties over a bounded time interval (i.e. the finite-time hyperbolicity) and the notion of loss or gain of (finite-time) hyperbolicity has proven useful for describing the transient behavior of a number of time-dependent structures in oceanographic flows. We will discuss examples of simple flows whose transitions are induced by the loss (or gain) of finite-time hyperbolicity in Sect. 3.3.1, 3.3.5, and 3.3.6.

In any case, it is important to realise that all of the finite-time dynamical systems notions that we mentioned above are *trajectory based*. That is, the finite-time hyperbolic trajectories are indeed trajectories and material curves contained in their finite-time stable and unstable manifolds are barriers to transport (see also Appendix B). Their usefulness for applications derives solely from their ability to explain new phenomena in applications, and this is assessed in the context of specific applications.

Another technique used in the finite-time transport analysis is based on determination of the so-called Lagrangian coherent structures (LCS) from finite-time Lyapunov exponent fields (FTLE). Lyapunov exponents are quantities associated with trajectories that are obtained as infinite time limits. For an n-dimensional continuous time dynamical system a trajectory has n Lyapunov exponents – one associated with a direction tangent to the trajectory (which is always zero) and $n-1$ Lyapunov exponents associated with the remaining directions. The Lyapunov exponents are measures of the growth of infinitesimal perturbations in these directions, i.e. growth rates of the linearized dynamics about the trajectory (cf. Appendix A). Of particular interest is the maximum Lyapunov exponent since the existence of a single positive Lyapunov exponent indicates that the trajectory is unstable. The fundamental theorem on the existence of Lyapunov exponents

---

[1]The Galilean invariance of hyperbolic trajectories is proven in Ide et al., 2002 for hyperbolicity determined with exponential dichotomies.

is expressed by the Osedelec multiplicative ergodic theorem (Oseledec, 1968). There are many excellent references on Lyapunov exponents that describe their properties (Katok and Hasselblatt, 1995; Lapeyre, 2002; Legras and Vautard, 1996) and algorithms for their computation (Dieci et al., 1997; Dieci and Eirola, 1999; Dieci and Vleck, 2002; Greene and Kim, 1987; Geist et al., 1990).

In the infinite-time setting, Lyapunov exponents are one measure of the hyperbolicity of a trajectory. If a trajectory has nonzero Lyapunov exponents (with the exception of the zero exponent associated with the direction tangent to the trajectory), it is said to be hyperbolic (Katok and Hasselblatt, 1995). Finite-time Lyapunov exponents are obtained by computing the same quantities, but restricting the computation to a finite time interval, rather than taking the limit as the time goes to positive infinity (for "forward-time" Lyapunov exponents) or minus infinity (for "backward-time" Lyapunov exponents)[2]. Clearly, one would like to know the length of the time interval on which they must be computed so that they are "close" to the infinite time limit. Some interesting arguments are given in Goldhirsch et al. (1987); Ershov and Potapov (1998) which indicate that the rate of convergence may be quite slow. The FLTE technique[3] is not immune to the non-uniqueness issues arising in the finite time setting mentioned earlier. These are highlighted by the fact that for any time instant in the considered time interval I one can compute a whole family of FTLE fields. We discuss implications of this fact in the following sections.

For each time instant t_n within the considered (or available) time interval I, forward FTLE fields are obtained by computing the forward Lyapunov exponents of the trajectory starting at an initial condition, $\boldsymbol{x}_i$, in a chosen grid for the length T of time available (and computable) and colour coding the initial condition according the the magnitude of the largest FTLE (e.g. bright colors for large values, light colors for small values). By performing such a computation for an ordered sequence of "observation times", $\{t_n\}_{n\in\mathbb{Z}}$, $t_n\in I$, one can examine the spatial evolution of the structures exhibited by the forward FTLE fields in time. Clearly, backward FTLE fields can also be computed by reversing the direction of time. Note here that for any t_n in such a sequence it is possible to compute an FTLE field for any T such that $t_n+T\in I$. It is often not obvious which length of the integration time interval T should be chosen in such computations especially when the structure of the resulting FTLE fields varies significantly for different values of T. We discuss these issues in most of the examples presented in Sect. 3.

Since Lyapunov exponents are a measure of the (linearized) growth rates of a set of orthogonal directions perpendicular to the tangent vector to a trajectory, FTLE fields have been more physically referred to as "stretching fields"[4]. Numerous groups have computed discrete approximations of FTLE fields over the years in the context of fluid transport (e.g., Pierrehumbert, 1991; Pierrehumbert and Yang, 1993; von Hardenberg et al., 2000) and have noted that these fields appear to exhibit a great deal of structure. A more precise quantification of such structures have led to the notion of LCS (Haller, 2000; Haller and Yuan, 2000; Haller, 2001a,b, 2002; Shadden et al., 2005; Lekien et al., 2007). In particular, since FTLE's are a measure of separation of nearby trajectories after some finite-time, regions of high values for the maximal FTLE would seem to be likely candidates for regions containing hyperbolic trajectories and their stable and unstable manifolds. Heuristic arguments supporting this assertion are given in the aforementioned references, and will not be reproduced here. Rather, in this paper we will focus upon the assumption that "maxima" of the FTLE fields are "approximations" to the stable manifolds of hyperbolic trajectories (forward time FTLE fields) and unstable manifolds of hyperbolic trajectories (backward time FTLE fields). We have put the word maxima in quotes since this notion needs careful consideration. This was done in Shadden et al. (2005) via the notion of a *ridge curve* of an FTLE field. Roughly speaking, a ridge curve has the property that moving transverse to the direction tangent to the curve corresponds to moving to a lower value of the FTLE. Precise definitions are given in Shadden et al. (2005) where ridges of the FTLE field are taken as the definition of LCS. This raises the question of precisely how "Lagrangian" are LCS's? In general, they are *not* material curves, and therefore not necessarily barriers to transport. In the following sections we will demonstrate this with several examples designed to highlight different aspects of the problem. Nevertheless, certain segments of an LCS

---

[2]We note that the notion of a "direct Lyapunov exponent" (DLE) has been introduced (Haller, 2001a). This has created some confusion in the literature in the sense that the acronyms "FTLE" and "DLE" are used somewhat synonymously. In recent years the consensus has become that there is no substantive difference between the two notions and "FTLE" has now returned to being the accepted acronym (e.g., see Shadden et al., 2005, 2006, 2007; Lekien et al., 2007).

[3]We note that in much of the literature concerning FTLEs, the phrase refers to the *maximum* FTLE.

[4]As we have noted, FTLE's are a measure of the growth of infinitesimal perturbations to a given trajectory, i.e. growth rates of the linearized dynamics about a trajectory. Finite size (or scale) Lyapunov exponents (FSLE's) are a technique to analyse the growth of finite perturbations to a given trajectory. Alternatively, FSLE quantify the relative dispersion of two particles, as discussed in Boffetta et al. (2001). In Boffetta et al. (2001); Koh and Legras (2002); Joseph and Legras (2002); d'Ovidio et al. (2007); Garcá-Olivares et al. (2007); d'Ovidio et al. (2009) Lagrangian structures are identified using FSLE's. The maxima of the FSLE fields look very much like the maxima of FTLE fields and bear a striking resemblance to the stable and unstable manifolds of hyperbolic trajectories. However, it must be emphasized that FSLE's are a non-rigorous numerical technique and, despite the strong numerical evidence, there are no theorems relate the results of the calculations to Lagrangian transport barriers. Much like the case with FTLE's, this must be assessed "after the fact".

may be "close" to a barrier to transport in the sense that the flux across the curve may be small. This issue was carefully considered in Shadden et al. (2005). However, the extent to which LCS's are barriers to transport must be assessed after they are computed. The stable and unstable manifolds of finite time hyperbolic trajectories are a priori barriers to transport since they are computed as curves of fluid particle trajectories.

A possible misconception that has appeared in several places in the LCS literature is that the concept of invariant manifold is somehow either not well defined or inapplicable, or not easily interpretable for aperiodically time-dependent flows (Haller and Yuan, 2000; Haller, 2001a,b; Shadden et al., 2006; Lekien and Coulliette, 2007). In particular, this point has been emphasized in the finite time dynamical systems context. While the approach to Lagrangian transport based on finite-time stable and unstable manifolds of finite-time hyperbolic trajectories certainly requires more complex algorithms and computational techniques, the results, being trajectory based, are certainly unambiguous (in that sense). Towards this end we note that Mancho et al. (2008) use finite-time hyperbolic trajectories and their (finite-time) stable and unstable manifolds which are computed in a realistic velocity field obtained from an oceanographic model (DieCAST) to give the first Lagrangian characterization of a salinity front in the Mediterranean Sea and provide an explanation and characterization of the notion of "leakiness" of the front. Of course, the finite time issues mentioned above do require careful consideration in the context of specific applications. It is incorrect to think that the LCS approach has somehow "solved" this problem.

A broader issue here, which keeps recurring throughout the following discussion, concerns the problem of description of the Lagrangian structure of a time-dependent flow in a way which would allow for a meaningful finite-time Lagrangian transport analysis. It is well known that in order to establish the existence of, for example, a transport barrier (i.e. a flow-invariant, Lagrangian structure) in the non-autonomous case, one requires non-local (in time and space) information about the governing flow. As already pointed out, the finite-time notions discussed above may provide ambiguous diagnostics due to their potential sensitivity to the time-interval chosen for extracting the relevant information. Consequently, it seems crucial for the development of a general theory of finite-time transport in aperiodically time-dependent velocity fields to understand and properly describe transient flow phenomena. Undoubtedly, this task requires development of tools which would adequately capture the finite-time flow properties. The examples discussed in the next section highlight a number of important points regarding the techniques of invariant manifolds and FTLE fields:

(1) One can obtain a good agreement between the ridges of the FTLE fields (i.e. the LCS) and the finite-time sta-

ble/unstable manifolds of relevant hyperbolic trajectories in sufficiently "well-behaved" flows,

(2) Both approaches may provide non-unique results, particularly in flows undergoing transitions (discussed later), and their interpretation may require a subjective interpretation. The main drawback affecting the invariant manifold computations lies in the need for identification of the "most important" (or distinguished) hyperbolic trajectories used for "seeding" the finite-time stable and unstable manifolds. The main drawback affecting the FTLE technique stems from the fact that it is a function of trajectory separation which depends, in general, on the time interval chosen for assessment of such a measure. Consequently, in flows undergoing transitions it is often difficult to decide which time interval is most suitable for assessing the (non-local) flow structure. Moreover, there is no guarantee that the time evolution of the ridges of locally strongest separation is continuous in time.

3 Tests

In this section, based on a wide range of example flows, we analyse and compare the information about the Lagrangian flow structure obtained from the backward/forward FTLE maps, and the information obtained from computing the unstable and stable manifolds of relevant (finite-time) hyperbolic trajectories. The algorithms used for computing the hyperbolic trajectories and their manifolds were developed in MATLAB, based on the ideas described in Ide et al. (2002); Ju et al. (2003); Mancho et al. (2003, 2004). The FTLE computations are performed also in MATLAB using an implementation of methods described in Haller (2001a); Shadden et al. (2005, 2006, 2007). We also compare our results with the LCS MATLAB Kit v.2.3, developed in the Biological Propulsion Laboratory at Caltech, which is available online (see Dabiri (weblink)). In the case of the LCS MATLAB Kit, several minor modifications were introduced in the code in order to enable FTLE computations from analytically defined vector fields.

All the examples considered here are based on analytically defined velocity fields. While the resulting flows are certainly not sufficiently complex to be of importance in practical applications, they provide an easily reproducible testbed for our analysis.

3.1 1-D non-autonomous configuration

We consider first a 1-D, non-autonomous ODE which can be solved analytically, and which illustrates in the simplest possible setting a number of issues which are important in the following sections. Based on three related examples, we highlight potential difficulties when trying the uncover the structure of a non-autonomous flow using the finite-time
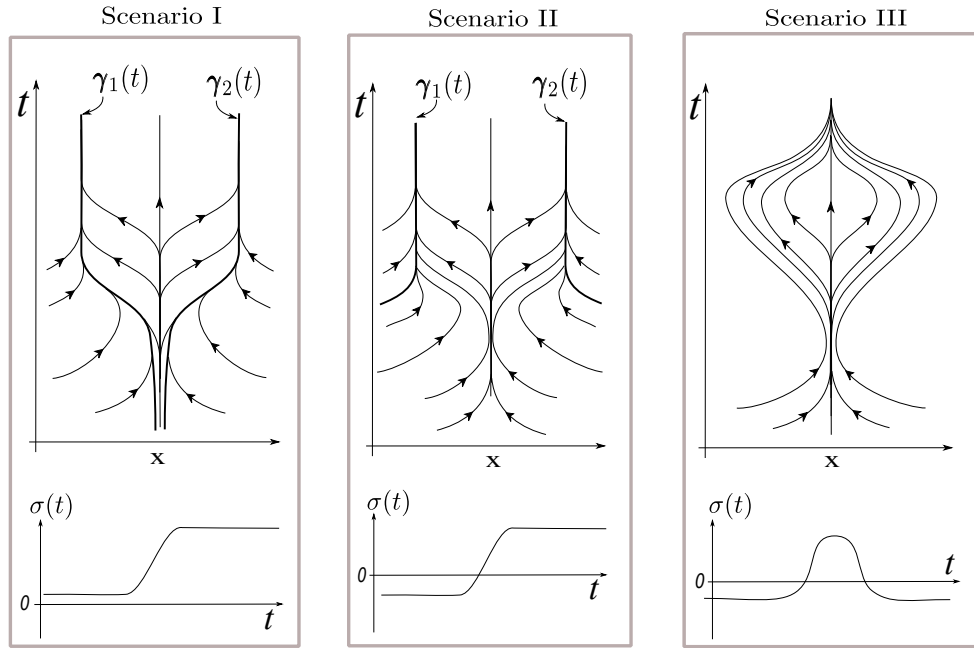
Fig. 1. Geometry of the 1-D flows (1) with the time dependence induced by $\sigma(t)$ characteristic of the three scenarios considered in Sect. 3.1. The trajectories $\gamma_1(t)$, $\gamma_2(t)$ are distinguished in the sense described in appropriate sections. Analysis of these flow structures using the FTLE technique are summarised in Figs. 2, 3, and 4.

Lyapunov exponents, or when trying to identify some "special" trajectories which play an important role in organising the global dynamics. Of course, in such a setting there are no non-trivial invariant manifolds in the (non-autonomous) flow. However, one can consider the 1-D geometry discussed below to represent some aspects of transverse dynamics in the neighbourhood of an invariant manifold in a higher-dimensional flow; in fact, we use this analogy in Sect. 3.3.6. Here, we are particularly interested in the properties of the FTLE maps and their behaviour during certain flow transitions characterised by changes of finite-time stability properties of some distinguished trajectories in the flow.

Consider a 1-D, non-autonomous dynamical system given by

$$\dot{x} = x\left(\sigma(t) - x^2\right), \quad x, t \in \mathbb{R}, \tag{1}$$

where $\sigma(t)$ is a prescribed function of time. In the autonomous configuration, with $\sigma=\text{const.}<0$, the trivial solution $x=0$, representing the only fixed point in the flow, attracts all trajectories as $t\to\infty$. When $\sigma=\text{const.}>0$, there are three fixed points in the flow: $x_1=0$, and $x_{2,3}=\pm\sqrt{\sigma}$. It can be easily checked by examining the linearisation of (1) about these points that x_1 is an unstable hyperbolic fixed point and $x_{2,3}$ are stable hyperbolic fixed points.

When $\partial\sigma/\partial t\neq 0$, it is more convenient to consider the resulting dynamics in the extended phase space, spanned by $\{\mathbf{e}_x, \mathbf{e}_t\}$, with coordinates (x, t); three distinct examples are shown in Fig. 1. We note here that (1) is, in fact, a Bernoulli equation with solutions given by the family

$$x(t; x_0, t_0)^2 = \cfrac{1}{\cfrac{1}{x_0^2}e^{-2\int_{t_0}^t \sigma(s)ds} + 2\int_{t_0}^t e^{-2\int_k^t \sigma(s)ds}dk}. \tag{2}$$

It can be easily verified using (2) that $x(t_0; x_0, t_0)=x_0$. For any trajectory $x(t; x_0, t_0)$, given by (2), we can consider a perturbation, $x(t; x_0+\delta_0, t_0)$, with $\delta_0\ll 1$, so that the growth of the perturbation after time T is given by

$$\delta(T, \delta_0, x_0, t_0) = |x(t_0+T; x_0, t_0) - x(t_0+T; x_0+\delta_0, t_0)|$$

$$= \left|\frac{\partial x(t_0+T; s, t_0)}{\partial s}\Big|_{s=x_0}\delta_0 + \mathcal{O}(\delta_0^2)\right|. \tag{3}$$

Thus, since the solutions (2) are continuous, the growth of an infinitesimal perturbation introduced at (x_0, t_0) after time T is given by

$$\Delta(T, x_0, t_0) = \lim_{\delta_0\to 0} \frac{\delta(T, \delta_0, t_0)}{\delta_0} \tag{4}$$

$$= \frac{e^{-2\int_{t_0}^{t_0+T}\sigma(s)ds}}{\left|e^{-2\int_{t_0}^{t_0+T}\sigma(s)ds} + 2x_0^2\int_{t_0}^{t_0+T}e^{-2\int_k^{t_0+T}\sigma(s)ds}dk\right|^{3/2}}.$$
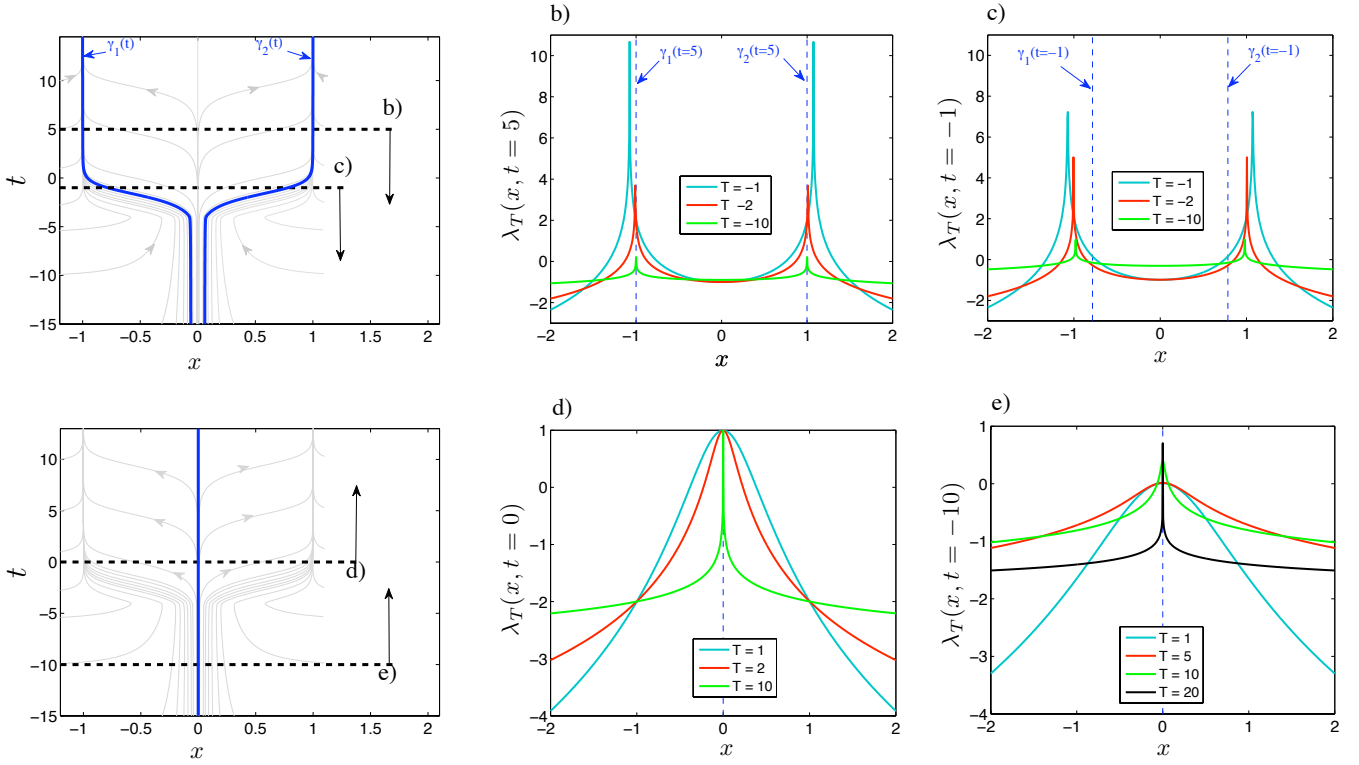
Fig. 2. (b–e) 1-D FTLE fields, $\lambda_T(x, t_0)$, for the flow (1) with $\sigma(t)$ given by (17) which is characteristic of Scenario I discussed in Sect. 3.1. The finite time Lyapunov exponents, λ_T, are computed over different time intervals of length T. In this configuration, there are three "distinguished" trajectories in the flow, $\gamma_{1,2}(t)$, (see (11)), and $x=0$, which play an important role in organising the dynamics (blue curves; left column). (b–c) Backward FTLE field computed, using (4) and (5), at (b) $t=5$ and (c) $t=-1$ with different values of the integration parameter T. Note that the maxima of the FTLE fields (i.e. the LCS) vary with T, and that they do not coincide with the location of $\gamma_{1,2}(t=-1)$ during the transition phase, e.g. (c), regardless of the value of T. See text for a discussion. (d–e) Forward FTLE field computed for the same flow at (d) $t=0$ and (e) $t=-10$ with different values of the parameter T.

We note further that (4) is related to the 1-D finite time Lyapunov exponent $\lambda_T(x_0, t_0)$ at time t_0 via

$$\lambda_T(x_0, t_0) = \frac{1}{|T|} \ln \Delta(T, x_0, t_0), \qquad (5)$$

which is computed over the time interval T, (see the Appendix A for a more general formulation).

Note that even if solutions satisfying a given system are only known numerically, an estimate on the separation rate of trajectories which were initially infinitesimally close can be obtained via finite differences. Therefore, λ_T can be estimated for any flow defined by sufficiently smooth velocity field on some time interval I. Consequently, the map

$$\mathbb{R} \ni x \mapsto \lambda_T(x, t_0) \in \mathbb{R}, \quad t_0 + T \in I \subset \mathbb{R}, \qquad (6)$$

can be used, in principle, as a straightforward diagnostic tool for uncovering time-dependent flow structures characterised by locally strongest separation of nearby trajectories. Note however, that at any time t_0 during the flow evolution one can construct the whole family of FTLE fields $\{\lambda_T(x, t_0)\}_{T+t_0 \in I}$ which generally results in a non-uniqueness of the computed

diagnostic. The ambiguities associated with choosing the "right" FTLE map from the family $\{\lambda_T(x, t_0)\}_{T+t_0 \in I}$ which "best" describes the flow structure at a given time are especially evident in analysis of flows displaying transient phenomena. We recall that this problem is not restricted to the FTLE method. In particular the techniques, mentioned in Sect. 2, based on identification of the so called "distinguished hyperbolic trajectories" and their invariant stable and unstable manifolds suffer from similar limitations in the case of flows defined on a finite time interval. We analyse these issues further below based on three different scenarios of evolution of the 1-D flow (1), characterised by different types of time dependence induced by the form of $\sigma(t)$ (see Fig. 1). Clearly, the dimensionality of the problem does not allow for existence of any non-trivial invariant manifold of a hyperbolic trajectory. Nevertheless, the discussed examples serve to highlight some important consequences of flow transitions (specified below) on the computed FTLE fields and their relationship to some (possibly non-unique) "special" trajectories in the space of solutions of (1). Moreover, we will show that the non-uniqueness of the FTLE diagnostic may lead to

detection of "ghosts" or "premonitions" of flow structures associated with the future, or past, stability properties of such "special" trajectories. We will later return to these examples in Sect. 3.3.1 in the context of locally transverse dynamics in a neighbourhood of a stable or unstable manifold of a hyperbolic trajectory in the 2-D non-autonomous case.

Scenario I: $0 < \sigma(t) < \infty$

With the above constraints imposed on $\sigma(t)$ (see Fig. 1), the trivial solution, $x(t)=0$, of (1) is (finite-time) unstable on any time interval $I=[t_a, t_b] \in I\!R$ in the sense that for each nonempty, simply-connected and bounded set $\tilde{x}_I=(0, x^*) \subset I\!R$, $0 < |x^*| < \infty$, there exists a trajectory, $x(t; x_0, t_0)$, with $x_0 \in \tilde{x}_I$, $t_0 \in I$, such that

$$\frac{\mathrm{d}}{\mathrm{d}t} |x(t; x_0, t_0)| > 0, \quad \forall t \in I. \tag{7}$$

A more general definition of instability of a trajectory in a non-autonomous dynamical system, which we do not require here, can be found, for example, in Langa et al. (2006). It can be easily verified that (7) is satisfied on $x(t)=0$ over any time interval $I \subset I\!R$, by noticing that

$$\frac{\mathrm{d}}{\mathrm{d}t} \left(\frac{1}{x(t; x_0, t_0)^2} \right) = \frac{2}{x_0^2} \left(-\sigma(t) e^{-2\int_{t_0}^t \sigma(t)\mathrm{d}s} \right. \tag{8}$$

$$\left. -2\sigma(t) x_0^2 \int_{t_0}^t e^{-2\int_k^t \sigma(s)\mathrm{d}s} \mathrm{d}k + x_0^2 \right), \tag{9}$$

which implies that (7) is satisfied at least for

$$x_0^2 < \frac{\sigma_{\min} e^{-2\sigma_{\min}(t_b - t_a)}}{1 - e^{-2\sigma_{\max}(t_b - t_a)}(e^{2\sigma_{\min}(t_b - t_a)} - 1)}. \tag{10}$$

We note further that there are two 'distinguished' trajectories in the space of solutions of (1) given by

$$\gamma_{1,2}(t)^2 = \frac{1}{2\int_{-\infty}^t e^{-2\int_k^t \sigma(s)\mathrm{d}s} \mathrm{d}k}, \tag{11}$$

which have the property that any trajectory of (1) $x(t; x_0, t_0)$, $x_0 < 0$ is "attracted" (in the sense we specify below) towards $\gamma_1(t)$ and any trajectory $x(t; x_0, t_0)$, $x_0 > 0$ is 'attracted' towards $\gamma_2(t)$. There are two different notions of attraction which we can utilise here. If we rewrite (2) as

$$x(t; x_0, t_0)^2 = \frac{1}{\frac{1}{x_0^2} e^{-2\int_{t_0}^t \sigma(t)\mathrm{d}s} + \frac{1}{\gamma(t)^2} - 2\int_{-\infty}^{t_0} e^{-2\int_k^t \sigma(s)\mathrm{d}s} \mathrm{d}k}, \tag{12}$$

it can be seen that the following are true (when $0 < \sigma(t) < \infty$)

$$\lim_{t \to \infty} \left(x(t; x_0, t_0) - \gamma_1(t) \right) = 0, \quad \forall x_0 < 0, t_0 \in I\!R, \tag{13}$$

$$\lim_{t \to \infty} \left(x(t; x_0, t_0) - \gamma_2(t) \right) = 0, \quad \forall x_0 > 0, t_0 \in I\!R, \tag{14}$$

and

$$\lim_{t_0 \to -\infty} \left(x(t; x_0, t_0)^2 - \gamma_1(t)^2 \right) = 0, \quad \forall x_0 < 0, t \in I\!R, \tag{15}$$

$$\lim_{t_0 \to -\infty} \left(x(t; x_0, t_0)^2 - \gamma_2(t)^2 \right) = 0, \quad \forall x_0 > 0, t \in I\!R. \tag{16}$$

Since we intend to minimise the amount of mathematical formalism here, we just remark that the property (13) implies that $\gamma_1(t)$ is *forwards attracting* (and *Lyapunov stable*) within $x_0 \in (-\infty, 0)$ and (15) implies that it is *pullback attracting* within $x_0 \in (-\infty, 0)$. Similarly, $\gamma_2(t)$ is both forwards and pullback attracting within $x_0 \in (0, \infty)$. A more formal introduction to the stability and bifurcation phenomena in non-autonomous dynamical systems can be found in Langa et al. (2006, 2002); Kloeden and Siegmund (2005); Duc and Siegmund (2008); Sell (1967, 1971). Pullback convergence is useful in constructing limiting sets, such as the distinguished trajectories in our 1-D toy example, provided that the flow is defined on the negative half-line $(-\infty, t^*]$, $t^* > -\infty$. Otherwise, we cannot uniquely define a distinguished trajectory. We will see in the next example that these two notions are not necessarily equivalent in the non-autonomous case.

We can now examine the 1-D FTLE fields, $\lambda_T(x, t_0)$, associated with scenario I which are obtained from (5) and (4) for different lengths of the integration time interval T. The results shown in Fig. 2 were computed for a sigmoidal function

$$\sigma(t) = \frac{1}{\pi} (\mathrm{atan}(10(t+4)) + \pi/2 + 0.01), \tag{17}$$

so that the flow (1) is asymptotically autonomous.

The top-row insets of Fig. 2 focus on detection of attracting structures in the (extended) phase space of the flow (1). Since such structures should be characterised by separation of trajectories in backward time, we compute a number of the backward FTLE fields at two different times $t=5$ (b) and $t=-1$ (c). The geometry of the two attracting distinguished trajectories $\gamma_{1,2}(t)$ is marked by the blue curves. Note that the maxima of the FTLE fields (i.e. the LCS) vary with T, and that they do not coincide with the location of $\gamma_{1,2}(t=-1)$ during the transition phase, e.g. (c), regardless of the value of T. The maxima of the forward FTLE fields, computed for the same flow at (d) $t=0$ and (e) $t=-10$, are all located at the trivial solution $x(t)=0$ which is unstable. However, during the flow phase when the unstable trivial solution is "sandwiched" between the two attracting "distinguished" solutions $\gamma_{1,2}$, the FTLE field has to be computed over sufficiently long time intervals in order to reveal a positive maximum (i.e. exponential growth of the infinitesimal perturbation to $x(t)=0$ over the considered time interval).
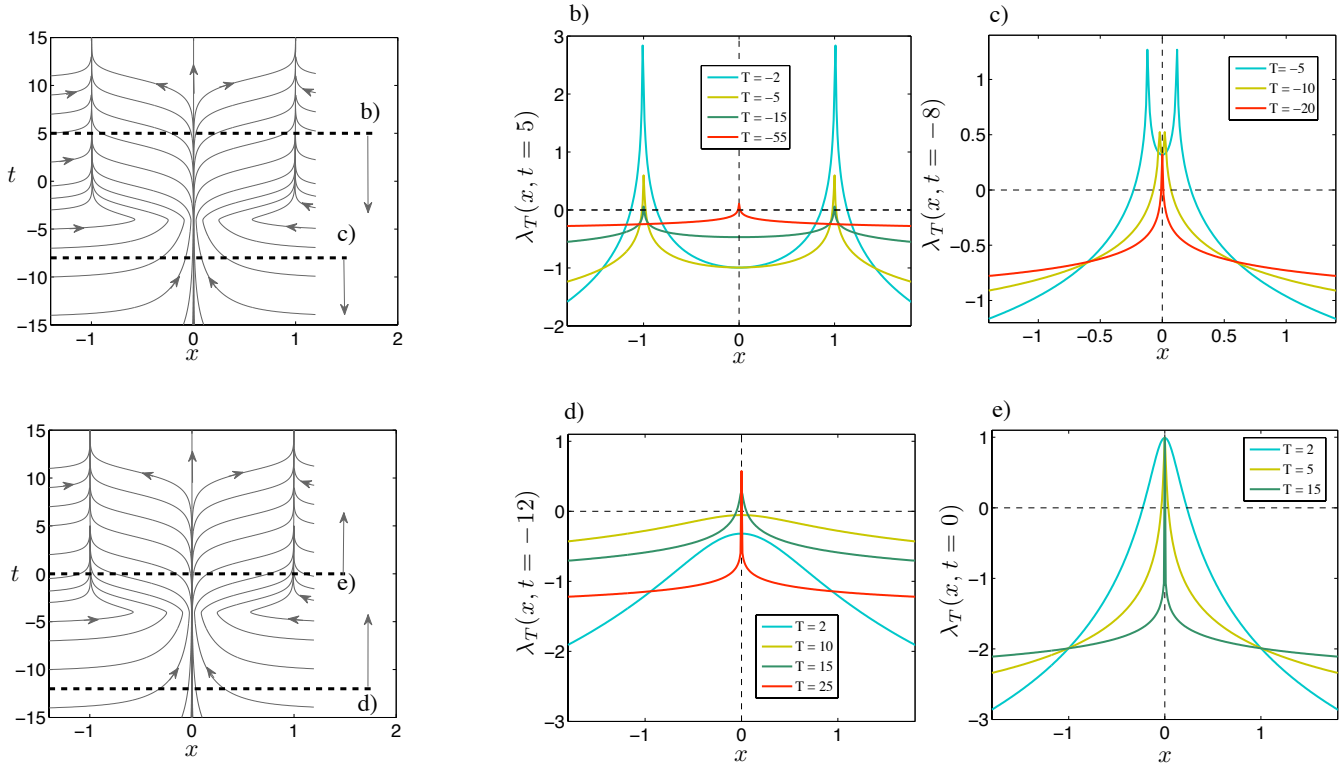
Fig. 3. **(b–e)** 1-D FTLE fields, $\lambda_T(x, t_0)$, for the flow (1) with $\sigma(t)$ given by (21) which is characteristic of Scenario II discussed in Sect. 3.1; the fields, λ_T, are computed over different time intervals of length T. **(b–c)** Backward FTLE field computed, using (4) and (5), at (b) $t=5$ and (c) $t=-8$ with different values of the integration parameter T. In this configuration there distinguished trajectories $\gamma_{1,2}(t)$ (cf. 11) dominate the flow structure after the transition when the trivial solution becomes unstable. Note that for sufficiently large values of the integration parameter T the maxima of the FTLE fields detect "ghosts" of the past stability of the trivial solution and not the situation at the time of computation t. See text for a discussion. **(d–e)** Forward FTLE field computed for the same flow at (d) $t=-12$ and (e) $t=0$ with different values of the parameter T. The trivial solution $x=0$ is globally attracting in the sense of (18) on any time interval $I = \left(-\infty, t_-^*\right]$, $t_-^* < t^*$ where $t^* \approx -4.105$. Note that, when computed over sufficiently long time intervals, the FTLE fields detect "premonitions" of the future (finite-time) stability properties of the trivial solution, cf. (d), which is repelling (in this case) on any time interval contained in $I = (-4.105, \infty)$.

Scenario II: $\lim\limits_{t \to -\infty} \sigma(t) < 0$, $\sigma(t^*) = 0$, and $\mathrm{d}\sigma/\mathrm{d}t > 0$

In this situation the trivial solution of (1), $x(t)=0$, is stable (in the pullback sense) on any time interval $I=(-\infty, t_-^*]$, $t_-^* < t^*$, i.e.,

$$\lim_{t_0 \to -\infty} x(t; x_0, t_0) = 0, \quad \forall \; t \in I, \tag{18}$$

and unstable, in the sense (7), on any time interval contained in $I = (t^*, \infty)$. Note that the trajectories $\gamma_{1,2}(t)$ (11), which are still solutions of (1), are now only asymptotically attracting, i.e.,

$$\lim_{t \to \infty} \left(x(t; x_0, t_0) - \gamma_1(t) \right) = 0, \quad \forall \, x_0 < 0, t_0 \in \mathbb{R}, \tag{19}$$

$$\lim_{t \to \infty} \left(x(t; x_0, t_0) - \gamma_2(t) \right) = 0, \quad \forall \, x_0 > 0, t_0 \in \mathbb{R}, \tag{20}$$

but they are not asymptotically pullback attracting. We will loosely refer to t^* as the transition time, since it corresponds to the boundary of the pullback stability of the trivial solution.

In Fig. 3 we analyse the phase-space geometry of the flow (1) with $\sigma(t)$ given by

$$\sigma(t) = \frac{1}{\pi/2 + 0.8}\left(\mathrm{atan}(10(t+4)) + 0.8 \right), \tag{21}$$

which satisfies the constraints characteristic of this scenario and changes sign at $t^* \approx -4.105$. Moreover, such a choice introduces an additional simplification to the problem, making it asymptotically autonomous. This configuration makes it easier to observe the emergence of an "attracting" structure developing around the trajectories $\gamma_{1,2}(t)$ after the transition (see Fig. 3). The FTLE fields, λ_T, shown in Fig. 3b–e are computed using (4) and (5) at four different times and over different time intervals of length T. The examples of the backward FTLE fields, computed at (b) $t=5$ and (c) $t=-8$ highlight some typical characteristics of this technique when applied to flows with transient phenomena. When computed at times after the transition, as in (b), over sufficiently short time interval lengths T, the maxima of the FTLE fields coincide well with the location of the distinguished trajectories
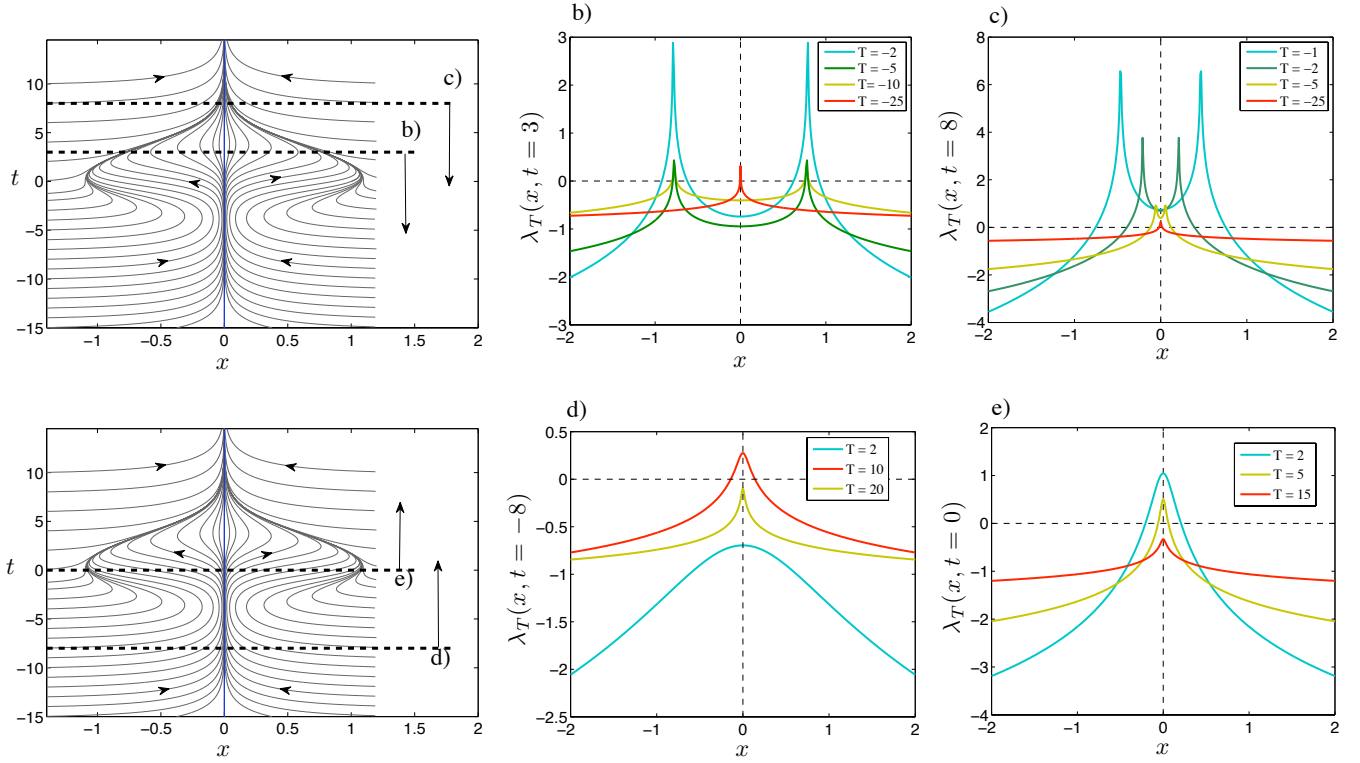
Fig. 4. (b–e) 1-D FTLE fields, $\lambda_T(x, t_0)$, for the flow (1) with $\sigma(t)$ given by (24) which is characteristic of Scenario III discussed in Sect. 3.1. The trivial solution, $x=0$, is asymptotically attracting on the time interval $I=\mathbb{R}$ and globally pullback stable, see (22), on any time interval $I = (-\infty, t_-^*]$, $t_-^*<t^*$ (in this case $t^*\approx-3.83$; see text). The trivial solution is unstable on any time interval contained (in this case) within $I=[-3.83, 3.83]$. (b–c) Backward FTLE field computed, using (4) and (5), at (b) $t=3$ and (c) $t=8$ with different values of the integration parameter T. Note that the maxima of the FTLE fields (i.e. the LCS) vary with T and, for sufficiently large T, the FTLE fields detect a 'ghost' of the past attracting phase of the trivial solution $x=0$, red curves in (b–c). See text for a discussion. (d–e) Forward FTLE field computed for the same flow at (d) $t=-8$ and (e) $t=0$ with different values of the parameter T. Note that at $t=-8$ (d), when $x=0$ is attracting and globally pullback attracting, the FTLE field computed over sufficiently long interval T detects a "premonition" of the future unstable phase of the trivial solution.

(dashed blue lines in Fig. 3b). Note, however, that for sufficiently large values of T the maxima of the FTLE fields detect "ghosts" (red) of the past stability of the trivial solution and not the situation at the time of computation t. It is worth remembering here that while the geometry of the flow trajectories and the transition time is known in the considered example, it may not be at all obvious what length of the time interval one should choose when computing FTLE fields for a realistic, higher-dimensional geophysical flow. A similar problem might occur when trying to identify structures characterised by trajectory separation in forward time via the computation of forward FTLE fields. We show examples of such computations for the same flow in Fig. 3d and e which are computed at d $t=-12$ and e $t=0$ with different values of the parameter T. As already mentioned above, the trivial solution $x=0$ is asymptotically pullback attracting at any t contained in $I=(-\infty, t_-^*]$, $t_-^*<t^*\approx-4.105$. Therefore, no trajectory separates, in the sense (7), from the trivial solution on I. The FTLE fields computed in Fig. 3d correspond to such a situation. However, if one computes the forward FTLE fields

at $t=-12$ for sufficiently large T a sharp positive maximum appears which might be interpreted as a "premonition" of the future (finite-time) stability properties of the trivial solution after the transition.

Scenario III: $\sigma(t)>0$ for $t\in[t^*, t^{**}]$, and $\sigma(t)<0 \ \forall \ t\in(-\infty, t^*] \cup [t^{**}, \infty)$

In this configuration the trivial solution is the only "distinguished" one. It is globally asymptotically pullback stable on any time interval $I = (-\infty, t_-^*]$, $t_-^*<t^*$, i.e.,

$$\lim_{t_0 \to -\infty} x(t; x_0, t_0) = 0, \quad \forall \ t \in I, x_0 \in \mathbb{R}, \quad (22)$$

and is globally asymptotically stable on any time interval $I=[t_+^{**}, \infty)$, $t_+^{**}>t^{**}$, i.e.,

$$\lim_{t \to \infty} x(t; x_0, t_0) = 0, \quad \forall \ t_0 \in I, x_0 \in \mathbb{R}. \quad (23)$$

However, it can be easily verified by examining (2) that $x(t)=0$ is unstable, in the sense of condition (7), on any time interval contained in $I=[t^*, t^{**}]$.

In order to illustrate the typical properties of the FTLE field in such a case we choose the time dependence in the following form

$$\sigma(t) = 2\left(e^{-t^2/16} - 0.4\right),\tag{24}$$

so that $t^* \approx -3.83$ and $t^{**} \approx 3.83$. In Fig. 4 we examine the backward (b, c) and forward (d, e) FTLE fields for this flow configuration, which are computed for different lengths, T, of the time test interval. The trivial solution is unstable on any time interval contained (in this case) within $I = [-3.83, 3.83]$. The backward FTLE fields, $\lambda_T(x, t_0)$, computed at $t=3$ show a similar behaviour as in Fig. 3b except that the magnitude of "ghost" maximum (red), indicating the past attracting properties of the trivial solution, is similar to those computed for $T=-5$ and $T=-10$. This simple example indicates the possible problems with interpretation of the families of FTLE fields at time t, $\{\lambda_T(x, t)\}_{T+t \in I}$, and the right choice of the time integration interval best describing the flow structure at the given time t. The forward FTLE computations reveal similar ambiguities when trying to detect structures characterised by separating trajectories in forward time. The FTLE field computed at $t=-8$ (d) with $T=2$ indicates correctly the lack of trajectory separation points. The profile of $\lambda_2(x, t=-8)$ is, however, rather broad and one might be tempted to increase the integration time interval T in order to obtain a more localised shape. If one then computes the forward FTLE field at $t=-8$ with $T=10$, the $\lambda_{10}(x, t=-8)$ reveals a positive maximum at $x=0$ (red curve in (d)) which indicates that the perturbations of the trivial solution will eventually separate with a positive λ_T. It is important to understand here that this is not an erroneous result. Indeed, we know that the trivial solution is unstable on the time interval $I = [-3.83, 3.83]$ and if one follows trajectories from $t=-8$ to a time contained within this interval, this is certainly what is going to happen. Moreover, if we follow such trajectories to times beyond I, the positive maximum disappears again (e.g. $\lambda_{20}(x, t=-8)$ in Fig. 4d). An important question arises in connection to this fact: Which FTLE fields from the T-parametrised family, $\{\lambda_T(x, t)\}_{T+t \in I}$, best describes the flow structure at t? As we showed above, it is not always the field with the 'sharpest' maxima.

3.2 2-D, time-dependent flows

In the remainder of this paper we consider a number of analytically defined, time-dependent 2-D flows. In each case we analyse and discuss the relationship between the stable and unstable manifolds of relevant hyperbolic trajectories and the LCS identified from the FTLE maps.

We note here that the characteristics of a "relevant", or distinguished, hyperbolic trajectory (DHT) in a finite-time setting are currently not well defined. We attempt a working definition of a DHT in the Appendix A which is "tied" to the initial finite-time hyperbolic guess via the iterative algorithm

described in Ide et al. (2002); Ju et al. (2003). The choice of the initial guess is often subjective and, consequently, a trajectory branded the DHT depends largely on applications. Determination of a general set of characteristics of a finite-time hyperbolic trajectory which would make it "more important" than others in the time-aperiodic is an open problem.

3.2.1 Two examples of dynamical systems where the Lyapunov exponents of every trajectory are equal

In this section we point out two situations where the Lyapunov exponents of *every* trajectory are equal. Interestingly, the two flows are, in some sense, almost exact *opposites* in terms of the complexity of the dynamics that they exhibit. The first example is the velocity field due to a linear, time-dependent straining flow defined on the plane. In this case we can derive the Lyapunov exponents analytically, and thus show explicitly that they do not depend of the initial condition of the trajectory (i.e., the Lyapunov exponents are identical for all trajectories). In this case the FTLE field reveals no LCS's, for any time over which the FTLE field is defined. The second example is the Arnold cat map. It is a linear map defined on a closed Riemannian phase manifold with doubly-periodic boundary conditions (i.e. the torus). The Lyapunov exponents for every trajectory can be again computed explicitly, and linearity of the map implies that all exponents are equal. Hence, also in the case of the Arnold cat map the FTLE fields reveal no LCS's. Contrasting these two examples is interesting. Neither example has LCS's as diagnosed by the FTLE field although the phase space of each does have hyperbolic trajectories with stable and unstable manifolds (the notion of a DHT becomes degenerate though). The considered velocity field given by the linear, time-dependent straining flow has "simple" trajectories, while the trajectories exhibited by the Arnold cat map are "extremely" chaotic. We will now describe each of these examples in more detail, and in the process provide more background and justification for these statements.

Linear, time-dependent strain

We consider here the simplest class of incompressible 2-D flows, defined for all $t \in I\!R$, which possess a hyperbolic trajectory at the origin. The flows are trivial, time-dependent extensions of the linear steady strain and the corresponding non-autonomous dynamical system is given by

$$\begin{bmatrix} \dot{x} \\ \dot{y} \end{bmatrix} = \mathcal{A}(t) \cdot \begin{bmatrix} -1 & 0 \\ 0 & 1 \end{bmatrix} \begin{bmatrix} x \\ y \end{bmatrix},\tag{25}$$

where $\mathcal{A}(t)$ is a time-dependent strain amplitude. When $\mathcal{A} = \text{const.}$, the point $(x, y) = (0, 0)$ is a hyperbolic saddle with a 1-D stable and unstable manifolds aligned with, respectively, $\mathbf{e}_x$ and $\mathbf{e}_y$. When $d\mathcal{A}/dt \neq 0$ and $\mathcal{A}(t) > 0$, it can be

easily verified that $\boldsymbol{\gamma}(t)=0$ is a trajectory of (25) in the extended phase space (x, y, t). Moreover, $\boldsymbol{\gamma}(t)$ is hyperbolic (and finite-time hyperbolic on any $I \subset I\!R$) and it has a 2-D stable and unstable manifolds spanned by, respectively, $\{\mathbf{e}_x, \mathbf{e}_t\}$ and $\{\mathbf{e}_y, \mathbf{e}_t\}$ in the extended phase space. The fundamental solution matrix, $\mathbf{X}(t, t_0)$, of (25) is given by

$$\mathbf{X}(t, t_0) = \begin{bmatrix} -e^{\tilde{\mathcal{A}}(t,t_0)} & 0 \\ 0 & e^{\tilde{\mathcal{A}}(t,t_0)} \end{bmatrix}, \tag{26}$$

where $\tilde{\mathcal{A}}(t, t_0) = \int_{t_0}^{t} \mathcal{A}(\tau) \mathrm{d}\tau$.

Note that the finite-time Lyapunov exponents, $\lambda_{1,2}$ (cf. Definition A.1), for the flow associated with (26) are given by

$$\lambda_T^{1,2}(x, y, t_0) = \pm \frac{\tilde{\mathcal{A}}(t_0 + T, t_0)}{2|T|}, \tag{27}$$

and are independent of the spatial coordinates. Consequently, the FTLE field given by

$$\lambda_T(x, y, t_0) = \max\left[\lambda_T^1(x, y, t_0), \lambda_T^2(x, y, t_0)\right],$$

is spatially homogeneous and does not reveal any structure despite the fact that the stable and unstable manifolds of the hyperbolic trajectory $\boldsymbol{\gamma}(t)=0$ are well defined. In this simple flow it is clear that the hyperbolic trajectory at the origin plays the dominant role in organising the flow dynamics. Moreover, since it trivially satisfies the requirements of Definition A.5, it represents a Distinguished Hyperbolic Trajectory of (25) in the considered frame of reference. Note, however, that the notion of a DHT is frame dependent (as opposed to a general hyperbolic trajectory). In particular, any trajectory $\boldsymbol{\gamma}(t)$ of (25) can become 'distinguished' by means of the transformation $\boldsymbol{x} = \boldsymbol{y} + \boldsymbol{\gamma}(t)$.

3.3 The Arnold cat map

The Arnold cat map, defined on the torus, is given by

$$p_{n+1} = p_n + q_n \quad (\text{mod } 1), \tag{28}$$
$$q_{n+1} = p_n + 2q_n \quad (\text{mod } 1). \tag{29}$$

This dynamical system has a number of remarkable properties that are amenable to explicit analysis resulting from the linearity of the map and the doubly periodic boundary conditions. In particular, *every* trajectory can be shown to be hyperbolic and explicit expressions for its stable and unstable manifolds can be computed (e.g. Arnold and Avez, 1968). The map can be shown to be ergodic, mixing, and to have the Bernoulli property, and each of these properties is present on the *entire* domain of the map. The proofs of these results are "well-known", but are often difficult to track down in the literature. Sturman et al. (2006) contains proofs, and also a guide to the original literature. However, for our purposes here we are only concerned with the Lyapunov exponents of

trajectories of the cat map. These can be explicitly computed from the map and are found to be

$$\Lambda_{1,2} = \pm \ln(3 + \sqrt{5})/2, \tag{30}$$

and they are the same for *every* trajectory. Therefore, we have a situation where, in some sense, the map is the "most chaotic possible" (i.e., it has the Bernoulli property) on its entire domain and every trajectory is hyperbolic (having one Lyapunov exponent with modulus greater than one and one Lyapunov exponent with modulus less than one). Nevertheless, since the Lyapunov exponents of every trajectory are identical the FTLE fields are constant, and thus they reveal no LCS's[5]. Similarly to the previously discussed case, the cat map is linear and the trivial trajectory located at the origin can be regarded as distinguished. The notion of a DHT is again degenerate (as in the previous linear case), since any trajectory $\boldsymbol{\gamma}_n$ of (28) can become distinguished upon an appropriate linear transformation $(p_n, q_n) = (k_n, l_n) + (\gamma_n^p, \gamma_n^q)$.

Summary

We have shown two examples where the Lyapunov exponents can be explicitly computed and shown to be identical for *every* trajectory. Dynamically, these two examples could not be more different. The flow defined by a linear, time-dependent strain on the plain does not possess complex dynamics, even though every trajectory in this flow has a positive Lyapunov exponent. The Arnold cat map defined on the torus is extremely chaotic on its entire domain (and every trajectory also has a positive Lyapunov exponent). Clearly, complexity of trajectories is not sufficient for the FTLE field to reveal "structure". Rather, spatial heterogeneity is required, and this does not occur for linear flows, or flows exhibiting "uniform" chaos, in the sense of identical Lyapunov exponents for (almost) every trajectory.

3.3.1 Strain-vortex-strain transition

We consider here an example which is designed to illustrate the geometry and fate of finite-time stable and unstable manifolds of a finite-time hyperbolic trajectory during a flow transition associated with a loss and subsequent re-gain of finite-time hyperbolicity by this trajectory. We show here what kind of information about transport properties of such a flow can be obtained by analysing this transition using, respectively, the invariant manifold approach and the FTLE approach.

---

[5]This paper is concerned with an understanding of the role of manifolds and LCSs in fluid transport. Consequently we have been dealing with flows that are defined for continuous time. The Arnold cat map is a discrete time dynamical system. We have chosen it to illustrate a specific point because of its familiarity, and the ease for which its various properties can be explicitly computed. Nevertheless, the Arnold cat map dynamics can be realized in continuous time flows; see Bowen (1973); Bowen and Ruelle (1975); Pollicott (1987) for details.
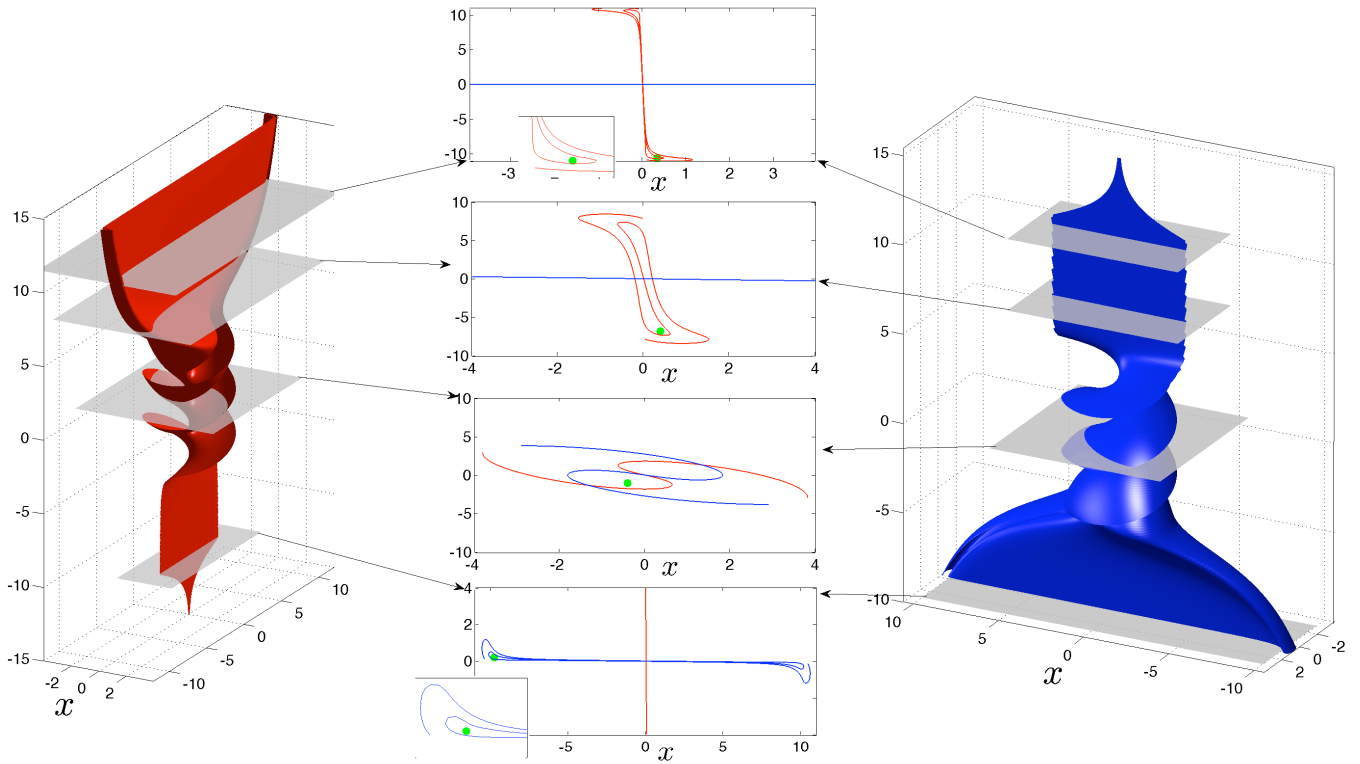
Fig. 5. Geometry of two material surfaces in the extended space (x, y, t) approximating the unstable manifold (red) and the stable manifold (blue) of the trivial solution, $\boldsymbol{x}(t)=0$, of the system (31). For the chosen form of the amplitudes $\mathcal{A}_S$, $\mathcal{A}_V$ (cf. 46), the trivial solution is (infinite-time) hyperbolic on $I=R$ but finite-time hyperbolic only on $I=(-\infty, -4.47]$ and $I=(4.47, \infty]$ (see Sect. 3.3.1 for a discussion of finite-time hyperbolicity on an interval).

Consider the following 2-D, non-autonomous dynamical system

$$\dot{\boldsymbol{x}} = \left(\mathcal{A}_S(t)\, \boldsymbol{S}(\boldsymbol{x}) + \mathcal{A}_V(t)\, \boldsymbol{\mathcal{V}}(\boldsymbol{x}) \right) e^{-\frac{\|\boldsymbol{x}\|^2}{\delta^2}}, \quad \boldsymbol{x}\in\mathbb{R}^2,\, t\in\mathbb{R}, \quad (31)$$

where δ is a constant and the terms in the brackets represent a linear superposition (with time-dependent coefficients $\mathcal{A}_S(t)$ and $\mathcal{A}_V(t)$) of a straining field given by

$$\boldsymbol{S}(\boldsymbol{x}) = \begin{bmatrix} -x \\ y \end{bmatrix}, \qquad (32)$$

and of a vector field with circular streamlines given by

$$\boldsymbol{\mathcal{V}}(\boldsymbol{x}) = \begin{bmatrix} -y \\ x \end{bmatrix}. \qquad (33)$$

Before proceeding to a discussion of concrete examples derived from (31), it is instructive to analyse the finite-time stability properties of the trivial solution, $\boldsymbol{x}(t)=0$. Some specific examples are discussed in the following subsection.

Stability of the trivial solution, $\boldsymbol{x}(t)=0$

The linearisation of (31) about $\boldsymbol{x}(t)=0$ is given by

$$\dot{\boldsymbol{x}} = \hat{\mathbf{A}}(t)\boldsymbol{x} = \begin{bmatrix} -\mathcal{A}_S(t) & -\mathcal{A}_V(t) \\ \mathcal{A}_V(t) & \mathcal{A}_S(t) \end{bmatrix} \begin{bmatrix} x \\ y \end{bmatrix}. \qquad (34)$$

Consider first a class of flows generated by (34) for which the coefficients, $\mathcal{A}_S(t)$, $\mathcal{A}_V(t)>0$, satisfy

$$\left. \begin{array}{l} \mathcal{A}_V(t) > \mathcal{A}_S(t), \quad \text{for}\ \ t \in [t^*, t^{**}],\ \ -\infty < t^* < t^{**} < \infty, \\ \mathcal{A}_V(t) < \mathcal{A}_S(t), \quad \text{for}\ \ t \in (\infty, t^*) \cup (t^{**}, \infty). \end{array} \right\} \quad (35)$$

In such a case, it can be shown that the trivial solution, $\boldsymbol{x}(t)=0$, $t\in\mathbb{R}$, has codimension-one unstable and stable manifolds[6] in the extended phase space $(\boldsymbol{x}, t)$. Consequently, it can be shown that the trivial solution is hyperbolic on $\mathbb{R}$

---

[6]We skip the proof here but the existence of the "infinite-time" stable and unstable manifolds of the trivial solution of (34) can be shown by using techniques analogous to those used in (Langa et al., 2002, cf. Sect. 4). The main difference here is the presence of the off-diagonal terms in $\hat{\mathbf{A}}$ (cf. 34) which invalidates the contraction mapping argument when $\mathcal{A}_V(t)>\mathcal{A}_S(t)$. However, one can show the existence of a codimension-one manifold of trajectories

in the classical, infinite-time sense. However, if we consider the finite-time stability properties of the trivial solution, some interesting issues arise. We note here that the theory of finite-time stability of non-autonomous dynamical systems is still an area of active research and, as a consequence, there exist, for example, at least two different ways of defining what is meant by *finite-time hyperbolicity* (cf. Definitions A.4 and A.11 in the Appendix A). Although, it is currently not clear if these two notions are equivalent, or which one is more suitable for a given application, we show below that they predict essentially the same stability changes in the configuration considered here.

As discussed briefly in the Appendix A, one approach to characterising finite-time stability properties of a given trajectory is via the notion of *finite-time exponential dichotomy* which is associated with a system linearised about this trajectory. While this notion of finite-time hyperbolicity seems more general and is very useful in more abstract considerations, it is often difficult to verify in practice. Nevertheless, provided that $\mathcal{A}_V(t)$ and $\mathcal{A}_S(t)$ are bounded and sufficiently slowly varying on a time interval I, it can be shown (Coppel, 1978, Propositions 1–2, p. 50, 52) that the trivial solution is finite-time hyperbolic on any time interval $J \subset I$ within which the real parts of the eigenvalues of the matrix $\hat{\mathbf{A}}(t)$ in (34) are non-zero and have opposite signs. Conversely, it can also be shown (Coppel, 1978, Proposition 2, p. 54) that a trajectory cannot be finite-time hyperbolic if the eigenvalues of $\hat{\mathbf{A}}(t)$ are imaginary over a sufficiently long time interval (the slower the variation of the coefficient matrix, the longer time interval needed). Since the eigenvalues of the matrix in (34) are given, at any $t \in I\!R$, by

$$\sigma(t)_{1,2} = \pm\sqrt{\mathcal{A}_S(t)^2 - \mathcal{A}_V(t)^2}, \qquad (36)$$

one can conclude that, if $\mathcal{A}_S$ and $\mathcal{A}_V$ satisfy (35) and $I = [t^*, t^{**}]$ is sufficiently long, the trivial solution is not finite-time hyperbolic on I.

Another approach to characterising the stability properties originates from the so-called EPH-partition (see the Appendix A and Haller, 2001b; Duc and Siegmund, 2008). This criterion relies upon considering the characteristics of the so-called *rate of strain tensor*, $\hat{\mathbf{S}}(t)$ (cf. Definition A.7), and the *strain acceleration tensor*, $\hat{\mathbf{M}}(t)$ (cf. Definition A.9), derived for a flow linearised about the considered trajectory. In particular, a trajectory is said to be in a hyperbolic region of the phase space within a time interval I if the restriction of $\hat{\mathbf{M}}(t)$ to the so called zero-strain set (cf. Definition A.8) is positive definite for all $t \in I$. In the case of our example system (34),

on $I = (-\infty, t^*)$ which converge to $\boldsymbol{x} = 0$ as $t \to -\infty$, In the linear case of (34) these solutions can be extended to $I = (t^*, \infty)$ with the help of the fundamental solution matrix. Similar procedure can be used to show existence of trajectories of (34) on $I = (t^{**}, \infty)$ converging to $\boldsymbol{x} = 0$ as $t \to \infty$, and then mapping them backwards using the fundamental solution matrix.

the rate of strain tensor

$$\hat{\mathbf{S}}(t) = \tfrac{1}{2}(\hat{\mathbf{A}}(t) + \hat{\mathbf{A}}(t)^T) = \begin{bmatrix} -\mathcal{A}_S(t) & 0 \\ 0 & \mathcal{A}_S(t) \end{bmatrix}, \qquad (37)$$

is indefinite for any $t \in I\!R$, and the zero-strain set, defined as $Z(t) = \{ \boldsymbol{x} \in I\!R^2 : \ \langle \boldsymbol{x}, \hat{\mathbf{S}}(t)\,\boldsymbol{x} \rangle = 0 \}$ is given by

$$Z(t) = \left\{ \boldsymbol{\xi}^+, \boldsymbol{\xi}^- \in I\!R^2 : \ \boldsymbol{\xi}^+ = \alpha \begin{bmatrix} 1 \\ 1 \end{bmatrix}, \ \boldsymbol{\xi}^- = \alpha \begin{bmatrix} 1 \\ -1 \end{bmatrix}, \ \alpha \in I\!R \right\}. \quad (38)$$

Finally, the strain acceleration tensor is

$$\hat{\mathbf{M}}(t) = \frac{\mathrm{d}}{\mathrm{d}t}\hat{\mathbf{S}}(t) + \hat{\mathbf{S}}(t)\hat{\mathbf{A}}(t) + \hat{\mathbf{A}}(t)^T \hat{S}(t)$$

$$= 2 \begin{bmatrix} \mathcal{A}_S(t)^2 & \mathcal{A}_S(t)\mathcal{A}_V(t) \\ \mathcal{A}_S(t)\mathcal{A}_V(t) & \mathcal{A}_S(t)^2 \end{bmatrix}, \qquad (39)$$

and its restriction to the zero-strain set yields

$$\langle \boldsymbol{\xi}^-, \hat{\mathbf{M}}(t)\boldsymbol{\xi}^- \rangle = \alpha^2 \mathcal{A}_S(t)\big(\mathcal{A}_S(t) - \mathcal{A}_V(t)\big), \qquad (40)$$

$$\langle \boldsymbol{\xi}^+, \hat{\mathbf{M}}(t)\boldsymbol{\xi}^+ \rangle = \alpha^2 \mathcal{A}_S(t)\big(\mathcal{A}_S(t) + \mathcal{A}_V(t)\big). \qquad (41)$$

Consequently, the restriction of $\hat{\mathbf{M}}(t)$ to $Z(t)$ is positive definite provided that $\mathcal{A}_S(t) - \mathcal{A}_V(t) > 0$. If the amplitudes $\mathcal{A}_S(t)$, $\mathcal{A}_V(t)$ satisfy (35), one can conclude, that the trivial solution leaves the hyperbolic region of the phase space at t^* and is contained in the elliptic region (cf. Definition A.10) for $t \in I = [t^*, t^{**}]$. According to Definition A.11, the trivial solution will not be finite-time hyperbolic on any time interval $J \in I\!R$ such that $J \cap I$ is sufficiently long (see Definition A.11 for more details).

Note that both of these characteristics of finite-time hyperbolicity depend on the time interval considered and cannot be attributed to a point on a trajectory. Rather, whether or not a given trajectory is finite-time hyperbolic on a given interval, I, depends on the relative length of subintervals of I within which the local dynamics has "undesirable" properties. In what follows we will say that a trajectory $\boldsymbol{\gamma}$ is not finite-time hyperbolic on an interval I if there exists interval(s) J such that $J \cap I \neq \emptyset$ and $\boldsymbol{\gamma}$ is not finite-time hyperbolic on J. Clearly, if a trajectory $\boldsymbol{\gamma}$ is finite-time hyperbolic on $I \in I\!R$ than it is finite-time hyperbolic on any $J \subset I$.

Note also that if, instead of (35), the amplitudes were chosen such that

$$\left. \begin{aligned} \mathcal{A}_V(t) &< \mathcal{A}_S(t), \quad \text{for} \quad t \in (-\infty, \ t^*\,], \\ \mathcal{A}_V(t) &> \mathcal{A}_S(t), \quad \text{for} \quad t \in (t^*, \infty), \end{aligned} \right\} \qquad (42)$$

one can only identify[6] an unstable manifold, $W^u[\boldsymbol{x} = 0]$, in the flow generated by (31). In such a case $\Re e\,[\sigma(t)] = 0$ for any $t \in [t^*, \infty)$ and the trivial solution is not finite-time hyperbolic on $t \in [t^*, \infty)$; i.e., $\boldsymbol{x}(t) = 0$ does not have the exponential dichotomy on $[t^*, \infty)$. Similarly, when

$$\left. \begin{aligned} \mathcal{A}_V(t) &> \mathcal{A}_S(t), \quad \text{for} \quad t \in (-\infty, t^*\,], \\ \mathcal{A}_V(t) &< \mathcal{A}_S(t), \quad \text{for} \quad t \in (t^*, \infty), \end{aligned} \right\} \qquad (43)$$
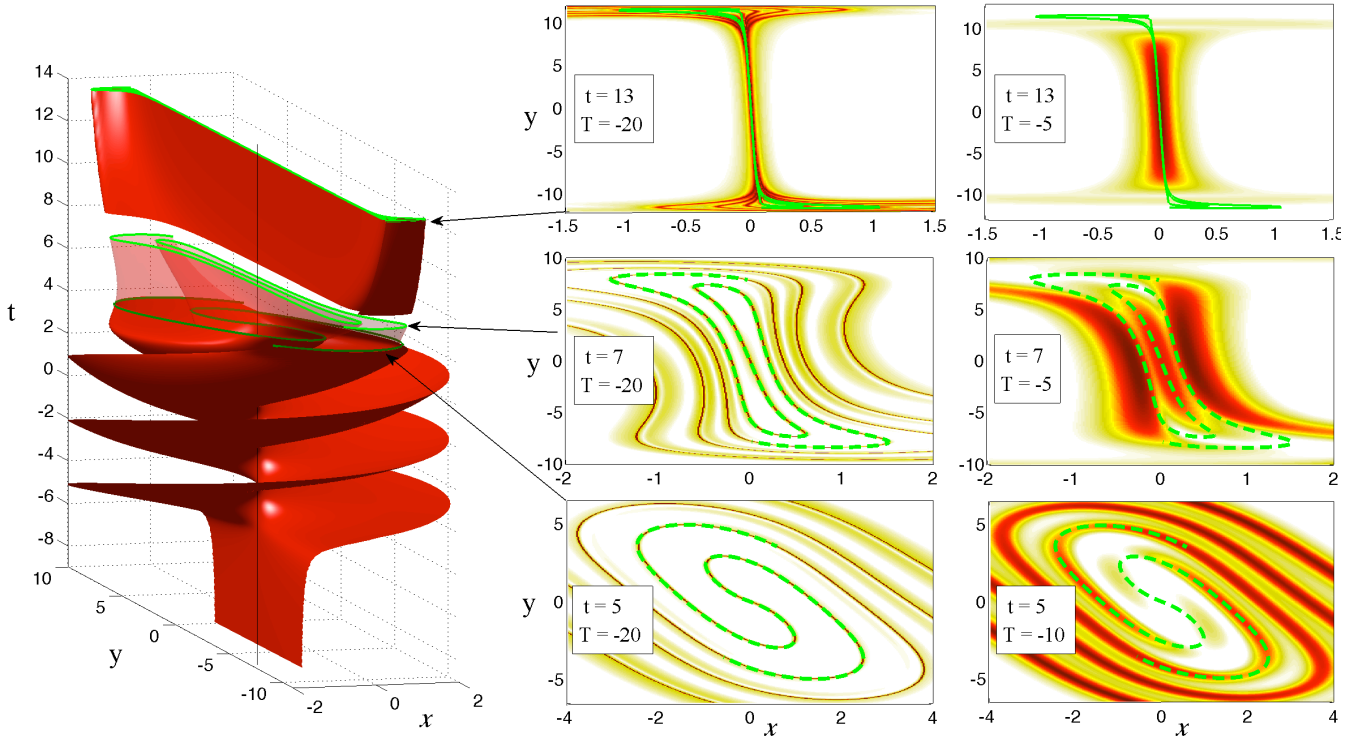
Fig. 6. (Left) Geometry (in the extended phase space (x, y, t)) of an unstable manifold of the trivial solution, $\boldsymbol{x}(t)=0$, in a flow generated by 31). (Right) Finite-time Lyapunov exponent fields, i.e., $\lambda_T(x, y, t)$ (cf. A.2), computed at three different times during the evolution $t=5$ (top row), $t=7$ (middle row), $t=13$ (bottom row); for each of these times the FTLE fields were computed over two time intervals of different lengths T. The green lines denote the instantaneous geometry of the unstable manifold. Only when computed over sufficiently long time intervals, the ridges of the backward FTLE fields coincide with the unstable manifold.

one could only define a stable manifold $W^s[\boldsymbol{x}=0]$. The trivial solution is in this case finite-time hyperbolic on (t^*, ∞) but not on $(-\infty, t^*)$.

Note finally that if we restrict the system (31) to a bounded time interval, $I=[t_a, t_b]\subset I\!\!R$, with $t_a>-\infty$, $t_b<\infty$, it is not possible to define[7] the stable and unstable manifolds of the trivial solution (in the classical, time-asymptotic sense) even if $\boldsymbol{x}(t)=0$ is hyperbolic for the same system considered on $I=I\!\!R$. This situation is by far the most common one in applications, especially when dealing with experimentally measured or numerically generated flows. However, if $\boldsymbol{x}(t)=0$ is finite-time hyperbolic on I (in the sense of Haller, 2001b), one can define (cf. Duc and Siegmund, 2008) the following two flow-invariant sets: the t-fibre of a finite-time stable set of $\boldsymbol{x}(t)=0$ on I is given by

$$\mathbb{W}^s_I[\boldsymbol{x}=0](t)=\left\{\boldsymbol{x}\in I\!\!R^2: \frac{\mathrm{d}}{\mathrm{d}m}\|\mathbf{X}(m, t)\boldsymbol{x}\|<0, m\in I\right\}, \quad (44)$$

and the finite-time unstable set of $x(t)=0$ on I is defined, for $t\in I$, as

$$\mathbb{W}^u_I[\boldsymbol{x}=0](t)=\left\{\boldsymbol{x}\in I\!\!R^2: \frac{\mathrm{d}}{\mathrm{d}m}\|\mathbf{X}(m, t)\boldsymbol{x}\|>0, m\in I\right\}. \quad (45)$$

In contrast to the classical (time asymptotic) definition of stable and unstable manifolds, the finite-time counterparts, $\mathbb{W}^u_I$ and $\mathbb{W}^s_I$, have the dimension of the extended phase space (rather than a lower dimension) and their t-fibres are open sets in $I\!\!R^2$. In such a case, a common approach used in the invariant-manifold Lagrangian transport analysis is to choose (non-unique) segments of initial conditions of length $\alpha\ll1$, $\mathfrak{U}^\alpha_{t_a}$ and $\mathfrak{S}^\alpha_{t_b}$, containing the trivial solution of the linearised system[8], and follow their forwards and backward time evolution. It can be shown (see Appendix B) that, if properly chosen, the material segments are contained in, respectively, $\mathbb{W}^u_I[\boldsymbol{x}(t)=0]$ and $\mathbb{W}^s_I[\boldsymbol{x}(t)=0]$. Moreover, due to the the embedding property of finite-time stable and unstable manifolds (see Duc and Siegmund, 2008, Theorem 37, p. 659) the effect of the non-unique choice of the initial material segments

---

[7]For systems defined on a finite time interval one can still consider non-unique extensions to $I=I\!\!R$ by applying the Lyapunov-Perron approach to an extension of the flow from $I = [a, b]$ to $I\!\!R$ as in Haller and Poje (1998); Haller (2000). Since such extensions can be accomplished in a non-unique way, the manifolds constructed in the extended system are unique up to an error $\mathcal{O}(e^{-c(b-a)})$, $c>0$.

[8]Note that, by construction, the trivial solution $\boldsymbol{\xi}(t)=0$ of a system linearised about some trajectory $\boldsymbol{\gamma}(t)$ corresponds to this trajectory.
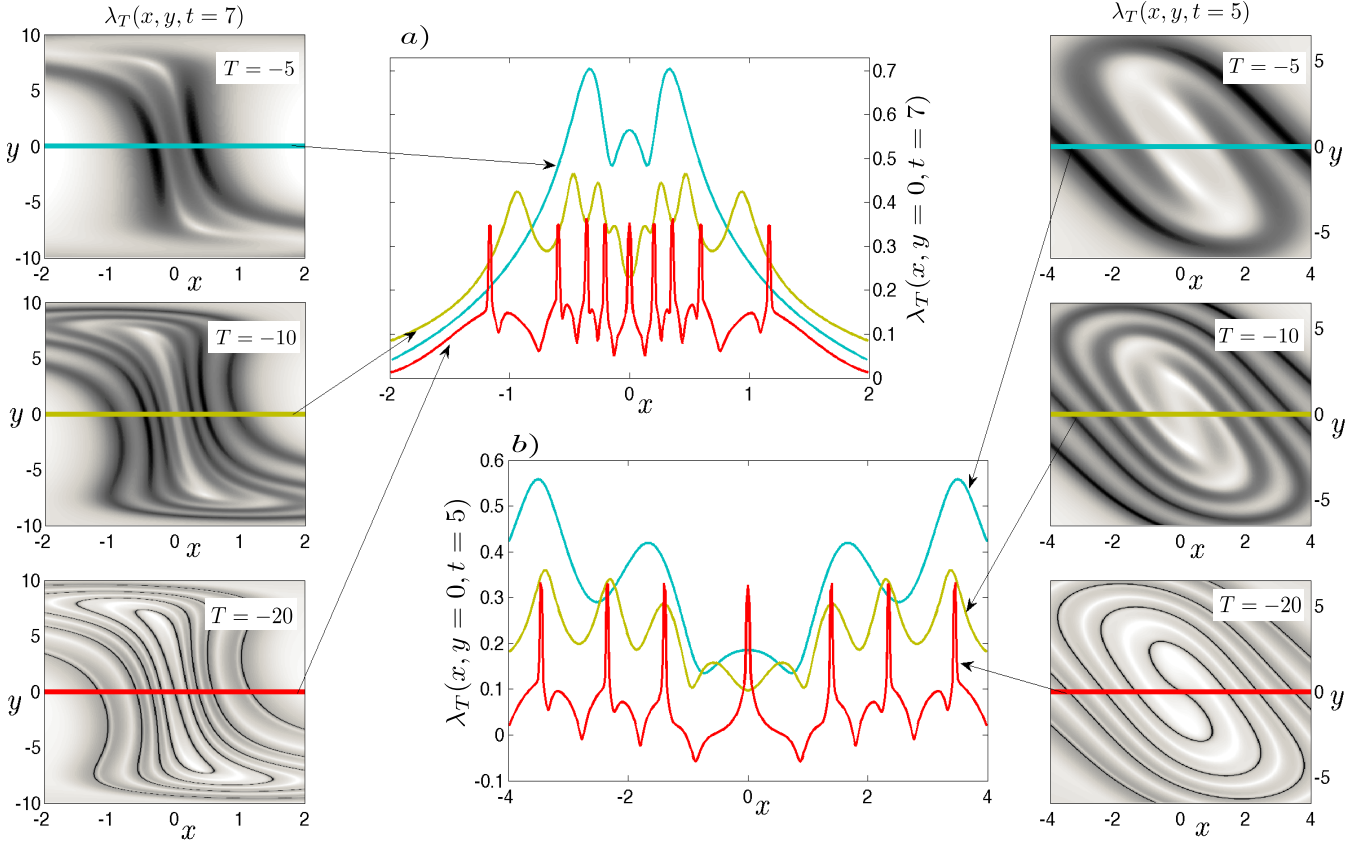
Fig. 7. Comparison of the 1-D sections (along $(x, y=0)$) of the backward FTLE fields (gray-shaded) computed for the flow (31) and discussed in Fig. 6. Three 1-D sections of the FTLE map computed at **(a)** $t=7$ and **(b)** $t=5$ over different integration intervals T. Note that the number of maxima and their location varies with T. In particular, the nature of the extremum at $x=0$ in the FTLE maps switches between minimum and maximum depending on T. The location of the finite-time unstable manifold of the (finite-time) hyperbolic trajectory $x(t)=0$ coincides, in this case, with the strongest maxima of the FTLE fields computed for $T=20$. However, this fact can be only established once the finite-time unstable manifold is computed.

diminishes with the length of the considered time interval I, provided that the considered trajectory is finite-time hyperbolic on I (see the Appendix B for more details).

Examples of flows generated by the system (31)

In our comparison of the invariant manifold and the FTLE analysis of flows generated by (31), we first choose the amplitudes $\mathcal{A}_S$ and $\mathcal{A}_V$ in such a way that the flow is not finite-time hyperbolic on a bounded interval; this can be achieved, for example, by setting $\mathcal{A}_S(t)=1$ and

$$\mathcal{A}_V(t) = \frac{2}{\pi}\left(\operatorname{atan}(10 - t^2/2) + \pi/2\right), \qquad (46)$$

in which case $t^*{\approx}-4.47$ and $t^{**}{\approx}4.47$ and the trivial solution is not finite-time hyperbolic on $I=[t^*, t^{**}]$. The results to computed for such a flow are discussed in Figs. 5–7.

In Fig. 6 we show the geometry of the numerically approximated unstable manifold of the trivial solution in the nonlinear flow (31) and compare these results with the back-

ward FTLE fields (cf. A.2) at three different times during the evolution $t=13$ (top row), $t=7$ (middle row) and $t=5$ (bottom row). The unstable manifold was approximated by following an evolution of appropriately chosen initial material segment (cf. Appendix B), using algorithms analogous to those described in Mancho et al. (2004, 2003). Clearly, for sufficiently long integration intervals the ridges of the backward FTLE field coincide very well with the instantaneous geometry of the unstable manifold (dashed green), as can be seen in the panels computed with $T=20$ at three different times (left column). Note, however, that for smaller values of T not only the ridges of the FTLE fields become less localised but their location changes as well. This effect is further highlighted in Fig. 7 where we show 1-D cross sections of the FTLE fields computed for different values of T. The non-uniqueness of the backward FTLE fields is a direct consequence of the fact that if one computes separation of nearby trajectories in non-autonomous flows, the outcome will depend, in general, on the starting time and the extent of the time interval over which such a diagnostic is evaluated. Therefore, in more
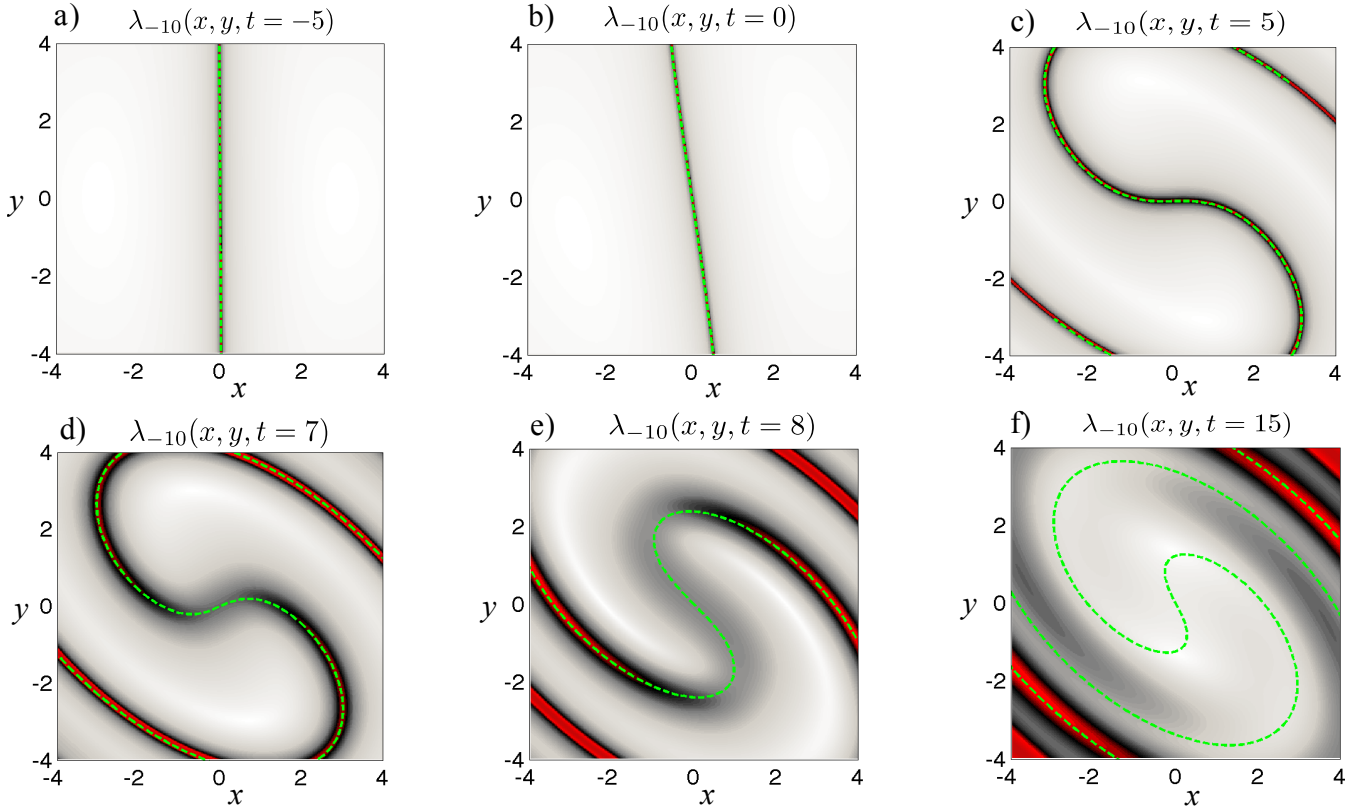
Fig. 8. A sequence of backward FTLE fields (grey/red shaded), $\lambda_T(x, y, t_i)$, $\{t_i\}_{i \in \mathbb{Z}}$ (cf. A.2), for the flow (31) with $\mathcal{A}_S$=1 and $\mathcal{A}_V(t)$ given by (47). The FTLE fields are computed with $|T|$=10. The flow undergoes a transition associated with the loss of finite-time hyperbolicity by the trivial solution. The dashed green lines denote the instantaneous geometry of a material curve which approximates the finite-time unstable manifold of $\boldsymbol{x}(t)$=0 before the transition (After the transition the trivial solution does not have f.t. unstable manifold but this curve remains a material transport barrier in the flow.) Note that, when computed with a fixed T, the ridges of the FTLE field fade away during the evolution as the flow transitions into the "non-hyperbolic" phase.

complex flows it might be not always clear which length, T, of the integration interval is the most suitable one for describing the flow structure based on the FTLE fields. It is also worth noting that in complicated flows, possibly known on only for a finite time, the identification of Distinguished Hyperbolic Trajectories on a finite time interval and their stable and unstable manifolds is also not unique, although for different reasons (see Ide et al., 2002 and the discussion following (44) and (45)).

We finish this section with an example of a flow associated with (31) with $\mathcal{A}_S(t)$=1 and

$$\mathcal{A}_V(t) = \frac{2}{\pi}\left(\operatorname{atan}(10t) + \pi/2\right), \qquad (47)$$

which corresponds to the case (42) mentioned above with $t^* \approx 0$. In Fig. 8 we consider a hypothetical situation of trying to record the time-dependent geometry of a transport barrier, given by the unstable manifold of $\boldsymbol{x}(t)$=0, using the backward FTLE fields. Note that, as discussed earlier, the trivial solution is not finite-time hyperbolic on any interval contained in I=(t^*, ∞) and, consequently, it does not have a finite-

time unstable (or stable) manifolds on I. Assume that we choose a time interval length T which leads to well localised ridges in the backward FTLE fields during the initial period of evolution. In this case $|T|$=10 seems satisfactory for determination of the LCS before the transition. Nevertheless, it can be seen that the ridge localisation deteriorates in the FTLE fields, $\lambda_T(x, y, t_i)$, computed at an ordered sequence of "observation" times $\{t_i\}_{i \in \mathbb{Z}}$ with increasing t_i.

3.3.2 Double gyre flow

The double gyre flow is considered in the domain D=[0, 2]×[0, 1] and is given by

$$\left. \begin{aligned} u(x, y, t) &= -\pi A \sin\left((\pi f(x, t)\right) \cos(\pi y), \\ v(x, y, t) &= \pi A \cos\left(\pi f(x, t)\right) \sin(\pi y) \frac{df}{dx}, \end{aligned} \right\} \qquad (48)$$

where $f(x, t)$ is chosen in such a way that $f(0, t)$=$f(2, t)$=0. This flow is frequently used for illustrating the LCS (e.g. Shadden et al. (2005); Shadden
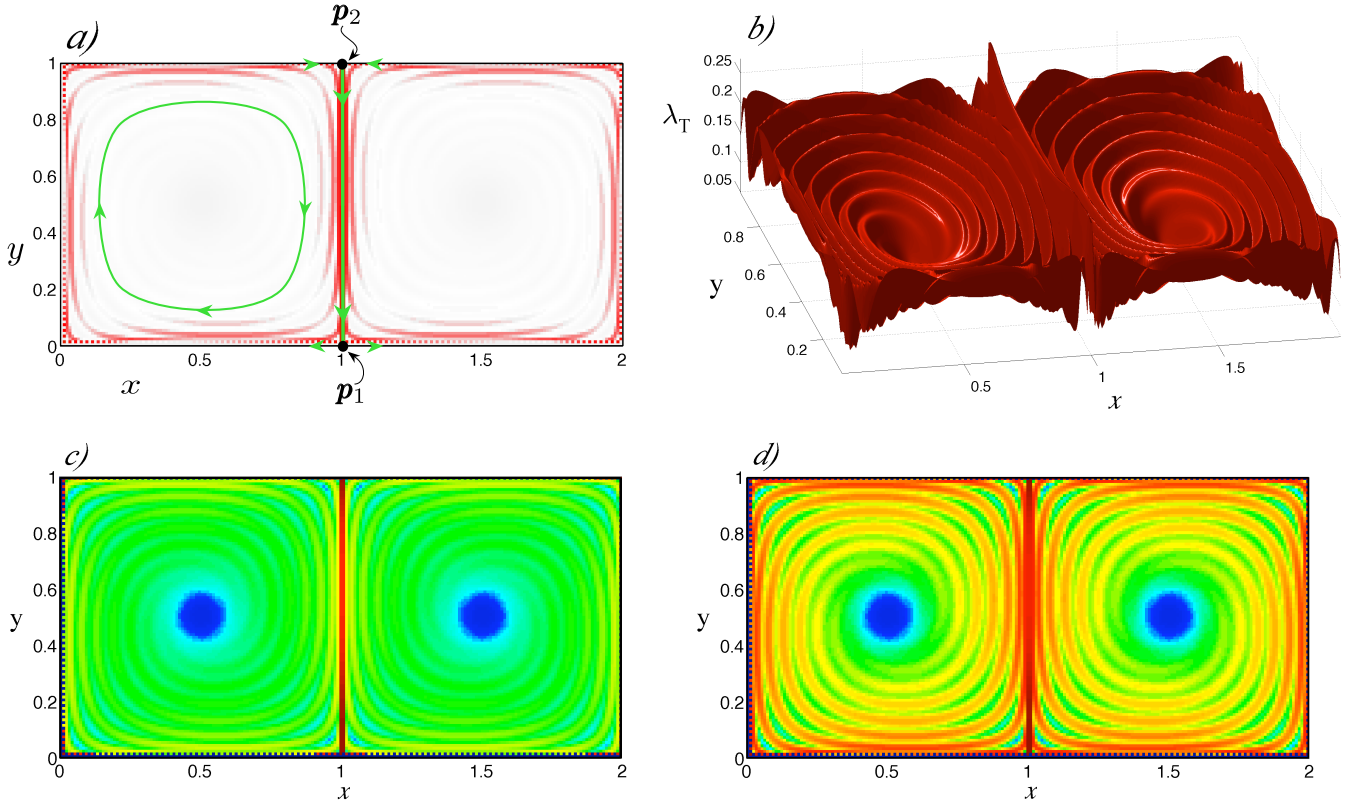
Fig. 9. Backward FTLE field, $\lambda_{-15}(x, y, t=0)$ (cf. A.2) computed with $T=-15$, the and invariant manifold structure for the double gyre flow (48) in the steady case. **(a)** The heteroclinic connection (green vertical line) between the two hyperbolic fixed points $\boldsymbol{p}_1$ and $\boldsymbol{p}_2$ coincides with the most pronounced ridge of the FTLE field, shown in more detail in **(b)**. Note that the FTLE field (b) possesses an inward spiralling ridge in each cell which does not correspond to an invariant manifold. Depending on the characteristics of the colour map, this spiralling structure can be suppressed **(c)** or enhanced **(d)**. However, in a time-dependent case it is not immediately clear whether or not similar spiralling ridges correspond to transport barriers.

(weblink)) and it is instructive to compare the LCS and stable/unstable manifolds of hyperbolic trajectories using this example. The (non-autonomous) dynamical system associated with (48) is simply given by

$$\left.\begin{array}{l} \dot{x} = u(x, y, t), \\ \dot{y} = v(x, y, t). \end{array}\right\} \tag{49}$$

When the flow is steady, i.e., when $\partial f(x, t)/\partial t=0$, there are two hyperbolic stagnation points in the system (49) located at $\boldsymbol{p}_1(x, y)=(1, 0)$ and $\boldsymbol{p}_2(x, y)=(1, 1)$. The unstable manifold of the stagnation point $\boldsymbol{p}_1$ coincides with the invariant boundary ($x=[0, 2]$, $y=0$) and the stable manifold is located within the domain. Similarly, the stable manifold of $\boldsymbol{p}_2$ is contained in the flow-invariant boundary ($x=[0, 2]$, $y=1$) and its unstable manifold coincides with the heteroclinic connection between $\boldsymbol{p}_1$ and $\boldsymbol{p}_2$. When $f(x, t)=x$ the heteroclinic connection is given by ($x=1$, $y=[0, 1]$). The steady situation is visualised in Fig. 9 where we overlap the forward FTLE field with the manifold structure associated with the

hyperbolic fixed points $\boldsymbol{p}_{1,2}$. Provided that the FTLE field is computed for sufficiently large T ($T=15$ in this case), the most pronounced FTLE ridge coincides with the heteroclinic connection discussed earlier. (If T is too small, the structure of the FTLE field does not reveal this heteroclinic connection; see Shadden (weblink).)

When $\partial f(x, t)/\partial t\neq0$, paths of the instantaneous stagnation points (ISPs, see A18) are not system trajectories. However, the paths of two (frozen-time) hyperbolic ISPs (see Definition A.6) given by

$$\boldsymbol{p}_1(t) = \{(x, y) \in \mathbb{R}^2 : y = 0, \, f(x, t) = 0\}, \tag{50}$$

$$\boldsymbol{p}_2(t) = \{(x, y) \in \mathbb{R}^2 : y = 1, \, f(x, t) = 0\}, \tag{51}$$

can be used to compute two Distinguished Hyperbolic Trajectories (DHTs, cf. Definition A.5, Appendix A), $\boldsymbol{\gamma}_1(t)$ and $\boldsymbol{\gamma}_2(t)$, which are contained in the flow-invariant, bottom and top and boundaries, respectively. These DHTs can be computed using techniques described in Ide et al. (2002); Mancho et al. (2003, 2004) (we stress again that the use of paths
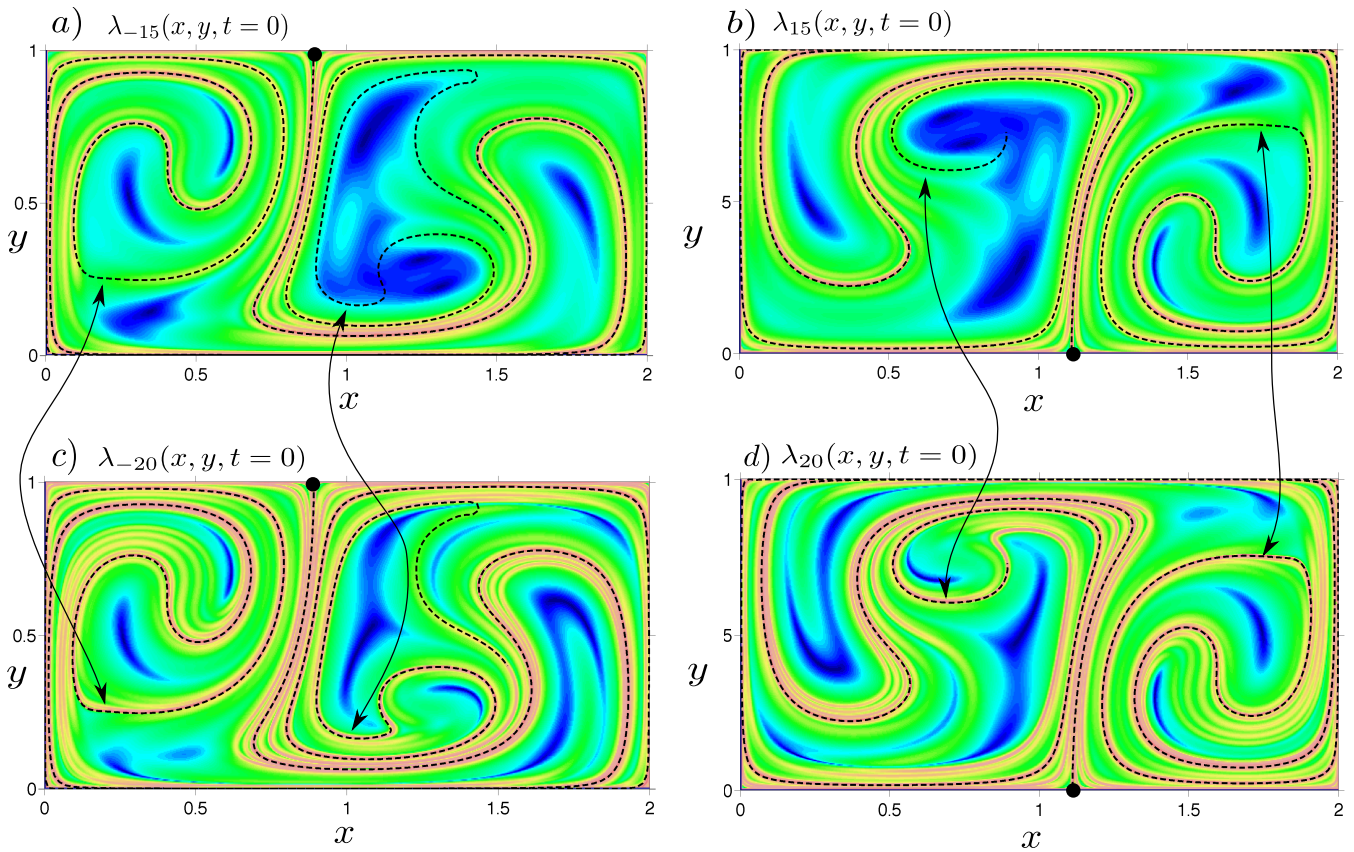
Fig. 10. Backward **(a, c)** and forward **(b, d)** FTLE maps for the double gyre flow (48) at t=0; computed over two different time intervals with lengths T=15 (a, b) and T=20 (c, d); Δt=0.01 in all cases. The parameters ω=$2\pi/10$, ϵ=0.25 and A=0.1 are chosen as in the online tutorial Shadden (weblink). The dashed black curves denote the instantaneous geometry of the unstable manifold (a, c) and of the stable manifold (b, d) of the Distinguished Hyperbolic Trajectories $\boldsymbol{\gamma}_2(t)$ (black dot in a and c), and $\boldsymbol{\gamma}_1(t)$ (black dot in b and d). For sufficiently long integration times, good agreement between the LCS (red) and the manifolds can be achieved. However, depending on T the FTLE map reveals ridges of different length and connectivity. Some most significant differences are marked by the black arrows. The correlation between the LCS and the invariant manifolds depends also on the integration method, the integration step Δt (see Fig. 11).
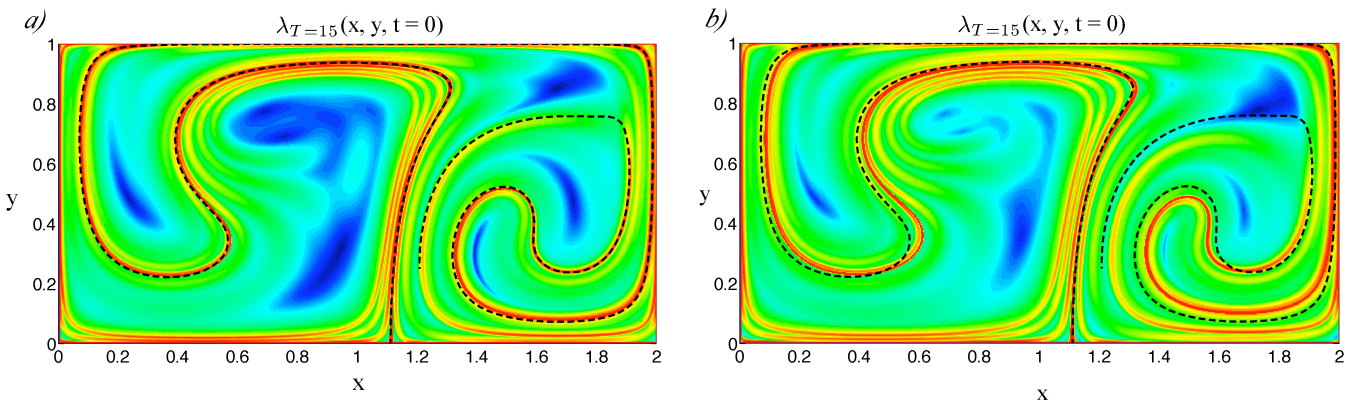
Fig. 11. Sensitivity of the FTLE field to the integration method (see also Fig. 14). Forward FTLE computed at t=0 with T=15 for the flow (48) using **(a)** 4th order Runge-Kutta and **(b)** forward Euler (used in the LCS MATLAB Kit, see Dabiri (weblink)); Δt=0.1 in both computations. The fact that the results depend on the integration method and the time step used are hardly surprising. However, it is particularly important to bear these effects in mind in situations when one does not have the control over the time discretisation (e.g., when dealing with experimental data recorded on a discrete space-time grid; see also figure 14). The dashed black curves show the instantaneous geometry of the stable manifold of $\boldsymbol{\gamma}_2$.
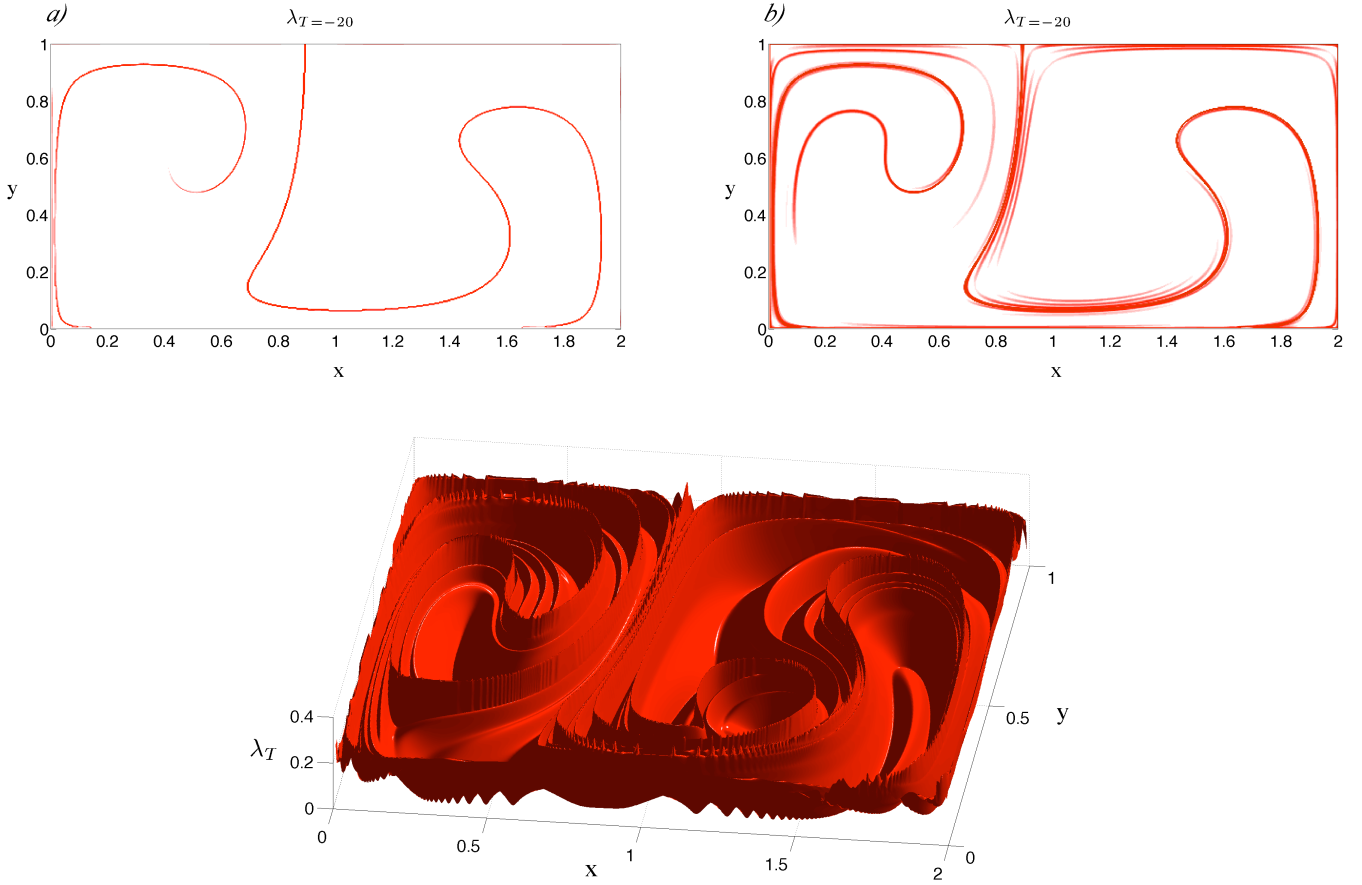
Fig. 12. When shading the FTLE fields one has to make a choice of a filtering threshold in order to reveal the ridges approximating the LCS. Different choices of the colour mapping, which serves here a height filter, may reveal or suppress disconnected segments of LCS (backward FTLE field at $t=0$ computed for $T=-20$ shown). This effect combined with the non-uniqueness of the FTLE maps (i.e., the one-parameter family $\{\lambda_T(x,y,t)\}_{t+T \in I}$) makes it difficult to identify long segments of the LCS which are necessary for transport analysis via the lobe dynamics.

of ISPs is a convenient but not a necessary choice of the initial guess). The stable manifold of $\boldsymbol{\gamma}_1(t)$ and the unstable manifold of $\boldsymbol{\gamma}_2(t)$ lie in the interior of the domain and they play a dominant role in organising transport within the flow. In Fig. 10 we show examples of backward FTLE fields (a, c) and forward FTLE fields (b, d) computed at a fixed time, $t=0$, over different lengths of the integration time interval T. We compare these results with the instantaneous geometry of the stable and unstable manifolds of $\boldsymbol{\gamma}_1(t)$ and $\boldsymbol{\gamma}_2(t)$ which are delineated by the dashed black curves. In the computations we used

$$f(x, t) = a(t)x^2 + b(t)x, \tag{52}$$

$$a(t) = \epsilon \sin \omega t, \tag{53}$$

$$b(t) = 1 - 2\epsilon \sin \omega t, \tag{54}$$

with $\omega = 2\pi/10$, $\epsilon = 0.25$ and $A=0.1$, which coincides with the choice used in Shadden (weblink). Since the flow (48) with $f(x, t)$ given by (52) is time-periodic, both the DHTs

and their stable and unstable manifolds are well defined and unique. Moreover, since these manifolds are composed of the system trajectories they represent barriers to Lagrangian transport. It can be seen in Fig. 10a and c that in this case the instantaneous geometry of the unstable manifold of $\boldsymbol{\gamma}_2(t)$ and the ridge of the backward FTLE map (i.e., the attracting LCS) are well correlated over long distances (in the arc length sense from the DHT). Similarly, the stable manifold of $\boldsymbol{\gamma}_1(t)$ and the repelling LCS associated with the forward FTLE map coincide provided that the FTLE field is computed over sufficiently long time interval (Fig. 10b and d). The issue of the length T of the time interval chosen to compute the FTLE field is worth reiterating here. Recall that (cf. Sect. 2 and the Appendix A), at each "observation" time the FTLE field, $\lambda_T(x, y, t)$, depends on the integration parameter T. Thus, the arclength of the strongest ridges of the FTLE field and, more importantly, the location of these ridges varies with T. This can be seen in Fig. 10c and d which is computed for the same values of the flow parameters as in Fig. 10a and b but for $T=\pm 20$. Note, in particular, the

changes in the FTLE fields occurring in the regions indicated by the arrows.

Another interesting aspect related to the FTLE computations is the identification the LCS (i.e., the ridges of the FTLE fields) and their connectivity. The ridge extraction was described in Shadden et al. (2005) and an example of the use of such a procedure can be found in Mathur et al. (2007), Fig. 2. However, it seems that such a ridge extraction is not commonly carried out. We note, for example, that the results discussed in Shadden et al. (2006, 2007); Shadden (weblink) and some results in Shadden et al. (2005) seem to be obtained not by ridge extraction but by appropriate "thresholding" of the colour map used for shading the FTLE fields. In Fig. 12 we show a few examples of different shading of the same FTLE field which reveal a "ridge landscape" of varying complexity with a number of disconnected ridges appearing (or disappearing), depending on the colour map threshold used.

In summary, we observe a good correlation between the stable and unstable manifolds of the relevant hyperbolic trajectories and the ridge segments identified in the forward/backward FTLE fields in the double gyre flow (48). However, for a given FTLE field, the choice of the parameters T and the filtering applied to extract the LCS is rather subjective and can be ambiguous. This is of particular concern when analysing transport in time-dependent flows via the mechanism of lobe dynamics. Such analysis requires the ability to follow the evolution of lobes associated with tangles of stable and unstable manifolds of relevant hyperbolic trajectories. Any numerical technique for identifying these tangles will provide, at best, a good approximation of these structures. However, the minimum requirement for this kind of analysis is that the numerical method is capable of approximating and identifying the evolution of the same (and sufficiently long) segments of the invariant manifolds involved. If the structure of the relevant stable and unstable manifolds of the DHTs is known, it is generally possible to adapt T and the colour map "threshold" so that sufficiently long and connected LCSs are revealed. However, if the manifold structure is not known a priori, this task may quickly become impossible. We also note that, while the methods based on computation of stable and unstable manifolds are capable of identifying and following in time long segments of hyperbolic structures, the necessary identification of the "distinguished" hyperbolic trajectory is not always easy. Thus, it is likely that a synergetic approach, combining the use of FTLEs for identifying the possible locations of the DHTs with a subsequent manifold computation, may offer the right way forward.

3.3.3 Time-dependent Hills' spherical vortex in the symmetry plane

Consider now a class of velocity fields obtained by perturbing the well known steady solution of equations of an inviscid incompressible fluid flow given by the Hill's spherical vortex (see, for example, Batchelor, 1967). The Hill's vortex flow,

H, is then perturbed by a time-dependent strain, S, so that the corresponding dynamical system is given by

$$\dot{x} = H(x, y, z) + S(x, y, z, t). \tag{55}$$

The components of the steady Hill's vortex in Cartesian coordinates are

$$\left. \begin{array}{l} H_x = (u_r \sin \Theta + u_\Theta \cos \Theta) \cos \Phi, \\ H_y = (u_r \sin \Theta + u_\Theta \cos \Theta) \sin \Phi, \\ H_z = (u_r \cos \Theta - u_\Theta \sin \Theta), \end{array} \right\} \tag{56}$$

where
$r = \sqrt{x^2 + y^2 + z^2}$, $\Theta = \mathrm{acos}(z/r)$, $\Phi = \mathrm{acos}\left(x/\sqrt{x^2 + y^2}\right)$
and, assuming that a denotes the radius of the vortex, the velocity components in the spherical coordinates are

$$u_r = \begin{cases} U(1 - a^3/r^3) \cos \Theta & \text{if} \quad r \geqslant a, \\ -\frac{3}{2}U(1 - r^2/a^2) \cos \Theta & \text{if} \quad r < a, \end{cases} \tag{57}$$

$$u_\Theta = \begin{cases} -U(1 + a^3/(2r^3)) \sin \Theta & \text{if} \quad r \geqslant a, \\ \frac{3}{2}U(1 - 2r^2/a^2) \sin \Theta; & \text{if} \quad r < a. \end{cases} \tag{58}$$

This unperturbed (steady) Hill's vortex flow has two hyperbolic stagnation points

$$h_1 = (0, 0, -a)^T, \quad h_2 = (0, 0, a)^T, \tag{59}$$

which are located on the (flow-invariant) axis of symmetry e_z of the vortex. The fixed point h_1 has a 2-D unstable manifold in $\mathbb{R}^3$ (1-D in any symmetry plane containing e_z), and the fixed point h_2 has a 2-D stable manifold in $\mathbb{R}^3$.

The perturbing, time-dependent straining flow is given by

$$S = \mathcal{A}(t) \cdot \begin{bmatrix} \alpha(t) & 0 & 0 \\ 0 & \beta(t) & 0 \\ 0 & 0 & \gamma(t) \end{bmatrix} \begin{bmatrix} x \\ y \\ z \end{bmatrix}, \tag{60}$$

where $\mathcal{A}(t)$ is a time-dependent amplitude, the strain rates are normalised so that $\max(\alpha, \beta, \gamma) = 1$ and they satisfy $\alpha + \beta + \gamma = 0$.

When $0 < \mathcal{A} \ll 1$ the fixed points h_1 and h_2 no longer exists but they are perturbed to two hyperbolic trajectories, $\gamma_1(t)$ and $\gamma_2(t)$, which possess, respectively, a 3-D unstable and 3-D stable manifolds in the extended phase space spanned by $\{e_x, e_y, e_z, e_t\}$. In other words, at any fixed time instant the unstable manifold of $\gamma_1(t)$ and the stable manifold of $\gamma_2(t)$ are given by surfaces embedded in $\mathbb{R}^3$. These trajectories can be computed using the algorithms of Ide et al. (2002); Ju et al. (2003). They are distinguished in the sense that their manifolds organise the overall flow dynamics.

a)

b)

c)
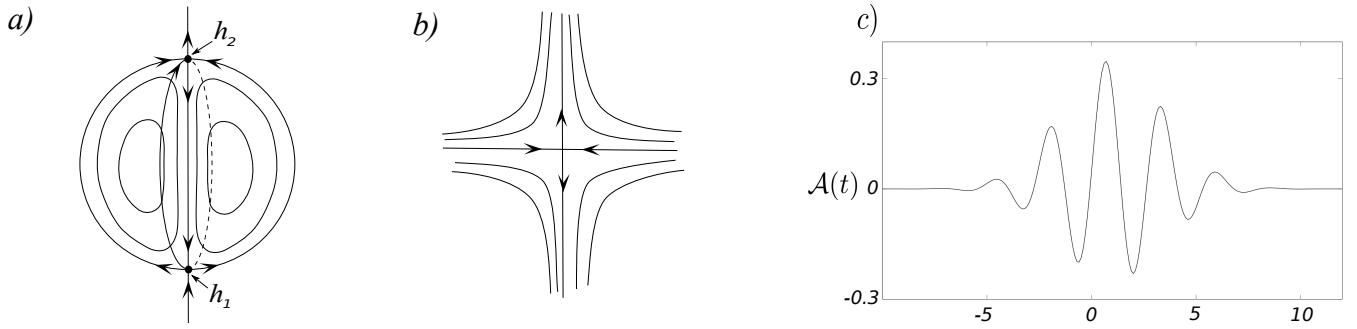
Fig. 13. Schematic representation of a 3-D flow used in computations of invariant manifolds and FTLE fields in Sect. 3.3.3. The steady Hill's spherical vortex **(a)**, sketched in a symmetry plane, is perturbed by a time-dependent strain **(b)**. One of the principal axes of the straining flow is aligned with the axis of symmetry of the Hill's vortex, $\boldsymbol{e}_z$. The amplitude of the strain changes with time as shown in **(c)**.

As long as one of the axes the perturbing straining flow (60) is aligned with the symmetry axis of the Hill's vortex, the flow (55) remains axisymmetric. Consequently, every plane containing $\boldsymbol{e}_z$ is invariant with respect to the flow (55), with $\boldsymbol{H}$ given by (56) and $\boldsymbol{S}$ given by (60). We therefore restrict the analysis to one such symmetry plane, namely $(x=0, y, z)$, in which the instantaneous geometry of the considered invariant manifolds is given by curves.

The hyperbolic trajectories, $\boldsymbol{\gamma}_1(t)$ and $\boldsymbol{\gamma}_2(t)$, which are confined to the symmetry axis, $\mathbf{e}_z$, can be computed using the same algorithms (cf. Ide et al., 2002; Ju and Wiggins, 2001) as used in the previous examples. Their stable and unstable manifolds are computed as in the previous examples using techniques described in Mancho et al. (2003, 2004) with the initial "seed" for these computations chooses in the way described in Appendix B. In Fig. 14 we compare the instantaneous geometry of the unstable manifold of $\boldsymbol{\gamma}_1$ with the corresponding backward FTLE field, both computed in the symmetry plane for the flow associated with (55) with the perturbing strain amplitude given by

$$\mathcal{A}(t) = (0.05 + 0.3\sin(2.33t))e^{-(t-1)^2/(3.5)^2}. \tag{61}$$

The strain rates are chosen as $\alpha=\beta=-0.5$, $\gamma=1$. The conclusions one may draw from these computations are similar as those drawn from the previous examples. Provided that the FTLE fields are computed with sufficient care the overall agreement between the ridges of the FTLE field (red) and the unstable manifold is rather striking (cf. Fig. 14a). As in the previous examples, the critical parameters for an accurate manifold computation are the maximum and minimum curvature cut-off parameters and accurate integration routine.

However, we intend to use this flow geometry to alert the reader to the potential problems which are particularly likely to appear when analysing experimentally measured flow fields or velocities obtained from numerical PDE solvers.

In order for the FTLE computations to be reliable, one needs to make sure that the computational grid is sufficiently refined to reveal the desired details and, most importantly, that the integration routine is chosen appropriate for the cho-

sen integration time step. Obviously, in the case of analytically defined flow fields, as the ones we are dealing with here, the choice of the integration time step is not a serious constraint. However, in the case of discrete data sets (numerical or experimental) the time-discretisation of the data set imposes limitations on Δt, requiring a trade-off between the time step chosen and the temporal data interpolation. In order to highlight, the kind of problems one might encounter in such a situation we show, in Fig. 14c and d results of the FTLE computations for the same flow as in Fig. 14a and b but using the first-order accurate forward Euler integration method. This method is in fact implemented in the LCS MATLAB Kit mentioned earlier Dabiri (weblink) which is combined with linear spatial interpolation of the discrete flow data required by the code. Note, in particular the erroneous structures in Fig. 14d which emerge in the FTLE fields computed using the forward Euler integration method with Δt=0.1. The main danger here is associated with the main advantage of the FTLE computations. Namely, it is straightforward to develop a basic algorithm computing FTLE fields which will generate reasonably looking output.

3.3.4 Boundary layer separation on a non-slip boundary

The technique of invariant manifolds and lobe dynamics for finite-time, aperiodically time-dependent velocity fields has not been extensively developed. An important area of application in this setting is separation from a non-slip boundary. In this setting Haller and co-workers have developed a comprehensive theory based on the FTLE and LCS approach Wang et al. (2003); Haller (2004); Alam et al. (2006); Surana et al. (2006, 2007). Related earlier work using non-hyperbolic separation points and manifolds can be found in Shariff et al. (1991); Duan and Wiggins (1997); Yuster and Hackborn (1997); Ghosh et al. (1998). Nevertheless, there has been extensive work in the mathematics literature on non-hyperbolic trajectories and their stable and unstable manifolds, e.g. McGehee (1973); Casasayas et al. (1992);
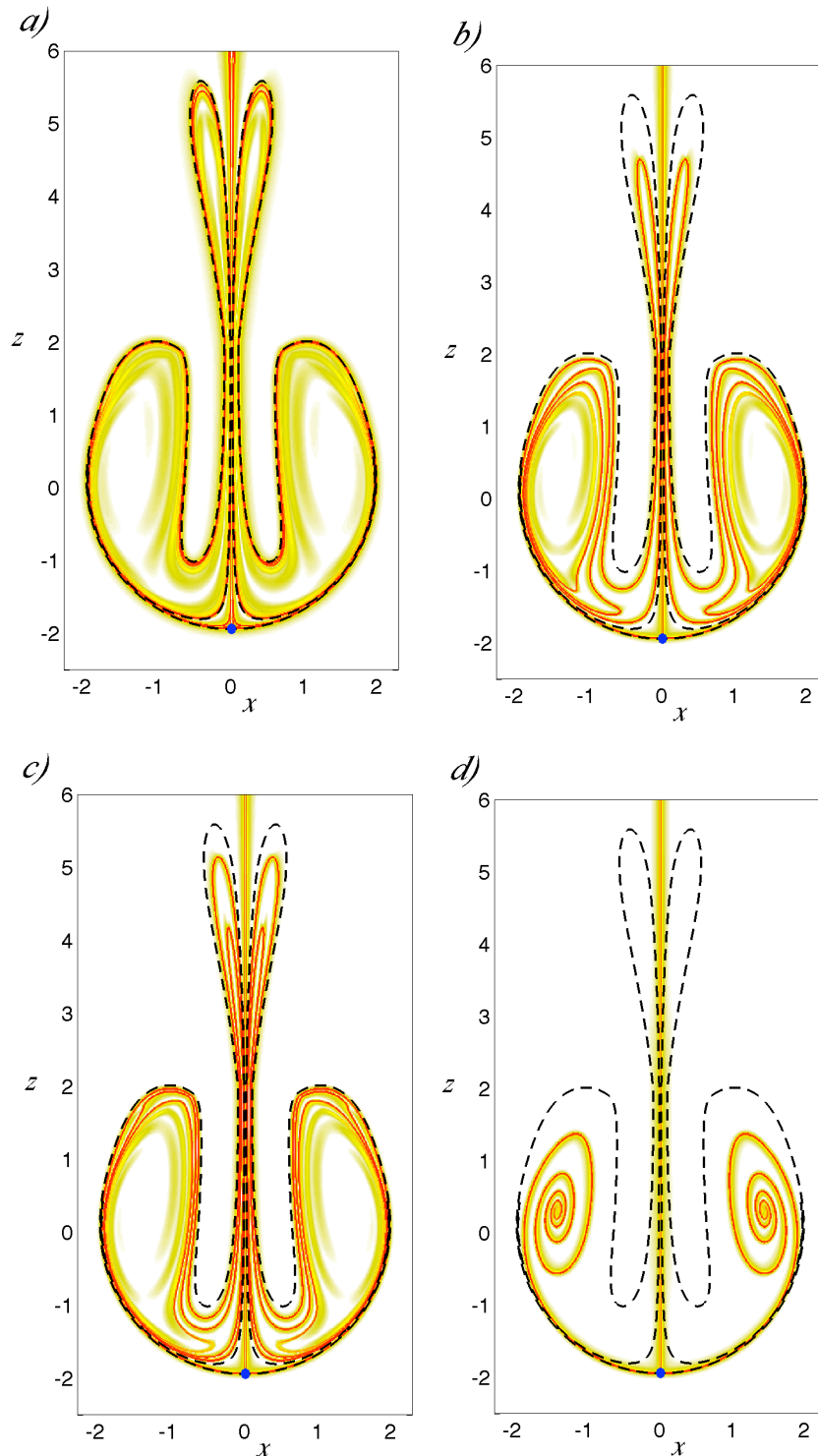
Fig. 14. Comparison of the backward FTLE fields, $\lambda_T(x, y, t)$ (cf. A.2), computed with $T = -15$ in a symmetry plane for the axisymmetric, time-dependent, perturbed Hill's vortex flow (55) at $t = 0$, and the instantaneous geometry of the unstable manifold of the DHT, $\gamma_1(t)$, denoted by the blue dot (see Sect. 3.3.3). The top row shows the FTLE fields computed using 4th order Runge-Kutta with **(a)** $\Delta t = 0.01$ and **(b)** $\Delta t = 0.1$. The bottom row shows analogous computations performed using the forward Euler method (as implemented in Dabiri (weblink)) with **(c)** $\Delta t = 0.01$ and **(d)** $\Delta t = 0.1$. Provided that an appropriate method is used for the integration of trajectories (i.e., not the forward Euler) a good agreement can be achieved (as in a) between the LCS and the invariant manifold computations.

Fontich (1999); Cicogna and Santoprete (1999); Casasayas et al. (2003); Baldoma and Fontich (2004); Bonckaert and Fontich (2005); Holland and Luzzatto (2006); Baldoma et al. (2007). This work should serve as an excellent foundation for developing a theory of "distinguished saddle-points" and their stable and unstable manifolds in finite time, aperiodically time-dependent velocity fields. Finally, we note that the algorithm for computing time-dependent invariant manifolds described in Mancho et al. (2003, 2004) does not require a hyperbolic trajectory as a starting point. Rather, it requires an appropriate "seed" from which the material curve, approximating an invariant manifold is "grown" according to the numerically integrated vector field. Depending on the choice of the "seed", the obtained results may, or may not, be relevant for transport considerations. Instead of selecting the location of some distinguished hyperbolic trajectory as the "seed", one could choose the instantaneous location of a non-hyperbolic saddle point. However, this situation has yet to be developed.

3.3.5 Eddy-pair system

In this example we focus on a flow exhibiting a transition between a configuration characterised by a single Lagrangian eddy and an eddy pair. As in all other examples in this section, our main objective is to establish how well the LCS, represented by ridges of the FTLE fields, correlate with invariant stable and unstable manifolds of relevant hyperbolic trajectories in aperiodically time-dependent flows.

The flow considered here is chosen in such a way that it undergoes a transition from a single Lagrangian eddy configuration to an eddy-pair configu-ration. The stream-function of the kinematic model we use in our analysis is given by

$$
\psi = \mathcal{M}(t) + \mathcal{A}_1(t)e^{-\left((x-x_1(t))^2+(y-y_1(t))^2\right)/\delta_1^2(t)}
$$
$$
+ \mathcal{A}_2(t)e^{-\left((x-x_1(t))^2+(y-y_1(t))^2\right)/\delta_2^2(t)}, \quad (62)
$$

where

$$
\mathcal{M}(t) = \mathcal{L}(t) - \alpha(t)\left(x\cos\theta(t) - y\sin\theta(t)\right)^2 \quad (63)
$$
$$
+ \beta(t)\left(x\sin\theta(t) + y\cos\theta(t)\right), \quad (64)
$$

and $\mathcal{L}=-1$, $\alpha=0.08$, $\beta=1$, $\theta=-\pi/4$. The second and the third term in (62) give rise, for appropriate values of the amplitudes $\mathcal{A}_1$ and $\mathcal{A}_2$, to the appearance of closed contours in the instantaneous streamline patterns. We refer to such patterns Eulerian eddies. We choose here $\mathcal{A}_1=10$, $\delta_1=4$, $x_1=y_1=4$, $x_2=y_2=0$, $\delta_2=0.9$ and the time-dependent amplitude of the second Eulerian eddy as

$$
\mathcal{A}_2(t)=-2/\pi\left(\text{atan}\,(t-1) - \text{atan}\,(-9)\right). \quad (65)
$$

With the above choice of the amplitudes $\mathcal{A}_1$ and $\mathcal{A}_2$ the flow is aperiodically time-dependent and asymptotically steady, so that the two DHTs present in the flow approach the location of the single fixed point in the system for $t\to-\infty$ and two fixed points at $t\to\infty$. The DHTs are again computed using the MATLAB implementation of the techniques introduced in Ide et al. (2002); Ju et al. (2003), and their manifolds are computed using the ideas based on Mancho et al. (2003, 2004).

Figure 15 shows the backward and forward FTLE fields (yellow/red shades, see Definition A.2) computed for the flow (62) at $t=0$, and stable (blue and cyan) unstable (magenta) manifolds of the two DHTs present in the flow. The location of this "observation" time relative to the geometry of the DHTs is shown in the top left panel. The top right panel shows the backward FTLE map computed with $T=25$ and an unstable manifold (of the two DHTs, they are extremely close if not identical). Clearly, the attracting LCS, corresponding to the ridge of the backward FTLE field, and the unstable manifolds of the two DHTs correlate very well over long arclength distances from the DHTs (black dots). The bottom panel shows a comparison between the stable manifolds (blue and cyan) of the DHTs and the forward FTLE map, showing a good agreement. Note also the spiral structure in the forward FTLE map (bottom) which is visible inside the small eddy. When computed over long time intervals the length and definition of the extracted ridges might increase (see, however, Sect. 3.1) but the method starts detecting "premonitions"/"ghosts" of the future/past phase space geometry. Note also that the significant inward curl of the LCSs inside the large eddy in both forward and backward FTLE fields which does not correspond to the manifold geometry.

We show two more snapshots of the instantaneous geometry of the FTLE fields and the stable and unstable manifolds of the DHTs at $t=-4$ (Fig. 16), and at $t=-8$ (Fig. 17). In all cases the agreement between the dominant FTLE ridges and the corresponding stable or unstable manifolds of the DHTs is good, provided that the FTLE fields are computed for sufficiently large T.

3.3.6 Eddy-quadrupole system

In this final example we focus on an incompressible flow characterised by the following streamfunction

$$
\psi(x, y, t)=\left(xy\left(\sigma(t)-x^2\right) -\alpha xy^3 + \beta xy^5\right)e^{-(x^4+y^4)/\delta^4}, \quad (66)
$$

where $\sigma(t)$ is some function of time and α, β, δ are constants. The dynamical system associated with the flow is given by

$$
\dot{x}=\partial\psi/\partial y, \quad \dot{y}=-\partial\psi/\partial x, \quad (x, y)\in\mathbb{R}^2, \quad t\in\mathbb{R}. \quad (67)
$$

We will choose here a particular form of time-dependence which will induce a symmetric transition of the flow associated with (67) from a four-eddy configuration to an
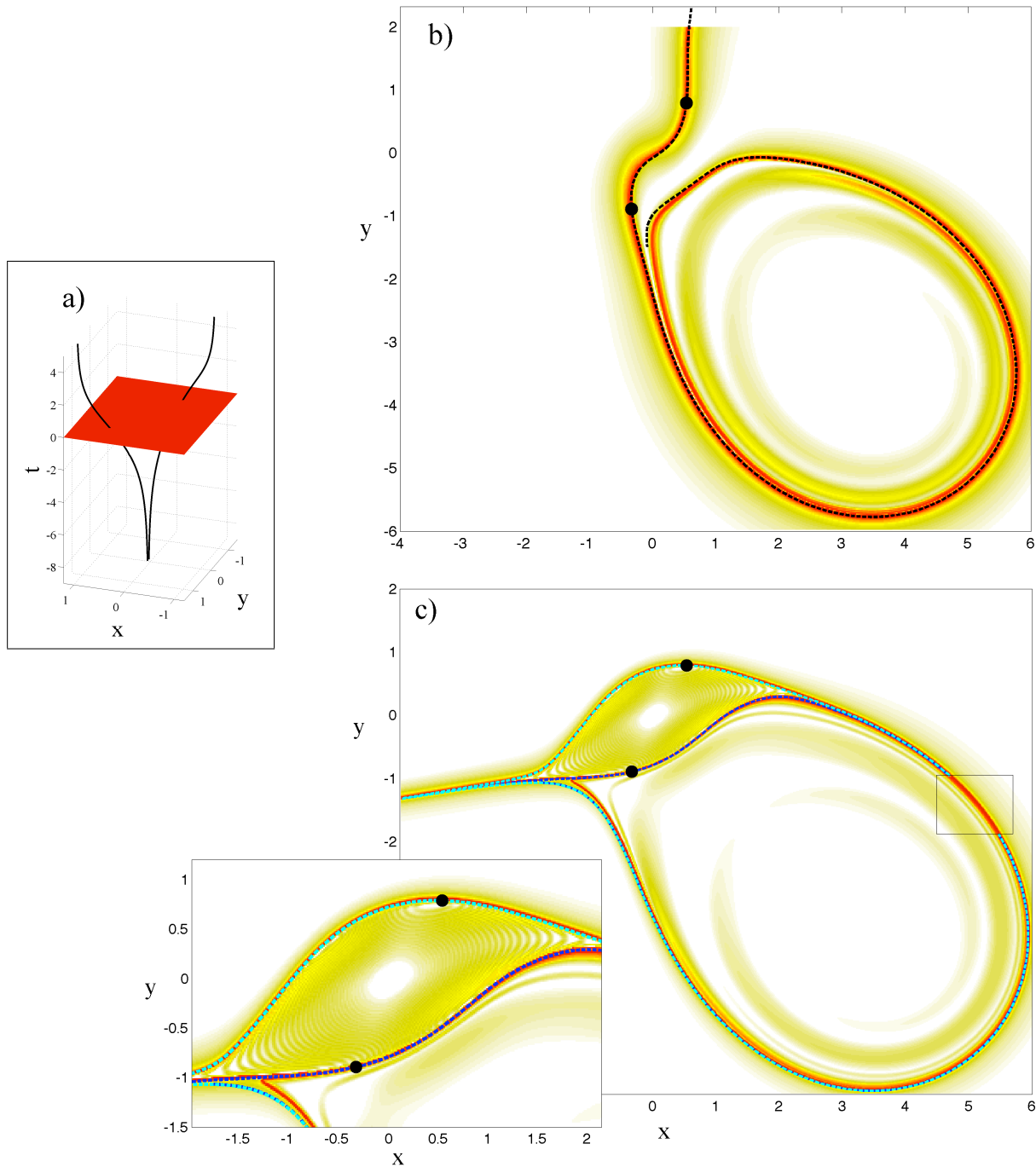
Fig. 15. FTLE fields (cf. A.2) shaded yellow and red, and stable/unstable manifolds of two DHTs (black curves in **a**) computed in the flow (62) at $t=0$ during a transition between the singe-eddy and eddy-pair configuration (see the Fig. 16, 17 for the geometry at earlier times). **(b)** backward FTLE field, computed with $T=-25$, superimposed with the unstable manifolds (dashed black) of the two DHTs (black dots); the LCS are delineated by the red ridges of the FTLE map and were enhanced by appropriate filtering of the colour map. **(c)** the forward FTLE field (yellow/red shades), computed with $T=25$, superimposed with the stable manifolds (cyan/blue) of the two DHTs (black dots). The manifold segments inside the black rectangle were removed in order to reveal the LCS underneath. When computed over sufficiently long time intervals, the length and definition of the strongest ridges (LCS, red) of the FTLE maps generally increases (see, however, Sect. 3.1) but the method starts detecting "premonitions"/"ghosts" of the future/past phase space geometry. Note, in particular, the spiral structure inside the small eddy visible in the forward FTLE map (c). Note also a significant inward curl of the weaker ridges of the forward and backward FTLE fields inside the large eddy which are not associated with the instantaneous geometry of the invariant stable/unstable manifolds.
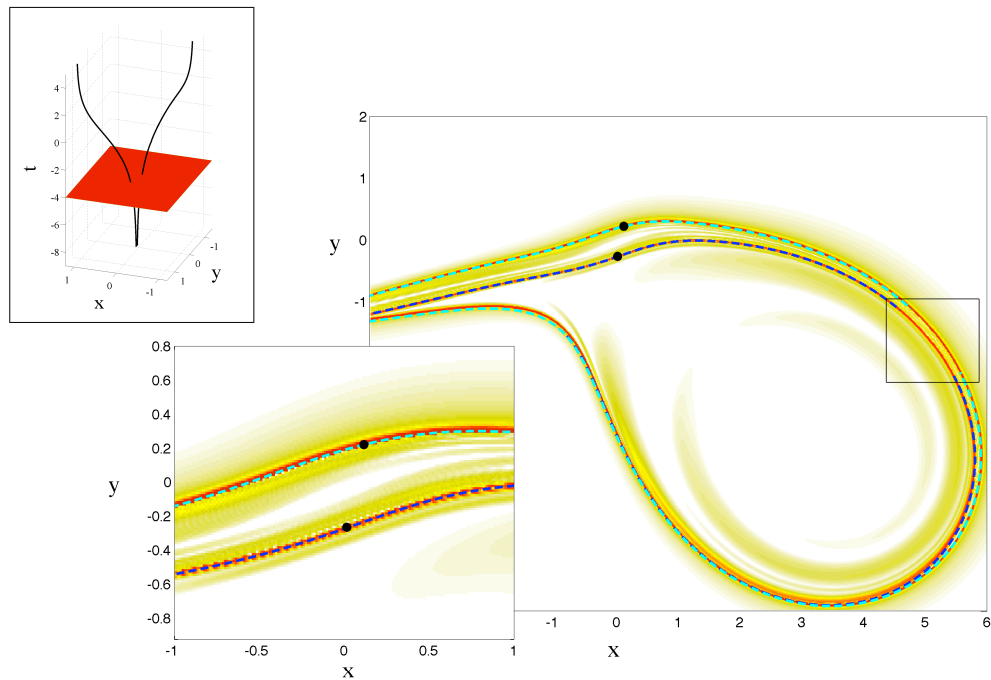
Fig. 16. Comparison between the forward FTLE map (yellow/red shades) and stable (blue, cyan) manifolds of two DHTs (black dots) computed in the flow (62) at $t=-4$. The FTLE field was computed with $T=25$ and the LCS, represented by the red ridges, were "extracted" by filtering the colour map. The manifolds inside the black rectangle were removed in order to reveal the LCS underneath. See Figs. 15 and 17 for the geometry at other times during the transition.
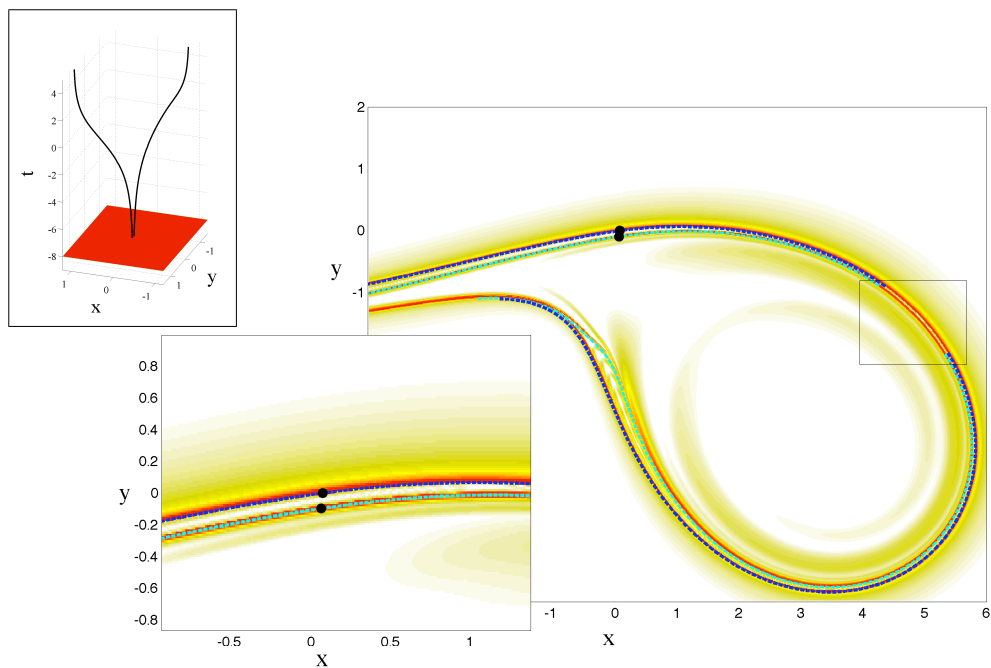
Fig. 17. The forward FTLE map (yellow/red shades) superimposed with the stable (blue, cyan) manifolds of two DHTs (black dots) computed in the flow (62) at $t=-8$. The FTLE field was computed with $T=25$ and the LCS, represented by the red ridges, were "extracted" by filtering the colour map. The manifolds inside the black rectangle were removed in order to reveal the LCS underneath. See Figs. 15 and 16 for the geometry at other times during the transition.
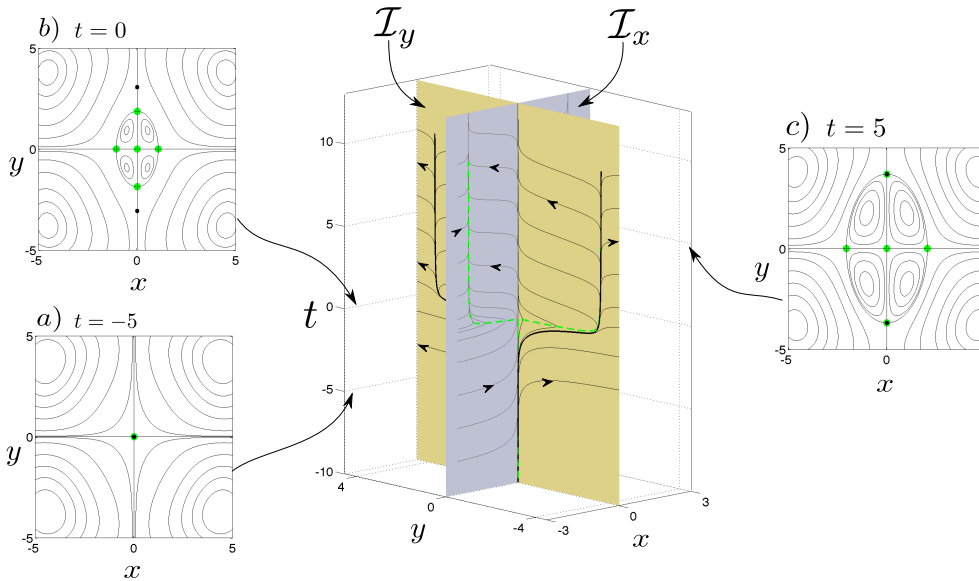
Fig. 18. centre Dynamics in the two invariant planes, $\mathcal{I}_x = \left\{(x, y, t) \in I\!\!R^2 \times I\!\!R : \quad y=0\right\}$ and $\mathcal{I}_y = \left\{(x, y, t) \in I\!\!R^2 \times I\!\!R : \quad x=0\right\}$, in the extended phase space of the flow associated with (67) with $\sigma(t)$ given by (72). The flow undergoes a transition associated with changes in finite-time stability properties of the trivial solution $\boldsymbol{x}(t)=0$ (see text). The Distinguished Hyperbolic Trajectories are marked by thick black lines and paths of instantaneous stagnation points (ISPs) are marked by dashed green lines (and by green dots in **a–c**). The dynamics in the invariant plane $\mathcal{I}_x$ corresponds to Scenario II in Sect. 3.1. (a–c) Instantaneous streamline patterns in the flow associated with (67) at three different times.
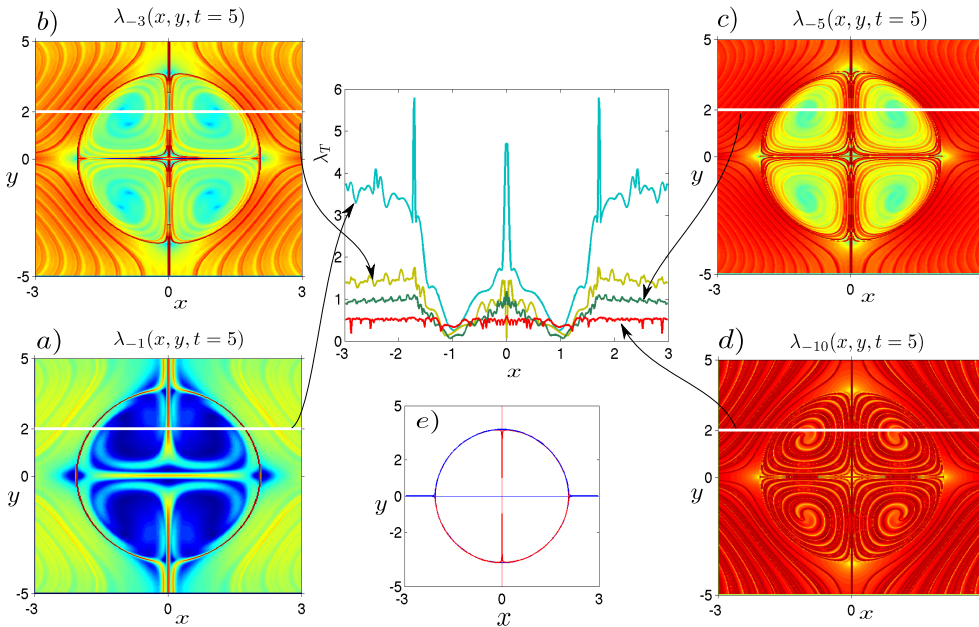
Fig. 19. Backward FTLE fields, $\lambda_T(x, y, t)$ cf. A.2, computed for the system (67) with $\sigma(t)$ given by (72) at $t=5$ and different integration time lengths **(a)** $|T|=1$, **(b)** $|T|=3$, **(c)** $|T|=5$, **(d)** $|T|=10$. 1-D cross sections of these fields along $(x, y=2)$ are shown in the central panel. The flow associated with (67) undergoes a transition which results in an emergence of four new eddies which are present in both the Eulerian and Lagrangian frameworks. Contrary to common intuition, the location of the strongest ridges in the FTLE fields varies with T and the overall strength of the ridges diminishes with T. This phenomenon is a direct consequence of the transition. Note also that the strongest ridge in **(d)**, located at $x=0$, is a "ghost" of the the dominant attracting structure before the transition. The stable manifolds (blue) and unstable manifolds (red) of four DHTs involved in this process are shown in **(e)**.

eight-eddy configuration (see Fig. 18). We use this setting to illustrate two issues affecting, respectively, the invariant manifold computations and the FTLE computations. Due to the type of transition considered here we are not able to identify DHTs throughout the time interval considered. The problem affecting the FTLE computations stems again from their non-uniqueness and the fact that, in this case, the FTLE fields computed for longer integration times show less pronounced ridges, detecting ghosts of pre-transition flow characteristics.

After a bit of algebra, one may notice that (67) has two invariant lines given by $y=0$ and $x=0$. Alternatively, in the extended phase space one may identify two invariant planes

$$\mathcal{I}_x = \{(x, y, t) \in \mathbb{R}^2 \times \mathbb{R} : \quad y = 0\}, \tag{68}$$

$$\mathcal{I}_y = \{(x, y, t) \in \mathbb{R}^2 \times \mathbb{R} : \quad x = 0\}. \tag{69}$$

Note further that the dynamics in $\mathcal{I}_x$ is given by

$$\begin{cases} \dot{x} = x\big(\sigma(t) - x^2\big)e^{-x^4/\delta^4} = x\big(\sigma(t) - x^2\big) + \mathcal{O}(x^5), \\ \dot{y} = 0, \end{cases} \tag{70}$$

and the dynamics in $\mathcal{I}_y$ is given by

$$\begin{cases} \dot{x} = 0, \\ \dot{y} = -y\big(\sigma(t) - \alpha\, y^2\big)e^{-y^4/\delta^4} \\ \quad = -y\big(\sigma(t) - \alpha\, y^2\big) + \mathcal{O}(y^5). \end{cases} \tag{71}$$

Clearly, we already analysed this type of 1-D dynamics in Sect. 3.1. In this example we will only consider the time-dependence that corresponds to Scenario II discussed in Sect. 3.1, i.e., we choose

$$\sigma(t) = 2\big(\text{atan}(10t) + \pi/2 - 1\big); \tag{72}$$

the remaining parameters in (66) are $\alpha=1/3$, $\beta=0.008/5$ and $\delta=5$.

With $\sigma(t)$ given by (72) so that $\sigma(t^*)=0$ at $t^*\approx0.0642$, one can easily see that within the plane $\mathcal{I}_x$ the trivial solution, $x(t)=0$, of (67) is pullback attracting (cf. 15 and Langa et al., 2006) on $I=(-\infty, t^*)$ and that it is repelling (in the sense of 7) on $I=(t^*, \infty)$. If we consider the dynamics within the invariant plane $\mathcal{I}_y$, the trivial solution is repelling on $I=(-\infty, t^*)$ and it is forwards attracting (cf. 13 and Langa et al., 2006) on $I=(t^*, \infty)$. Consequently, while $\boldsymbol{x}(t)=0$ is not hyperbolic on $\mathbb{R}$ (in the traditional, infinite-time sense) it is certainly finite-time hyperbolic on any time interval which does not contain t^*. Moreover, while for $J\subset(-\infty, t^*)$ any finite-time unstable manifold of $\boldsymbol{x}(t)=0$, i.e., $\mathbb{W}_J^u[\boldsymbol{x}(t)=0]$ (cf. Appendix B and Sect. 3.3.1), contains a subset of $\mathcal{I}_y$, for any $J\subset(t^*, \infty)$ the unstable manifold $\mathbb{W}_J^u[\boldsymbol{x}(t)=0]$ contains a subset of $\mathcal{I}_x$. The converse is true for the finite-time stable manifolds, $\mathbb{W}_J^s[\boldsymbol{x}(t)=0]$, for, respectively, $J\subset(-\infty, t^*)$ and $J\subset(t^*, \infty)$.

Similarly to the 1-D dynamics considered in Sect. 3.1, the changes in stability properties of the trivial solution are accompanied by a transition in the Lagrangian flow structure,

which is associated with changes in the geometry of certain distinguished, hyperbolic trajectories. Due to the presence of higher order terms in (70) and (71) we cannot compute the distinguished trajectories in a way analogous to (11). However, one can resort here to the iterative algorithm (cf. Appendix A and Ide et al., 2002; Ju et al., 2003) as in most other cases discussed in this work. Recall that, as it was shown in Ide et al. (2002); Ju et al. (2003), if the iterative algorithm converges, it returns a hyperbolic trajectory. Such a trajectory is branded "distinguished" if it is also bounded (cf. Definition A.5) on the considered time-interval[9]. Since we are concerned in this example with a system which is defined on $I=\mathbb{R}$ and asymptotically autonomous due to the form of (72), the obvious candidates for the location of the DHTs for $t\to\pm\infty$ are given by the hyperbolic stagnation points of the autonomous dynamical systems given respectively by (67) with $\sigma^*=\lim_{t\to\pm\infty}\sigma(t)$. One would then expect the existence of five DHTs after the transition and the presence of only one DHT before the transition. Since the DHTs are trajectories, they cannot bifurcate. Consequently, all of the five trajectories which would be branded "DHTs" after the transition must exist in the flow before the transition. For a given time interval $I\subset\mathbb{R}$ the finite-time DHTs can be located using the iterative algorithm provided that one can choose an initial guess, given by a C^1 finite-time hyperbolic path (see Definition A.4) which lies sufficiently close to the sought DHT (cf. Definition A17 in the Appendix A). Often, a satisfactory initial guess can be constructed from the paths of instantaneous stagnation points which are frozen-time hyperbolic. This strategy is also useful here for finding two DHTs contained in the invariant plane $\mathcal{I}_y$. However, due to the nature of the dynamics in $\mathcal{I}_x$ (which is identical with that considered in Scenario II of Sect. 3.1) we are unable to construct a guess on intervals containing t^* which would lie sufficiently close to the DHT. Identification of DHTs on intervals contained in (t^*, ∞) does not pose such difficulties but the outcome depends on the chosen time interval, i.e., the iterative algorithm converges onto different hyperbolic trajectories depending on the considered time interval. We compare the stable manifolds of the identified DHTs with ridges of FTLE fields computed for this flow in Fig. 19.

When attempting to characterise the flow associated with (67) and (72) using the FTLE fields, one can, as in the previous examples, identify the one-parameter family of FTLE fields, $\{\lambda_T(x, y, t)\}_{T\in\mathbb{R}}$, which are computed over different integration time intervals. Despite this non-uniqueness of the FTLE diagnostic, in most examples presented so far one could obtain good agreement between the invariant manifold calculations and the LCS obtained from

---

[9]Note that on a finite time interval this notion is non-unique since any trajectory of a smooth vector field is bounded on a bounded time interval. However, the ambiguities due to the non-uniqueness are, in general, only non-negligible near the end points of the time interval; cf. Ju et al. (2003); Ide et al. (2002).

λ_T for sufficiently large T. In this case, however, the situation is rather different and in many ways analogous to the 1-D configuration discussed in Sect. 3.1. In Fig. 19 we show results of backward FTLE computations at t=5 for the flow associated with (67) and $\sigma(t)$ given by (72). The panels (a–d) show results of computations over four different lengths of the integration time interval (a) $|T|$=1, (b) $|T|$=3, (c) $|T|$=5, (d) $|T|$=10; the central panel show 1-D cross-sections of these fields at $(x, y$=2). Three issues affecting the ridges of the shown FTLE fields are worth noting: (i) the geometry of the ridges (i.e., the LCS) and their connectivity changes with T, (ii) the relative and absolute strength of the ridges diminishes with T, (iii) for sufficiently long (backward) integration times the strongest ridge in the FTLE field corresponds to a "ghost" of the pre-transition flow structure (see y=0 in d). Consequently, in this case it is rather difficult to obtain a coherent picture of the flow structure based on the family, $\left\{\lambda_T(x, y, t)\right\}_{T \in \mathbb{R}}$, of FTLE's.

4 Conclusions

In this paper we have considered issues associated with the characterising the notion of hyperbolicity for aperiodically time-dependent vector fields that are only known on a finite time interval. We explored the concepts of finite-time hyperbolic trajectories, their finite time stable and unstable manifolds, as well as (one-parameter) families of finite-time Lyapunov exponent (FTLE) fields and associated Lagrangian coherent structures. Our approach has been to consider a collection of diverse examples where explicit phenomena can be exhibited and controlled.

In Sect. 3.1 we considered a 1-D vector field where the aperiodic time-dependence was specified in three distinct ways. This enabled us to probe the phenomenon of flow transitions and show how they may give rise to ambiguities in the effort to determine flow barriers from non-unique FTLE fields. Similarly, we used this configuration to illustrate issues associated with the lack of a unique, locally distinguished hyperbolic trajectories organising the structure of the flow. In Sect. 3.2.1 we considered two essentially dynamically opposite examples where the Lyapunov exponents of every trajectory could be determined analytically. In each example all Lyapunov exponents were identical, hence the FTLE fields did not give rise to LCSs. This highlighted the point that the emergence of LCSs is a consequence of spatial heterogeneity in the FTLE field and not just due to a rapid separation of nearby trajectories. In Sect. 3.3.1 we considered a velocity field exhibiting the strain-vortex-strain transition. This example illustrated some crucial issues associated with attempts to understand the nature of transport barriers in a transitioning flow in the finite-time setting. In this case, depending on the length and location of the "observation window", different diagnostics could be obtained

when employing the invariant manifold approach as compared with FTLE fields. In Sect. 3.3.2 we considered a double-gyre flow which has become a common benchmark flow in the LCS literature. We used this example to show that essentially the same information about the flow structure can be obtained from both techniques provided sufficient care is taken. This seems to be a common situation in flows which do not undergo transitions. We also illustrated there the sensitivity of the results to the order of the integrator used in computation of the trajectories as well as the importance of the cut-off level for the filtering procedure used in extracting LCSs. These conclusions and, in particular, the need for accurate trajectory integration, is further stressed in Sect. 3.3.3 where we considered an axisymmetric, time-dependent perturbation of the Hills spherical vortex. This flow serves as a good illustration of how inaccurate integration of flow trajectories can lead to plausible yet incorrect FTLE fields. The two closing examples, considered in Sect. 3.3.5 and 3.3.6, were linked to the 1-D examples discussed in Sect. 3.1. The kinematic model of an "eddy-pair system", discussed in Sect. 3.3.5, resembles a common feature in geophysical flows and both the invariant manifold and the FTLE methods yield correlated diagnostics of the flow structure in this case. The "eddy-quadrupole" system, discussed in Sect. 3.3.6, further highlights the problems that might arise when trying to select the most suitable FTLE field from the family parametrised by the integration time length. In particular, this example illustrates the ambiguities one may encounter when attempting to increase the length of the integration time interval in order to obtain longer (in the arc length sense) and more pronounced ridges in the FTLE field. Finally, in the appendices, we collect a number of technical details on finite-time hyperbolicity and its use in understanding fluid transport, as well as a detailed discussion of an important technical detail concerning the choice of the initial material segment for the computation of finite time stable and unstable manifolds of finite time hyperbolic trajectories.

The phenomena discovered and analysed in our examples point the way to a variety of directions for rigorous mathematical research in this rapidly developing, and important, new area of dynamical systems theory.

Appendix A

Some important definitions

In order to make the discussion presented in this paper relatively self-contained, we recapitulate here some fundamental notions and definitions which are important for the analysis presented in the preceding sections. All of the material included in this section can be found in existing literature and we provide references, which are not exhaustive, to some relevant material.

Consider a velocity field $\boldsymbol{v} : \mathbb{R}^n \times I \to \mathbb{R}^n$ defined over a time interval $I = [t_i, t_f] \subset \mathbb{R}$ and a system of ODE's

$$\dot{\boldsymbol{x}} = \boldsymbol{v}(\boldsymbol{x}, t), \quad \boldsymbol{x} \in \mathbb{R}^n, \quad t \in I. \tag{A1}$$

The curves, $\boldsymbol{\gamma}(t) : I \to \mathbb{R}^n$ that satisfy (A1), i.e., $\dot{\boldsymbol{\gamma}}(t) = \boldsymbol{v}(\boldsymbol{\gamma}(t), t)$, are referred to as $\mathbb{R}^n$−embedded trajectories of the non-autonomous dynamical system associated with $\boldsymbol{v}$ (other embeddings are possible; for example, $\tilde{\boldsymbol{\gamma}}(t) : I \to \mathbb{R}^n \times I$, but we do not require such notions here. Also, one could define the system (A1) in a subset $\mathcal{D} \subset \mathbb{R}^n$ but this is not important here.)

Consider now a transformation of the system (A1) to a frame moving along an arbitrary C^r ($r \geqslant 1$) path, $\tilde{\boldsymbol{x}}(t) : I \to \mathbb{R}^n$, given by

$$\dot{\boldsymbol{\xi}} = \hat{\mathbf{A}}_{\tilde{x}}(t)\, \boldsymbol{\xi} + \mathbf{f}_{\tilde{x}}(\boldsymbol{\xi}, t), \tag{A2}$$

where $\boldsymbol{\xi} = \boldsymbol{x} - \tilde{\boldsymbol{x}}$, $\hat{\mathbf{A}}_{\tilde{x}}(t)$ is the Jacobian of $\boldsymbol{v}(\boldsymbol{x}, t)$ evaluated at $\boldsymbol{x} = \tilde{\boldsymbol{x}}(t)$, i.e.,

$$\hat{\mathbf{A}}_{\tilde{x}}(t) = \partial_{\mathbf{x}} \boldsymbol{v}(\tilde{\boldsymbol{x}}(t), t), \tag{A3}$$

and

$$\mathbf{f}_{\tilde{x}}(\boldsymbol{\xi}, t) = \boldsymbol{v}(\boldsymbol{\xi} + \tilde{\boldsymbol{x}}(t), t) - \partial_{\mathbf{x}} \boldsymbol{v}(\tilde{\boldsymbol{x}}(t), t)\boldsymbol{\xi} - \dot{\tilde{\boldsymbol{x}}}(t). \tag{A4}$$

If $\tilde{\boldsymbol{x}} = \boldsymbol{\gamma}(t)$ is a trajectory of the system (A1), i.e., when $\dot{\boldsymbol{\gamma}}(t) = \boldsymbol{v}(\boldsymbol{\gamma}(t), t)$, then (A2) is homogeneous with $\mathbf{f}_{\gamma}(\boldsymbol{\xi}, t) \sim \mathcal{O}(\boldsymbol{\xi}^2)$, and the linearised equation

$$\dot{\boldsymbol{\xi}} = \hat{\mathbf{A}}_{\gamma}(t)\, \boldsymbol{\xi}, \tag{A5}$$

describes the dynamics in the neighbourhood of the trajectory $\boldsymbol{\gamma}(t)$ in the frame moving at speed $\dot{\boldsymbol{\gamma}}$.

Thus, if $\boldsymbol{\delta}_{t_i}$ denotes the perturbation of $\boldsymbol{\gamma}(t)$ at $t = t_i$, we find that it evolves according to

$$\|\boldsymbol{\delta}(t)\| = \sqrt{\langle \mathbf{X}(t, t_i)\boldsymbol{\delta}_{t_i}, \mathbf{X}(t, t_i)\boldsymbol{\delta}_{t_i} \rangle} \tag{A6}$$

$$= \sqrt{\langle \boldsymbol{\delta}_{t_i}, \mathbf{X}(t, t_i)^T \mathbf{X}(t, t_i)\boldsymbol{\delta}_{t_i} \rangle}, \tag{A7}$$

where $\Delta = \mathbf{X}(t, t_i)^T \mathbf{X}(t, t_i)$ is commonly referred to as the finite-time Cauchy-Green tensor. We let $\mathbf{X}(t, t_i)$ denote the fundamental solution matrix of (A5), i.e., it is the map $\mathbf{X}(t, t_i)(\cdot) : \mathbb{R}^n \to \mathbb{R}^n$ which is linear in $t_i \in I$ and Lipschitz in $t \in I$. Moreover, if $\boldsymbol{\xi}(t, \boldsymbol{\xi}_i, t_i)$ is a solution of (A5), then $\boldsymbol{\xi}(t, \boldsymbol{\xi}_i, t_i) = \mathbf{X}(t, t_i)\boldsymbol{\xi}_i$, and $\mathbf{X}(t, s)\mathbf{X}(s, t_i) = \mathbf{X}(t, t_i)$. Since Δ is real and symmetric, it can be diagonalised in an orthogonal basis of eigenvectors which denote the principal axes of growth of the infinitesimal perturbation. It then follows that the tensor

$$\mathcal{M} = \left(\mathbf{X}(t, t_i)^T \mathbf{X}(t, t_i)\right)^{1/2(t - t_i)}, \tag{A8}$$

is also diagonalisable in the same orthogonal basis. We note that an alternative definition of the Cauchy-Green tensor can

be given (e.g., Shadden et al., 2005) in terms of a flow map induced by (A1) defined as

$$\Phi_{t_i}^t : \mathbb{R}^n \to \mathbb{R}^n, \quad \boldsymbol{x}_{t_i} \mapsto \Phi_{t_i}^t(\boldsymbol{x}_{t_i}) = \boldsymbol{\gamma}(t, \boldsymbol{x}_{t_i}, t_i), \tag{A9}$$

where $\boldsymbol{\gamma}$ is a trajectory of (A1). Then, Δ can be expressed as

$$\Delta = \left(\partial_{\boldsymbol{x}} \Phi_{t_i}^t(\boldsymbol{x}_{t_i})\right)^T \partial_{\boldsymbol{x}} \Phi_{t_i}^t(\boldsymbol{x}_{t_i}), \tag{A10}$$

where $\partial_{\boldsymbol{x}} \Phi_{t_i}^t(\boldsymbol{x}_{t_i})$ denotes the Jacobian of $\Phi_{t_i}^t$ evaluated at $\boldsymbol{x}_{t_i}$. We used a 1-D variant of this definition in (4).

Definition A.1 (Finite-time Lyapunov exponents, $\lambda_T^i(\boldsymbol{x}, t)$)**.** The logarithms of the eigenvalues of $\mathcal{M}$ and are called the finite-time Lyapunov exponents computed at time t over the time interval T. If $T > 0$, $\lambda_T^i(\boldsymbol{x}, t)$ is called the i-th *forward* finite-time Lyapunov exponent. If $T < 0$, $\lambda_T^i(\boldsymbol{x}, t)$ is called the i-th *backward* finite-time Lyapunov exponent.

For more details regarding properties of Lyapunov exponents the reader is referred to (Katok and Hasselblatt, 1995; Lapeyre, 2002; Legras and Vautard, 1996), and for description of algorithms allowing their computation see, for example, (Dieci et al., 1997; Dieci and Eirola, 1999; Dieci and Vleck, 2002; Greene and Kim, 1987; Geist et al., 1990).

Definition A.2 (Finite-time Lyapunov exponent field, $\lambda_T(\boldsymbol{x}, t)$)**.** Assume that

$$\lambda_T^1(\boldsymbol{x}, t), \lambda_T^2(\boldsymbol{x}, t), \ldots, \lambda_T^n(\boldsymbol{x}, t), \tag{A11}$$

represent the finite-time Lyapunov exponents computed for a trajectory of (A1) passing through $\boldsymbol{x} \in \mathbb{R}^n$ at t. The scalar field

$$\lambda_T(\boldsymbol{x}, t) = \max \left[\lambda_T^1(\boldsymbol{x}, t), \lambda_T^2(\boldsymbol{x}, t), \ldots, \lambda_T^n(\boldsymbol{x}, t) \right], \tag{A12}$$

is called the finite-time Lyapunov exponent field at time t computed over a time interval of length T. If $T > 0$, it is called a forward FTLE field and if $T < 0$, it is called a backward FTLE field.

Definition A.3 (Finite-time exponential dichotomy)**.** We say that the linear Eq. (A5) has an *exponential dichotomy* on the finite time interval I if there exists a (constant) projection operator $\mathbf{P} \in \mathbb{R}^{n \times n}$, $\mathbf{P}^2 = \mathbf{P}$, and positive constants K, L, α, β such that (for $t, s \in I$):

$$|\mathbf{X}(t, t_i)\mathbf{P}\mathbf{X}^{-1}(s, t_i)| \leqslant K e^{-\alpha(t-s)}, \quad \text{for} \quad t \geqslant s,$$

$$|\mathbf{X}(t, t_i)(\mathbf{Id} - \mathbf{P})\mathbf{X}^{-1}(s, t_i)| \leqslant L e^{-\beta(s-t)}, \quad \text{for} \quad s \geqslant t. \tag{A13}$$

For more details see, for example, Coppel (1978); Henry (1981). The notion of a *generalised exponential dichotomy*, where $\mathbf{P}$ does not have to be constant, is discussed for example, in Zhang (1992). Numerical methods for calculating the constants $K, L, \alpha,$ and β are given in Dieci et al. (1997).

Using the notion of exponential dichotomy, we can provide one possible definition of finite-time hyperbolicity.

Definition A.4 (Finite-time hyperbolicity). We say that the path $\tilde{\boldsymbol{x}}(t) : I \rightarrow I\!\!R^n$ is *finite-time hyperbolic* on the interval I if the linearisation of the homogeneous part of (A2), given by

$$\dot{\boldsymbol{\xi}} = \partial_{\mathbf{x}} \boldsymbol{v}(\tilde{\boldsymbol{x}}(t), t) \, \boldsymbol{\xi}, \tag{A14}$$

has exponential dichotomy on I. Furthermore, if $\boldsymbol{\gamma}(t)$ is a trajectory of the system (A1), then $\boldsymbol{\gamma}$ is called a *finite-time hyperbolic trajectory* on the interval I if the equation (A5) has exponential dichotomy on I.

Remark: In the limit $t_i \rightarrow -\infty$, $t_f \rightarrow \infty$ and $\tilde{\boldsymbol{x}} = \boldsymbol{\gamma}(t)$, the above definition becomes equivalent to the standard notion of a hyperbolic trajectory.

Roughly speaking, finite-time hyperbolicity of a trajectory $\boldsymbol{\gamma}(t)$ implies that there exists a k-dimensional ($k \leqslant n$) subspace in $I\!\!R^n$ of solutions approaching $\boldsymbol{\gamma}$ at an exponential rate in forward time, and a $(n-k)$-dimensional subspace of solutions approaching $\boldsymbol{\gamma}$ at an exponential rate in backward time; no assumptions are made the about the fate of these neighbouring trajectories beyond I even if the velocity field $\boldsymbol{v}(\boldsymbol{x}, t)$ is known outside this interval.

Given a finite-time hyperbolic path, $\tilde{\boldsymbol{x}}(t)$, a corresponding finite-time hyperbolic trajectory can be derived using the techniques described in Ide et al. (2002); Ju et al. (2003). This is accomplished by considering (A1) in a frame "moving" with $\tilde{\boldsymbol{x}}$ (cf. A2). It can be easily checked that the particular solution of (A2) satisfies the following integral equation

$$\boldsymbol{y}(t) = \mathbf{X}(t, t_i) \int_{t_i}^{t} \mathbf{P} \mathbf{X}^{-1}(s, t_i) \mathbf{f}(\boldsymbol{y}(s), s) \mathrm{d}s \tag{A15}$$
$$- \mathbf{X}(t, t_i) \int_{t}^{t_f} (\mathbf{Id} - \mathbf{P}) \mathbf{X}^{-1}(s, t_i) \mathbf{f}(\boldsymbol{y}(s), s) \mathrm{d}s,$$

where $\mathbf{P}$ is the projection operator associated with the exponential dichotomy (A13) and $\mathbf{X}$ is the fundamental solution matrix associated with the linearisation of the homogeneous part of (A2). Furthermore, using very similar techniques to those employed in Ju and Wiggins (2001), it can be shown that, for given $\tilde{\boldsymbol{x}}(t)$, the solution of (A15) is finite-time hyperbolic and unique on the time interval I provided that the following holds for all $t \in I$:

$$\|\boldsymbol{v}(\boldsymbol{y}(t) + \tilde{\boldsymbol{x}}(t), t) - \partial_{\mathbf{x}} \boldsymbol{v}(\tilde{\boldsymbol{x}}(t), t) \boldsymbol{y}(t) - \dot{\tilde{\boldsymbol{x}}}(t)\|_{\infty} < \infty, \tag{A16}$$

and

$$\|\partial_{\mathbf{x}} \boldsymbol{v}(\boldsymbol{y}(t) + \tilde{\boldsymbol{x}}(t), t) - \partial_{\mathbf{x}} \boldsymbol{v}(\tilde{\boldsymbol{x}}(t), t)\|_{\infty} < \left(\frac{K}{\alpha} + \frac{L}{\beta}\right)^{-1}. \tag{A17}$$

The constants K, L, α, β are associated with the exponential dichotomy of the linear part of (A2) (cf. Definition A.3).

Definition A.5 (Distinguished, Finite-time Hyperbolic Trajectory.). Let $\tilde{\boldsymbol{x}}(t)$ be a finite-time hyperbolic path which does not have an exponential component within $I \subset I\!\!R$. A trajectory $\boldsymbol{\gamma}(t)$ of the system (A1) is called a *Finite-time Distinguished Hyperbolic Trajectory* if it can be represented as $\boldsymbol{\gamma}(t) = \boldsymbol{y}(t) + \tilde{\boldsymbol{x}}(t)$ where $\boldsymbol{y}(t)$ satisfies the integral Eq. (A15) subject to the conditions (A16) and (A17), and the path $\tilde{\boldsymbol{x}}$ is finite-time hyperbolic within I.

Remarks. Two issues are worth mentioning here:

(i) The notion of a distinguished, finite-time hyperbolic trajectory is, in general, non-unique on any finite time (or semi-finite) interval.

(ii) The finite-time hyperbolic path $\tilde{\boldsymbol{x}}(t)$ used in Definition A.5 can be given, in particular, by a path of *Instantaneous stagnation points* (ISPs) which are frozen-time hyperbolic (cf. Definition A.6). Given the velocity field $\boldsymbol{v}$: $I\!\!R^n \times I \rightarrow I\!\!R^n$, a path of ISPs is given by a continuous curve, $\boldsymbol{x}_{\mathrm{isp}}: I \rightarrow I\!\!R^n$, $t \mapsto \boldsymbol{x}_{\mathrm{isp}}(t)$, such that

$$\boldsymbol{v}(\boldsymbol{x}_{\mathrm{isp}}(t), t) = 0, \qquad t \in \tilde{I}, \tag{A18}$$

where $\tilde{\mathcal{T}} \subset I$ is a time interval within which the Jacobian, $\partial_{\mathbf{x}} \boldsymbol{v}(\boldsymbol{x}_{\mathrm{isp}}(t), t)$, does not vanish, as required by the Implicit Function Theorem for the existence of a solution to (A18).

Definition A.6 (Frozen-time hyperbolicity). We say that the path of instantaneous stagnation points, $\boldsymbol{x}_{\mathrm{isp}}(t)$ is *frozen-time hyperbolic* on the interval I if the eigenvalues of the Jacobian, $\partial_{\mathbf{x}} \boldsymbol{v}(\boldsymbol{x}_{\mathrm{isp}}(t), t)$, in (A2) have non-zero real parts for any fixed $t \in I$.

Remark. A frozen-time hyperbolic path of ISPs, $\boldsymbol{x}_{\mathrm{isp}}(t)$, is also finite-time hyperbolic if Eq. (A14) with $\tilde{\boldsymbol{x}}(t) = \boldsymbol{x}_{\mathrm{isp}}(t)$ has (finite-time) exponential dichotomy. This generally requires $\partial_{\mathbf{x}} \boldsymbol{v}(\tilde{\boldsymbol{x}}_{\mathrm{isp}}(t), t)$ to be sufficiently slowly varying (see Coppel, 1978, Propositions 1–2, p. 50, 52). A numerical approach to solving this problem was described in Ide et al. (2002) (see also Ju et al., 2003). The method is based on a numerical determination of the finite-time Lyapunov exponents in a frame where the linear part of (A2) is given by a diagonal matrix with constant coefficients.

Definition A.7 (Rate-of-strain tensor). The symmetric part

$$\hat{\mathbf{S}}_{\gamma}(t) = \frac{1}{2}[\hat{\mathbf{A}}_{\gamma}(t) + \hat{\mathbf{A}}_{\gamma}(t)^T], \tag{A19}$$

of $\hat{\mathbf{A}}_{\gamma}(t) = \partial_{\mathbf{x}} \boldsymbol{v}(\boldsymbol{\gamma}(t), t)$ is called the *rate of strain tensor*.

The rate of strain tensor describes the growth or decay of solutions $\boldsymbol{\xi}(t)$ of the linearised system (A5). This can be seen by directly evaluating $\mathrm{d}\|\boldsymbol{\xi}(t)\|^2/\mathrm{d}t$, i.e.,

$$\frac{\mathrm{d}}{\mathrm{d}t}\|\boldsymbol{\xi}(t)\|^2 = \frac{\mathrm{d}}{\mathrm{d}t}\langle \boldsymbol{\xi}(t), \boldsymbol{\xi}(t)\rangle \tag{A20}$$
$$= \langle \boldsymbol{\xi}(t), [\hat{\mathbf{A}}_{\gamma}(t) + \hat{\mathbf{A}}_{\gamma}(t)^T]\boldsymbol{\xi}(t)\rangle = 2\langle \boldsymbol{\xi}(t), \hat{\mathbf{S}}(t)\boldsymbol{\xi}(t)\rangle,$$

where $\langle \cdot, \cdot \rangle$ denotes the canonical inner product on $I\!\!R^n$,

which induces the canonical norm $\|\boldsymbol{\xi}\|=\sqrt{\langle\boldsymbol{\xi},\boldsymbol{\xi}\rangle}$ in $I\!R^n$. Thus, if $\hat{\mathbf{S}}(t)$ is negative definite, all solutions of the linearised system are strictly monotonically decaying (in the sense of their norm) to the trivial solution. When $\hat{\mathbf{S}}(t)$ is positive definite, all solutions of the linearised system are strictly monotonically growing (in the sense of their norm). If the strain tensor is indefinite or semi-definite one can define the following set:

Definition A.8 (Zero-strain set, cf. Haller, 2001b)**.** The set

$$Z_\gamma(t) = \left\{ \boldsymbol{\xi} \in I\!R^n : \langle \boldsymbol{\xi}, \hat{\mathbf{S}}_\gamma(t)\boldsymbol{\xi} \rangle = 0 \right\}, \qquad (A21)$$

is called the *zero-strain set* associated with linearisation about $\boldsymbol{\gamma}(t)$.

Definition A.9 (Strain acceleration tensor; or Cotter-Rivlin tensor)**.** The time-dependent operator

$$\hat{\mathbf{M}}_\gamma(t) = \frac{\mathrm{d}}{\mathrm{d}t}\hat{\mathbf{S}}_\gamma(t) + \hat{\mathbf{S}}_\gamma(t)\hat{\mathbf{A}}_\gamma(t) + \hat{\mathbf{A}}_\gamma(t)^T\hat{\mathbf{S}}_\gamma(t), \qquad (A22)$$

is called the *strain acceleration tensor* associated with the linearisation of (A1) about $\boldsymbol{\gamma}(t)$. The strain acceleration tensor is associated with the second derivative of $\|\boldsymbol{\xi}(t)\|$, i.e.,

$$\frac{\mathrm{d}^2}{\mathrm{d}t^2}\|\boldsymbol{\xi}(t)\|^2 = \frac{\mathrm{d}}{\mathrm{d}t}\langle\boldsymbol{\xi}(t),\hat{\mathbf{S}}_\gamma(t)\boldsymbol{\xi}(t)\rangle = \langle\boldsymbol{\xi}(t),\hat{\mathbf{M}}_\gamma(t)\boldsymbol{\xi}(t)\rangle. \qquad (A23)$$

The restriction of $\hat{\mathbf{M}}_\gamma$ to the zero-strain set is denoted by $\hat{\mathbf{M}}_\gamma^Z$.

For $n=2$ and $\nabla\cdot\boldsymbol{v}=0$ in (A1), i.e., the case associated with unsteady and incompressible 2-D flows, the characteristics of $\hat{\mathbf{S}}_\gamma$ and $\hat{\mathbf{M}}_\gamma^Z$ were used in Haller (2001b) to partition $I\!R^2$ into time-dependent regions containing system trajectories with distinct stability properties. (Some generalisations of this framework to $n=3$ were discussed in Haller, 2005.) The following definition (see Duc and Siegmund, 2008) extends the dynamic partition of $I\!R^2$ to the compressible flow setting:

Definition A.10 (Dynamic partition of $I\!R^2$)**.** Consider the extended phase space, $I\!R^2 \times I$, associated with the flow induced by (A1). For each $t\in I$ one can define the following sets

(i) Attracting region:
$$\mathcal{A}(t) = \{\boldsymbol{x} \in I\!R^2 : \hat{\mathbf{S}}_x(t) \text{ is negative definite}\},$$

(ii) Repelling region:
$$\mathcal{R}(t) = \{\boldsymbol{x} \in I\!R^2 : \hat{\mathbf{S}}_x(t) \text{ is positive definite}\},$$

(iii) Elliptic region:
$$\mathcal{E}(t) = \{\boldsymbol{x} \in I\!R^2 : \quad \hat{\mathbf{S}}_x(t) \text{ is indefinite},$$
$$\hat{\mathbf{M}}_x^Z(t) \text{ is indefinite } \},$$

(iv) Hyperbolic region:
$$\mathcal{H}(t) = \{\boldsymbol{x} \in I\!R^2 : \quad \hat{\mathbf{S}}_x(t) \text{ is indefinite},$$
$$\hat{\mathbf{M}}_x^Z(t) \text{ is positive definite} \},$$

(iii) Quasi-hyperbolic region:
$$\mathcal{Q}(t) = \{\boldsymbol{x} \in I\!R^2 : \quad \hat{\mathbf{S}}_x(t) \text{ is indefinite},$$
$$\hat{\mathbf{M}}_x^Z(t) \text{ is negative definite } \},$$

(iii) Degenerate region:
$$\mathcal{D}(t) = I\!R^2 \backslash [\mathcal{A}(t) \cup \mathcal{R}(t) \cup \mathcal{E}(t) \cup \mathcal{H}(t) \cup \mathcal{Q}(t)]\}.$$

Definition A.11 (Finite-time hyperbolicity based on the dynamic partition; Haller, 2001b)**.** Assume that $n=2$ in (A1) and that the velocity field satisfies $\nabla \cdot \boldsymbol{v}=0$. A trajectory $\boldsymbol{\gamma}(t) : I \rightarrow I\!R^2$ of (A1) is called *finite-time hyperbolic* on the interval I if

(i) $\boldsymbol{\gamma}(t)$ intersects $\mathcal{D}(I)$ at isolated points.

(ii) If $I_\mathcal{E}$ denotes a time interval that the trajectory spends in $\mathcal{E}(I)$, then

$$\int_{I_\mathcal{E}} \sqrt{2}|\hat{\mathbf{S}}_\gamma(t)|\mathrm{d}t < \frac{\pi}{2}, \qquad (A24)$$

where

$$|\hat{\mathbf{S}}| = \sqrt{\sum_{i,j=1}^{2} |\hat{S}_{ij}|^2} \,.$$

The condition (ii) implies that if $\boldsymbol{\gamma}(t)$ is finite-time hyperbolic, its finite-time stable and unstable manifolds of are nonempty. See Haller (2001b) for details. See also Appendix B and (Duc and Siegmund, 2008, Theorem 42).

Appendix B

On the choice of the initial material segment in numerical computations of stable and unstable manifolds of (finite-time) hyperbolic trajectories.

We briefly discuss here the problem of approximating stable and unstable manifolds of flow trajectories which are finite-time hyperbolic (see Definitions A.4 and A.11).

Consider the linearisation (A5) of the dynamical system (A1) about a system trajectory (i.e., $\boldsymbol{x}=\boldsymbol{\xi}+\boldsymbol{\gamma}(t)$ and $\dot{\boldsymbol{\gamma}}(t)=\boldsymbol{v}(\boldsymbol{\gamma}(t),t)$ for $t\in I$. In such a case the the stability properties of the trivial solution, $\boldsymbol{\xi}(t)=0$, of (A5) correspond to the linear stability properties of $\boldsymbol{\gamma}(t)$ in (A1). As already noted in Sect. 3.3.1, if the system (A1) is only known (or defined) on a bounded interval $I\subset I\!R$, it is not possible to define the stable and unstable manifolds of $\boldsymbol{\xi}(t)=0$ in the traditional "infinite-time" sense (even the trivial solution of the system (A5) considered on $I=I\!R$ is hyperbolic). In the finite-time setting one can define the following two flow-invariant, "stable" and "unstable" sets of the linearised equation (A5) (see Duc and Siegmund, 2008 for a more general treatment in the nonlinear case): The finite-time stable set of the trivial solution of (A5) on I, $\boldsymbol{\xi}(t)=0$, is given in the extended phase

space, $\mathcal{S}=I\!\!R^2 \times I$, by

$$\mathbb{W}_I^s[\boldsymbol{\xi}=0] = \left\{ (\boldsymbol{\xi}_t, t) \in \mathcal{S}: \ \frac{\mathrm{d}}{\mathrm{d}m}\|\mathbf{X}(m, t)\boldsymbol{\xi}_t\| < 0, \ \forall\, m \in I \right\}, \quad \text{(B1)}$$

and the finite-time unstable set of $\boldsymbol{\xi}(t)=0$ on I is defined, for $t \in I$, as

$$\mathbb{W}_I^u[\boldsymbol{\xi}=0] = \left\{ (\boldsymbol{\xi}_t, t) \in \mathcal{S}: \ \frac{\mathrm{d}}{\mathrm{d}m}\|\mathbf{X}(m, t)\boldsymbol{\xi}_t\| > 0, \ \forall\, m \in I \right\}, \quad \text{(B2)}$$

where $\mathbf{X}$ is the fundamental solution matrix associated with (A5) and $\|\cdot\|$ is the norm induced by the canonical inner product on $I\!\!R^2$, i.e., $\|\boldsymbol{x}\|=\sqrt{\langle \boldsymbol{x}, \boldsymbol{x}\rangle}$. The instantaneous geometry of (B1) and (B2) is given by

$$\mathbb{W}_I^s[\boldsymbol{\xi}=0](t) = \left\{ \boldsymbol{\xi}_t \in I\!\!R^2: \ \frac{\mathrm{d}}{\mathrm{d}m}\|\mathbf{X}(m, t)\boldsymbol{\xi}_t\| < 0, \ \forall\, m \in I \right\}, \quad \text{(B3)}$$

and

$$\mathbb{W}_I^u[\boldsymbol{\xi}=0](t) = \left\{ \boldsymbol{\xi}_t \in I\!\!R^2: \ \frac{\mathrm{d}}{\mathrm{d}m}\|\mathbf{X}(m, t)\boldsymbol{\xi}_t\| > 0, \ \forall\, m \in I \right\}, \quad \text{(B4)}$$

referred to as t-fibres of $\mathbb{W}_I^s[\boldsymbol{\xi}=0]$ and $\mathbb{W}_I^u[\boldsymbol{\xi}=0]$ respectively.

In contrast to the classical (time asymptotic) definition of stable and unstable manifolds, the finite-time counterparts, $\mathbb{W}_I^u$ and $\mathbb{W}_I^s$, have the dimension of the extended phase space (rather than a lower dimension) and their t-fibres are open sets in $I\!\!R^n$. If $\boldsymbol{\xi}(t)=0$ is finite-time hyperbolic on I, these sets are nonempty. In such a case, a common approach used in the invariant-manifold Lagrangian transport analysis is to choose (non-unique) segments of initial conditions of length $\alpha \ll 1$, $\mathfrak{U}_{t_a}^\alpha$ and $\mathfrak{S}_{t_a}^\alpha$, containing the trivial solution of the linearised system and follow their forwards and backward time evolution. We show below (cf. Proposition B.2) how to choose the (non-unique) material segments in such a way that they are contained in, respectively, the finite-time stable and unstable manifolds of the linearised system (A5).

Recall first that the trivial solution $\boldsymbol{\xi}(t)=0$ of the linearised equation corresponds to $\boldsymbol{\gamma}(t)$ of (A1). If $\boldsymbol{\gamma}(t) \in \mathcal{H}(t)$ for all $t \in I$, then the (symmetric) rate of strain tensor, $\hat{\mathbf{S}}_\gamma(t)$, is indefinite on I (see Definition A.10) so that the zero-strain set contains two orthogonal lines for each $t \in I$, and it is given by

$$Z_\gamma(t) = \big\{ \boldsymbol{z}_1, \boldsymbol{z}_2 \in I\!\!R^2: \ \langle \boldsymbol{z}_1(t), \boldsymbol{z}_2(t)\rangle = 0,$$

$$\langle \boldsymbol{z}_1(t), \hat{S}_\gamma(t)\boldsymbol{z}_2(t)\rangle = 0\big\}. \quad \text{(B5)}$$

We now define a subset of nondecreasing solutions at t as

$$\Psi^+(t) = \left\{ \boldsymbol{\xi}_t \in I\!\!R^2: \ \frac{\mathrm{d}}{\mathrm{d}m}\|\mathbf{X}(m, t)\boldsymbol{\xi}_t\|\Big|_{m=t} \geqslant 0 \right\}, \quad \text{(B6)}$$

a subset of nonincreasing solutions at t in as

$$\Psi^-(t) = \left\{ \boldsymbol{\xi}_t \in I\!\!R^2: \ \frac{\mathrm{d}}{\mathrm{d}t}\|\mathbf{X}(m, t)\boldsymbol{\xi}_t\|\Big|_{m=t}\| \leqslant 0 \right\}, \quad \text{(B7)}$$

so that $\Psi^+(t) \cap \Psi^-(t) = Z_\gamma(t)$. Moreover, for $\boldsymbol{\gamma}(t) \in \mathcal{H}(t)$ the restriction of the strain acceleration tensor to $Z_\gamma(t)$, $\hat{\mathbf{M}}_\gamma^Z(t)$, is positive definite, i.e., $\langle \boldsymbol{\xi}_1(t), \hat{\mathbf{M}}(t)\boldsymbol{\xi}_1(t)\rangle > 0$ and $\langle \boldsymbol{\xi}_2(t), \hat{\mathbf{M}}(t)\boldsymbol{\xi}_2(t)\rangle > 0$ which, based on (A23), implies that solutions, $\boldsymbol{\xi}(t, \boldsymbol{\xi}_{t^*}, t^*)$, $\boldsymbol{\xi}_{t^*} \in Z_\gamma(t^*)$, of (A5) cross the zero strain set $Z_\gamma(t^*)$ at $t=t^*$ from the region of decreasing norm to the region of increasing norm.

Proposition B.1. Consider a trajectory $\boldsymbol{\gamma}(t)$ of (A1) and the corresponding trivial solution, $\boldsymbol{\xi}(t)=0$, of the linearised system (A5) on $I=[t_a, t_b]$ with the fundamental solution matrix $\mathbf{X}(t, t_a)$. The finite-time unstable set, $\mathbb{W}_I^u[\boldsymbol{\xi}=0]$ and the finite-time stable set, $\mathbb{W}_I^s[\boldsymbol{\xi}=0]$ are invariant under the action of $\mathbf{X}(t, t_a)$. Moreover, if $\boldsymbol{\gamma}(t) \in \mathcal{H}(t)$ for $t \in I$, the set $\Psi_I^+ = \{\boldsymbol{\xi} \in I\!\!R^2: \ \exists\, t \in I, \ \boldsymbol{\xi} \in \Psi^+(t)\}$ is forward-time invariant and the set $\Psi_I^- = \{\boldsymbol{\xi} \in I\!\!R^2: \ \exists\, t \in I, \ \boldsymbol{\xi} \in \Psi^-(t)\}$ is backward time invariant. In particular, $\mathbb{W}_I^u[\boldsymbol{\xi}=0](t_a) = \Psi^+(t_a)$ and $\mathbb{W}_I^s[\boldsymbol{\xi}=0](t_b) = \Psi^-(t_b)$.

Proof. The invariance of $\mathbb{W}_I^u[\boldsymbol{\xi}=0]$ and $\mathbb{W}_I^s[\boldsymbol{\xi}=0]$, as well as the forward-time invariance of $\Psi^+(t)$ and the backward-time invariance of $\Psi^-(t)$, was discussed in Duc and Siegmund (2008), cf. Remark 23, Theorem 44. In order to show that $\mathbb{W}_I^u[\boldsymbol{\xi}=0](t_a) = \Psi^+(t_a)$ we appeal to the forward invariance of $\Psi^+(t)$ under the action of $\mathbf{X}(t, t_a)$.

Assume first that the opposite holds, i.e., that $\boldsymbol{\xi}_{t^*} \in \Psi^+(t^*)$ and that $\boldsymbol{\xi}(t^{**}, \boldsymbol{\xi}_{t^*}, t^*) \notin \Psi^+(t^{**})$ for $t^* < t^{**}$, $t^*, t^{**} \in I$. Due to continuity of $\boldsymbol{\xi}(t)$, the trajectory has to cross the zero strain set at some time $t^* < t^\times < t^{**}$ which requires that $\boldsymbol{\xi}(t^\times, \boldsymbol{\xi}_{t^*}, t^*) \in Z_\gamma(t^\times)$ and

$$\frac{\mathrm{d}^2}{\mathrm{d}t^2}\|\boldsymbol{\xi}(t, \boldsymbol{\xi}_{t^*}, t^*)\|\Big|_{t=t^\times} = \langle \boldsymbol{\xi}(t^\times), \hat{\mathbf{M}}(t^\times)\boldsymbol{\xi}(t^\times)\rangle < 0, \quad \text{(B8)}$$

which contradicts the fact that if $\boldsymbol{\gamma}(t) \in \mathcal{H}(t)$ for $t \in I$, $\hat{\mathbf{M}}(t)$ is positive definite on $Z_\gamma(t)$ for $t \in I$. Consequently, if $\boldsymbol{\gamma}(t) \in \mathcal{H}(t)$ and $\boldsymbol{\xi}_{t^*} \in \Psi^+(t^*)$, then $\boldsymbol{\xi}(t) \in \Psi^+(t)$ for $t > t^*$, t, $t^* \in I$, which implies that Ψ^+ is forward-time invariant on I. Note that Ψ^+ is not backward time invariant. In order to see this, it is sufficient to consider trajectories crossing the zero strain set, $Z_\gamma(t^*)$, at $t^* \in (t_a, t_b)$. Since $\partial \Psi^+(t^*) = Z_\gamma(t^*)$, any trajectory $\boldsymbol{\xi}(t, \boldsymbol{\xi}_{t^*}, t^*)$, $\boldsymbol{\xi}_{t^*} \in Z_\gamma(t^*)$ leaves Ψ^+ for $t < t^*$ in backward time. We finally note that the set $\Psi^+(t_a)$ is invariant under the action of $\mathbf{X}(t, t_a)$, which implies that $\Psi^+(t_a) \subset \mathbb{W}_I^u[\boldsymbol{\xi}=0](t_a)$. However, based on Definitions (B6) and (B3) it is clear that $\mathbb{W}_I^u[\boldsymbol{\xi}=0](t) \subset \Psi^+(t)$, which implies that $\Psi^+(t_a) = \mathbb{W}_I^u[\boldsymbol{\xi}=0](t_a)$. Similar procedure can be used in backward time to show that Ψ^- is backward-time invariant on I. $\square$

Proposition B.2. Consider the linearised flow (A5) over the time interval I so that the trivial solution is finite-time hyperbolic on I (in the sense that $\boldsymbol{\gamma}(t) \in \mathcal{H}$ for $t \in I$). If the material segments, $\mathfrak{U}_{t_a}^\alpha$, $\mathfrak{S}_{t_b}^\alpha$, are chosen as

$$\mathfrak{U}_{t_a}^\alpha = \left\{ \boldsymbol{x} \in I\!\!R^2: \ \boldsymbol{x} = \beta \boldsymbol{S}^+(t_a), \quad \beta \in \left[-\frac{\alpha}{2}, \frac{\alpha}{2} \right] \subset I\!\!R \right\}, \quad \text{(B9)}$$

and

$$\mathfrak{S}_{t_b}^\alpha = \left\{ \boldsymbol{x} \in I\!R^2 : \ \boldsymbol{x} = \beta \boldsymbol{S}^-(t_b) \quad \beta \in \left[-\frac{\alpha}{2}, \ \frac{\alpha}{2} \right] \subset I\!R \right\}, \quad (B10)$$

where $\boldsymbol{S}^+(t)$ and $\boldsymbol{S}^-(t)$ are the eigenvectors of the rate of strain tensor, $\hat{\mathbf{S}}(t)$, corresponding to the eigenvalues $\mathfrak{s}^+(t) > 0$, $\mathfrak{s}^-(t) < 0$. Then, $\mathfrak{U}_{t_a}^\alpha \subset \mathbb{W}_{t_a}^u [\boldsymbol{\xi} = 0]$ and $\mathfrak{S}_{t_a}^\alpha \subset \mathbb{W}_{t_b}^s [\boldsymbol{\xi} = 0]$.

Proof. For any point $\mathfrak{u}_{t_a} = \beta \boldsymbol{S}^+(t_a) \in \mathfrak{U}_{t_a}^\alpha$, $|\beta| \leqslant \alpha/2$, we have

$$\langle \mathfrak{u}_{t_a}, \hat{\mathbf{S}}(t_a) \mathfrak{u}_{t_a} \rangle > 0, \quad (B11)$$

which implies that $\mathfrak{u}_{t_a} \in \Psi^+(t_a) = \mathbb{W}_I^u [\boldsymbol{\xi} = 0] (t_a)$. The invariance of the unstable manifold $\mathbb{W}_I^u [\boldsymbol{\xi} = 0]$ implies that $\boldsymbol{\xi} (t, \mathfrak{u}_{t_a}, t_a) \in \mathbb{W}_I^u [\boldsymbol{\xi} = 0] (t)$ for $t \in I$. Similarly, for any point

$$\mathfrak{s}_{t_b} = \beta \boldsymbol{S}^-(t_a) \in \mathfrak{S}_{t_a}^\alpha, |\beta| \leqslant \alpha/2,$$

we have

$$\langle \mathfrak{s}_{t_b}, \hat{\mathbf{S}}(t_b) \mathfrak{s}_{t_b} \rangle < 0, \quad (B12)$$

which implies that $\mathfrak{s}_{t_b} \in \Psi^-(t_b) = \mathbb{W}_I^s [\boldsymbol{\xi} = 0] (t_b)$. The invariance of the stable manifold, $\mathbb{W}_I^s [\boldsymbol{\xi} = 0]$, implies that $\boldsymbol{\xi} (t, \mathfrak{s}_{t_b}, t_b) \in \mathbb{W}_I^u [\boldsymbol{\xi} = 0] (t)$ for $t \in I$. $\square$

Note finally that, due to the the embedding property of finite-time stable and unstable manifolds (see Duc and Siegmund, 2008, Theorem 37, p. 659), the stable and unstable manifolds of $\boldsymbol{\xi}(t) = 0$, for two time intervals I, J, such that $I \subset J$, satisfy the following

$$\mathbb{W}_I^s \subset \mathbb{W}_J^s \quad \text{and} \quad \mathbb{W}_I^u \subset \mathbb{W}_J^u. \quad (B13)$$

Thus, the effect of the non-unique choice of the initial material segments diminishes with the length of the considered time interval, provided that the considered trajectory is finite-time hyperbolic on I.

References

Acrivos, A., Aref, H., and Ottino, J. M. (Eds.): Symposium on Fluid Mechanics of Stirring and Mixing, Part 2, Phys. Fluids A, 3(5), 1009–1469, 1991.

Alam, M.-R., Liu, W., and Haller, G.: Closed-loop separation control: An analytic approach, Phys. Fluids, 158, 18(4), 043601, doi 10.1063/1.2188267, 2006.

Aref, H. and El Naschie, M. S. (Eds.): Chaos Applied to Fluid Mixing, Chaos Soliton. Fract., 4(6), 370 pp., 1994.

Arnold, V. and Avez, A.: Ergodic Problems of Classical Mechanics, W.A. Benjamin Inc., 1968.

Babiano, A., Provenzale, A., and Vulpiani, A. (Eds.): Chaotic Advection, Tracer Dynamics, and Turbulent Dispersion, in: Proceedings of the NATO Advanced Research Workshop and EGS Topical Workshop on Chaotic Advection, Conference Centre Sereno di Gavo, Italy, 24–28 May 1993, Physica D, vol. 76, 329 pp., 1994.

Baldoma, I. and Fontich, E.: Stable manifolds associated to fixed points with linear part equal to identity, J. Differ. Equations, 197, 45–72, 2004.

Baldoma, I., Fontich, E., de la Llave, R., and Martin, P.: The parametrization method for one-dimensional invariant manifolds of higher dimensional parabolic fixed points, Discrete Cont. Dyn. S., 17, 835–865, 2007.

Batchelor, G. K.: An Introduction to Fluid Dynamics, Cambridge University Press, Cambridge, 1967.

Berger, A., Son, D. T., and Siegmund, S.: Nonautonomous finite-time dynamics, Discrete Cont. Dyn. B, 9, 463–492, 2008.

Boffetta, G., Lacorata, G., Redaelli, G., and Vulpiani, A.: Detecting barriers to transport: a review of different techniques, Physica D, 159, 58–70, 2001.

Bonckaert, P. and Fontich, E.: Invariant manifolds of dynamical systems close to a rotation: Transverse to the rotation axis, J. Differ. Equations, 214, 128–155, 2005.

Bowen, R.: Symbolic Dynamics for Hyperbolic Flows, Am. J. Math., 95, 429–460, 1973.

Bowen, R. and Ruelle, D.: The ergodic theory of axiom A flows, Invent. Math, 29, 181–202, 1975.

Brown, G. L. and Roshko, A.: Density effect and large structure in turbulent mixing layers, J. Fluid Mech., 64, 775–816, 1974.

Casasayas, J., Fontich, E., and Nunes, A.: Invariant manifolds for a class of parabolic points, Nonlinearity, 5, 1193–1210, 1992.

Casasayas, J., Faisca, J., and Nunes, A.: Melnikov method for parabolic orbits, NODEA-Nonlinear Diff., 10, 119–131, 2003.

Cicogna, G. and Santoprete, M.: Nonhyperbolic homoclinic chaos, Phys. Lett. A, 256, 25–30, 1999.

Coddington, E. A. and Levinson, N.: Theory of Ordinary Differential Equations, McGraw-Hill, New York, 1955.

Coppel, W. A.: Dichotomies in Stability Theory, in: Lecture Notes in Mathematics, Springer-Verlag, New York, Heidelberg, Berlin, 629, 97 pp., 1978.

Dabiri, J. O.: LCS MATLAB Kit, available at: http://dabiri.caltech.edu/software.html, last access: 2009.

de Blasi, F. S. and Schinas, J.: On the stable manifold theorem for discrete time dependent processes in Banach spaces, B. Lond. Math. Soc., 5, 275–282, 1973.

Dieci, L. and Eirola, T.: On smooth decompositions of matrices, SIAM J. Matrix Anal. A., 20(3), 800–819, 1999.

Dieci, L. and Vleck, E. S. V.: Lyapunov spectral intervals: Theory and computation, SIAM J. Numer. Anal., 40(2), 516–542, 2003.

Dieci, L., Russell, R. D., and Vleck, E. S. V.: On the computation of Lyapunov exponents for continuous dynamical systems, SIAM J. Numer. Anal., 34(1), 402–423, 1997.

d'Ovidio, F., Fernández, V., a, E. H.-G., and López, C.: Mixing structures in the Mediterranean Sea from finite-size Lyapunov exponents, Geophys. Res. Lett., 31, L17203, doi:10.1029/2004GL020328, 2007.

d'Ovidio, F., Isern-Fontanet, J., Lopez, C., Hernandez-Garcia, E., and Garcia-Ladon, E.: Comparison between Eulerian diagnostics and finite-size Lyapunov exponents computed from altimetry in the Algerian basin, Deep-Sea Res. Pt. I, 56, 15–31, 2009.

Duan, J. and Wiggins, S.: Lagrangian transport and chaos in the near wake of the flow around an obstacle: a numerical implementation of lobe dynamics, Nonlin. Processes Geophys., 4, 125–136, 1997,
http://www.nonlin-processes-geophys.net/4/125/1997/.

Duc, L. H. and Siegmund, S.: Hyperbolicity and invariant manifolds for planar nonautonomous systems on finite time intervals, Int. J. Bifurcat. Chaos, 18, 641–674, 2008.

Ershov, S. V. and Potapov, A. B.: On the concept of stationary Lyapunov basis, Physica D, 118, 167–198, 1998.

Fontich, E.: Stable curves asymptotic to a degenerate fixed point, Nonlinear Anal.-Theor., 35(6), 711–733, 1999.

Garcá-Olivares, A., Isern-Fontanet, J., and Garcá-Ladona, E.: Dispersion of passive tracers and finite-scale Lyapunov exponents in the Western Mediterranean Sea, Deep-Sea Res. Pt. I, 54, 15–31, 2007.

Geist, K., Parlitz, U., and Lauterborn, W.: Comparison of Different Methods for Computing Lyapunov Exponents, Prog. Theor. Phys., 83(5), 875–893, 1990.

Ghosh, S., Leonard, A., and Wiggins, S.: Diffusion of a passive scalar from a no-slip boundary into a two-dimensional chaotic advection field a two-dimensional chaotic advection field, J. Fluid Mech., 372, 119–163, 1998.

Goldhirsch, I., Sulem, P.-L., and Orszag, S. A.: Stability and Lyapunov Stability of Dynamical Systems: A Differential Approach and a Numerical Method, Physica D, 27, 311–337, 1987.

Greene, J. M. and Kim, J.-S.: The Calculation of Lyapunov Spectra, Physica D, 24, 213–225, 1987.

Haller, G.: Finding finite-time invariant manifolds in two-dimensional velocity fields, Chaos, 10(1), 99–108, 2000.

Haller, G.: Distinguished material surfaces and coherent structure in three-dimensional fluid flows, Physica D, 149, 248–277, 2001a.

Haller, G.: Lagrangian structures and the rate of strain in a partition of two-dimensional turbulence, Phys. Fluids, 13, 3365–3385, 2001b.

Haller, G.: Lagrangian coherent structures from approximate veolcity data, Phys. Fluids, 14, 1851–1861, 2002.

Haller, G.: Exact theory of separation for two-dimensional flows, J. Fluid Mech., 512, 257–311, 2004.

Haller, G.: An objective definition of a vortex, J. Fluid Mech., 525, 1–26, 2005.

Haller, G. and Poje, A.: Finite time transport in aperiodic flows, Physica D, 119, 352–380, 1998.

Haller, G. and Yuan, G.: Lagrangian coherent structures and mixing in two-dimensional turbulence, Physica D, 147, 352–370, 2000.

Henry, D.: Geometric theory of semilinear parabolic equations, in: Lecture Notes in Mathematics, Springer-Verlag: New York, Heidelberg, Berlin, 840, 348 pp., 1981.

Holland, M. and Luzzatto, S.: Stable manifolds under very weak hyperbolicity conditions, J. Differ. Equations, 221, 444–469, 2006.

Ide, K., Small, D., and Wiggins, S.: Distinguished hyperbolic trajectories in time-dependent fluid flows: analytical and computational approach for velocity fields defined as data sets, Nonlin. Processes Geophys., 9, 237–263, 2002,
http://www.nonlin-processes-geophys.net/9/237/2002/.

Irwin, M. C.: Hyperbolic time dependent processes, B. Lond. Math. Soc., 5, 209–217, 1973.

Jones, C. K. R. T. and Winkler, S.: Invariant manifolds and Lagrangian dynamics in the ocean and atmosphere, in: Handbook of dynamical systems, North-Holland, Amsterdam, 55–92, 2002.

Joseph, B. and Legras, B.: Relation between kinematic boundaries, stirring and barriers for the Antarctic polar vortex, J. Atmos. Sci., 59, 1198–1212, 2002.

Ju, N. and Wiggins, S.: On roughness of exponential dichotomy, J. Math. Anal. Appl., 262, 39–49, 2001.

Ju, N., Small, D., and Wiggins, S.: Existence and Computation of Hyperbolic Trajectories of Aperiodically Time-Dependent Vector Fields and Their Approximations, Int. J. Bif. Chaos, 13, 1449–1457, 2003.

Katok, A. and Hasselblatt, B.: Introduction to the Modern Theory of Dynamical Systems, Cambridge University Press, Cambridge, 1995.

Kloeden, P. and Siegmund, S.: Bifurcations and continuous transitions of attractors in autonomous and nonautonomous systems, Int. J. Bif. Chaos, 15, 743–762, 2005.

Koh, T. Y. and Legras, B.: Hyperbolic trajectories and the Antarctic polar vortex, Chaos, 12(2), 382–394, 2002.

Langa, J., Robinson, J. C., and Suàrez, A.: Bifurcations in non-autonomous scalar equations, J. Differ. Equations, 221, 1–35, 2006.

Langa, J. A., Robinson, J. C., and Suàrez, A.: Stability, instability, and bifurcation phenomena in non-autonomous differential equations, Nonlinearity, 15, 887–903, 2002.

Lapeyre, G.: Characterization of finite-time Lyapunov exponents and vectors in two-dimensional turbulence, Chaos, 12(3), 688–698, 2002.

Legras, B. and Vautard, R.: A Guide to Liapunov Vectors, in: Proceedings of the 1995 ECMWF Seminar on Predictability, edited by: Palmer, T., 143–156, 1996.

Lekien, F. and Coulliette, C.: Chaotic stirring in quasi-turbulent flows, Philos. T. Roy. Soc. A, 365 pp., 2007.

Lekien, F., Shadden, S., and Marsden, J. E.: Lagrangian coherent structures in n-dimensional systems, J. Math. Phys., 48, 065404, 2007.

Mancho, A. M., Small, D., Wiggins, S., and Ide, K.: Computation of Stable and Unstable Manifolds of Hyperbolic Trajectories in Two-Dimensional, Aperiodically Time-Dependent Vector Fields, Physica D, 182, 188–222, 2003.

Mancho, A. M., Small, D., and Wiggins, S.: Computation of hyperbolic trajectories and their stable and unstable manifolds for oceanographic flows represented as data sets, Nonlin. Processes Geophys., 11, 17–33, 2004,
http://www.nonlin-processes-geophys.net/11/17/2004/.

Mancho, A. M., Small, D., and Wiggins, S.: A tutorial on dynamical systems concepts applied to Lagrangian transport in oceanic flows defined as finite time data sets: Theoretical and computational issues, Phys. Rep., 437, 55–124, 2006.

Mancho, A. M., Hernández-García, E., Small, D., and Wiggins, S.: Lagrangian transport through an ocean front in the

North-Western Mediterranean Sea, J. Phys. Oceanogr., 38, 1222–1237, 2008.

Mathur, M., Haller, G., Peacock, T., Ruppert-Felsot, J. E., and Swinney, H. L.: Uncovering the Lagrangian Skeleton of Turbulence, Phys. Rev. Lett., 98, 144502, 2007.

McGehee, R.: Stable manifolds theorem for degenerate fixed-points with applications to celestial mechanics, J. Differ. Equations, 14, 70–88, 1973.

Miller, P. D., Jones, C. K. R. T., Rogerson, A. M., and Pratt, L. J.: Quantifying transport in numerically generated velocity fields, Physica D, 110, 105–122, 1997.

Oseledec, V.: A multiplicative ergodic theorem: Lyapunov characteristic numbers for dynamical systems, Trans. Moscow Math. Soc., 19, 197–231, 1968.

Ottino, J.: The Kinematics of Mixing: Stretching, Chaos, and Transport, Cambridge University Press, Cambridge, 1989.

Pierrehumbert, R. T.: Large-scale horizontal mixing in planetary atmospheres, Phys. Fluids A, 3(5), 1250–1260, 1991.

Pierrehumbert, R. T. and Yang, H.: Global chaotic mixing on isentropic surfaces, J. Atmos. Sci., 50, 2462–2480, 1993.

Pollicott, M.: Symbolic Dynamics for Smale Flows, Am. J. Math., 109, 183–200, 1987.

Samelson, R. and Wiggins, S.: Lagrangian Transport in Geophysical Jets and Waves: The Dynamical Systems Approach, Springer-Verlag, New York, 2006.

Sell, G. R.: Non-autonomous differential equations and dynamical systems, T. Am. Math. Soc., 127, 241–83, 1967.

Sell, G. R.: Lectures on Topological Dynamics and Differential Equations, Van-Nostrand-Reinhold, Princeton, NJ, 1971.

Shadden, S., Lekien, F., and Marsden, J. E.: Definition and properties of Lagrangian coherent structures from finite-time Lyapunov exponents in two-dimensional aperiodic flows, Physica D, 212, 271–304, 2005.

Shadden, S., Dabiri, J. O., and Marsden, J. E.: Lagrangian analysis of fluid transport in empirical vortex ring flows, Phys. Fluids, 18, 047105, 2006.

Shadden, S., Katija, K., Rosenfeld, M., Marsden, J. E., and Dabiri, J. O.: Transport and stirring induced by vortex formation, J. Fluid Mech., 593, 315–331, 2007.

Shadden, S. C.: Online LCS tutorial: available at: www.cds.caltech.edu/~shawn/LCS-tutorial/, last access: 2009.

Shariff, K., Pulliam, T. H., and Ottino, J. M.: A dynamical systems analysis of kinematics in the time-periodic wake of a circular cylinder, in: Vortex dynamics and vortex methods (Seattle, WA, 1990), Amer. Math. Soc., Lectures in Appl. Math., 28, 613–646, 1991.

Sturman, R., Ottino, J. M., and Wiggins, S.: The Mathematical Foundations of Mixing, in: Cambridge Monographs on Applied and Computational Mathematics, Cambridge University Press, vol. 22, 281 pp., 2006.

Surana, A., Grunberg, O., and Haller, G.: Exact theory of three-dimensional flow separation. Part 1. Steady separation, J. Fluid Mech., 564, 57–103, 2006.

Surana, A., Jacobs, G. B., and Haller, G.: Extraction of Separation and Attachment Surfaces from Three-Dimensional Steady Shear Flows, AIAA Journal, 45, 1290–1302, 2007.

von Hardenberg, J., Fraedrich, K., Lunkeit, F., and Provenzale, A.: Transient chaotic mixing during a baroclinic life cycle, Chaos, 10(1), 122–134, 2000.

Wang, Y., Haller, G., Banaszuk, A., and Tadmor, G.: Closed-loop Lagrangian separation control in a bluff body shear flow model, Phys. Fluids, 15, 2251–2266, 2003.

Wiggins, S.: The Dynamical Systems Approach to Lagrangian Transport in Oceanic Flows, Annu. Rev. Fluid Mech., 37, 295–328, 2005.

Yuster, T. and Hackborn, H. W.: On invariant manifolds attached to oscillating boundaries in Stokes flows, Chaos, 7, 769–776, 1997.

Zhang, W.: Invariant manifolds for differential equations, Acta Math. Sin., 8, 375–398, 1992.